Machine-verified Kerr–Newman horizons, nonsingular gravitational collapse, and quantum horizon obstructions

Jonathan Washburn [1*]

[1]Recognition Physics Institute, Austin, Texas 78701, USA.

Corresponding author: Jonathan Washburn, e-mail: jon@recognitionphysics.org

Abstract

We present a machine-verified framework of strong-field black-hole theorems, effective nonsingular gravitational collapse models, and sharp horizon obstructions, extending our linearized body-centred hypercubic lattice gravity analysis into the nonlinear regime. First, direct four-dimensional Fréchet differentiation proves all **16** nonlinear Einstein and coupled Einstein–Maxwell equations on Kruskal–Szekeres Schwarzschild, smooth ingoing Kerr across both horizons (paired with local first-variation stationarity of the **104**-hinge discrete curvature action directly on the horizon), and horizon-penetrating ingoing Kerr–Newman spacetimes without $\mathbf{1/\Delta}$ denominators. We establish both four-dimensional horizon Zeroth Laws, the Smarr and three-parameter First Law, Komar and Gauss charges, Petrov Type D Weyl scalars and the exact **8**-index Kretschmann scalar, unconditional sub-extremal Kerr light rings and equatorial innermost stable circular orbits, charged-scalar superradiance, Kerr Teukolsky separation, the four-dimensional ADM constraint and evolution system, spherical and inverse-mean-curvature-flow Penrose rigidity, pure-vacuum Christodoulou gravitational-wave memory, and the classical Bondi–Metzner–Sachs soft-graviton Ward identity. Second, imposing a finite energy-density ceiling $\boldsymbol{\rho_c = 3/(8\pi G\ell^2)}$ organized around the canonical reciprocal cost $\boldsymbol{J(x) = \frac{1}{2}(x+x^{-1})-1}$ yields nonsingular homogeneous dust bounces ($\mathbf{0 \le K_{ext} \le 360/\ell^4}$, exact $\mathbf{9+9}$ Israel–Darmois matching), a two-sided inhomogeneous Lemaître–Tolman–Bondi theorem separating global boundedness ($\boldsymbol{|\eta_{sh}| < 1}$) from genuine post-turn shell-crossing blow-up ($\boldsymbol{\eta_{sh} = 5/4}$), a supercritical horizon obstruction ($\mathbf{27G^2M^2 > 64\ell^2}$) preventing causal bounce return to the original exterior, and global completeness bounds on static Hayward rain trajectories and rotating Gürses–Gürsey principal null rays ($\boldsymbol{|K| \le 896/\ell^4}$, with direction-dependent ring curvature $\mathbf{0}$ versus $\boldsymbol{24/\ell^4}$). Third, we prove a universal $\mathbf{3/2}$ three-dimensional Voronoi Crofton area overcount across $\boldsymbol{\mathbb{Z}^3}$, $\boldsymbol{D_3}$, and $\boldsymbol{D_3^*}$, forced uniqueness of the logarithmic entropy coefficient $\boldsymbol{\gamma_{log} = 3/2}$ across arbitrary $\boldsymbol{SU(2)}$ spin ceilings, and deterministic exterior-only Yoshida–Kitaev Grover and Uhlmann decoding bounds. Every theorem is formally checked in Lean 4 with zero unfinished proofs and cross-checked by an independent symbolic–numerical suite.

Keywords: Kerr–Newman black holes, Petrov Type D, Teukolsky equation, ADM constraints, BMS symmetry, gravitational-wave memory, nonsingular gravitational collapse, Lemaître–Tolman–Bondi shell crossing, black-hole echoes, regular black holes, logarithmic black-hole entropy, Hayden–Preskill decoding

1 Introduction

Classical general relativity describes macroscopic gravity with extraordinary accuracy, yet breaks down precisely where its own dynamics concentrate energy most strongly. Under generic energy conditions, gravitational collapse drives spacetime curvature to infinity and terminates timelike and null geodesics in finite proper or affine parameter [10;16;18]. Any microscopic formulation of gravity that aims to extend

general relativity beyond the Planck scale therefore confronts three coupled questions in the strong-field regime:

1. *Exact nonlinear black-hole recovery.* Does the theory reproduce the full nonlinear vacuum and electrovacuum black-hole solutions of general relativity—Schwarzschild, rotating Kerr[11], and charged rotating Kerr–Newman[12]—directly across both event and inner horizons, together with their Killing-horizon mechanics[22], Petrov algebraic structure[27;29], linear perturbation separability[23;24], initial-value constraint and evolution structure[31;33], and asymptotic Bondi–Metzner–Sachs (BMS_4) radiation and memory laws[39–41]?
2. *Nonsingular collapse, geodesic completeness, and sharp obstructions.* When collapsing matter reaches a microscopic energy-density ceiling set by a fundamental length ℓ, does the dynamics replace central and cosmological singularities with finite-curvature, geodesically complete spacetimes—and what sharp obstructions govern inhomogeneous shell crossings[49] and claimed gravitational-wave "echoes" returning to an exterior observer[60–62]?
3. *Quantum horizon microstructure and information recovery.* What exact geometric and Hilbert-space theorems control horizon-area lattice counting, logarithmic area-entropy corrections[76;77;80], and deterministic post-Page-time information decoding[81–83;85]?

A recurring hazard in regular-black-hole and discrete-gravity work is mistaking homogeneous toy models for general theorems. Homogeneous bounces can conceal inhomogeneous shell-crossing singularities; finite curvature invariants at $r = 0$ do not by themselves imply global geodesic completeness[57]; local bounce geometries are frequently assumed to reflect causal waves back into the original black-hole exterior without verifying global horizon matching; and raw lattice face counts can silently distort horizon area by a fixed geometric factor. The purpose of this paper is to resolve these strong-field questions cleanly, establishing exact positive theorems alongside constructive counterexamples and sharp causal and geometric obstructions.

1.1 From linearized D_4^* gravitons to the nonlinear strong-field frontier

This work directly extends our linearized Lorentzian lattice analysis[1] (and its companion study of area-weighted hinge actions[2]). There we derived the exact full-sphere dimension-six graviton dispersion of Lorentzian length and area Regge calculus[8] on the 15-edge Kuhn triangulation of the hypercubic lattice across every flat timelike-triangle background parameterized by the light-cone reach parameter $\kappa_{\mathrm{cone}} > \frac{1}{2}$. That calculation established four structural obstructions on the single-posting Kuhn triangulation: tetrahedral linear birefringence and opposite-direction non-reciprocity at relative order $(k\lambda)^2$; a $(2\kappa_{\mathrm{cone}} - 1)^{-1}$ divergence of the length-Regge dispersion coefficients as $\kappa_{\mathrm{cone}} \to \frac{1}{2}^+$; four spurious gapless Brillouin-zone corner doublers at $\kappa_{\mathrm{cone}} = 1$; and a strict graviton-below-scalar speed ordering opening vacuum gravitational Cherenkov radiation for ultra-high-energy cosmic rays.

That study[1] then proved how lifting the single-posting triangulation to the 24-bond double-entry body-centred hypercubic lattice D_4^* at $\kappa_{\mathrm{cone}} = \frac{1}{2}$—governed by the 1,152-element crystallographic Weyl group F_4, the unique irreducible four-dimensional reflection group possessing no quartic polynomial invariant beyond $(k^2)^2$[9]—resolves all four linearized obstructions simultaneously. Direct exact-rational Schur elimination on the canonical 12-bond D_4^* linearized gravity operator proves that all dimension-six dispersion and birefringence vanish identically ($s_{D_4^*} = 0$), that dimension-eight birefringence also vanishes with strictly subluminal dispersion

$$\frac{\omega_{\pm}^{D_4^*}(\hat{n})}{|\mathbf{q}|} = 1 - \frac{(1 - I_4) - 2I_3^2}{80} \, (a_{\mathrm{lat}}|\mathbf{q}|)^4 + O\big((a_{\mathrm{lat}}|\mathbf{q}|)^6\big), \tag{1}$$

where $\hat{n} = \mathbf{q}/|\mathbf{q}| \in S^2$ is the spatial propagation direction and $I_3 := \hat{n}_1\hat{n}_2\hat{n}_3$ and $I_4 := \sum_{i=1}^{3} \hat{n}_i^4$ are the elementary cubic invariants. Furthermore, the gauge-fixed 12×12 Hermitian carrier has exact $(11, 1)$ signature throughout the punctured Brillouin zone (eliminating all corner doublers), and vacuum gravitational Cherenkov emission against the nearest-neighbour D_4^* scalar is kinematically closed through dimension eight.

Linearized plane waves on flat spacetime, however, leave the nonlinear strong-field physics of gravity untested. Accordingly, this paper separates three distinct layers cleanly: (a) exact machine-verified theorems of nonlinear classical general relativity, initial-value constraints, and asymptotic radiation

(Sections 3 and 4); (b) effective capacity-ceiling models of nonsingular gravitational collapse and static/rotating regular cores parameterized around the canonical reciprocal cost $J(x)$ (Sections 5 and 6), situated directly alongside modern effective polymerized collapse models [66–71]; and (c) universal discrete horizon-area geometry and finite-dimensional quantum-information recovery bounds (Section 7).

1.2 Summary of main results and sharp obstructions

The results of this paper are organized into five thematic theorem blocks and two decisive strong-field obstructions (paired with a universal 50% raw-face horizon-counting obstruction), all established by direct four-dimensional differential-geometric computation and machine-verified formal proof (Section 2.3):

1. **Exact nonlinear black holes, Petrov Type D structure, and horizon mechanics (Section 3).** Evaluating the four-dimensional Levi–Civita connection, Riemann tensor, Ricci tensor, and Einstein tensor directly via Fréchet derivatives proves that all 16 nonlinear vacuum Einstein and coupled Einstein–Maxwell equations vanish identically on maximally extended Kruskal–Szekeres Schwarzschild [13;14], on smooth ingoing rotating Kerr across outer (r_+), inner (r_-), and extremal ($\Delta = 0$) horizons—paired with local periodic-patch stationarity of the full 104-hinge D_4^* action directly across the horizon—and on smooth ingoing charged rotating Kerr–Newman spacetimes [12] with zero $1/\Delta$ denominators. Directly at $\Delta = 0$ without punctured limits, we establish both four-dimensional horizon Zeroth Laws (polar-independent surface gravity $\kappa_H = \kappa_+$ and corotating electric potential Φ_H), the Smarr and three-parameter First Law [22], exact Komar mass and angular momentum ($M, J_{\rm BH} = Ma$) [28], Gauss's law electric charge Q, Petrov Type D Weyl scalars ($\Psi_0 = \Psi_1 = \Psi_3 = \Psi_4 = 0$, exact Ψ_2) and the complete 8-index Kerr–Newman Kretschmann scalar $K_{\rm KN}$ [29], unconditional sub-extremal Kerr light rings and Bardeen–Press–Teukolsky equatorial innermost stable circular orbits [20], exact Kerr shadow contours [21], Kerr–Newman Penrose extraction ($E \geq \Omega_H L + \Phi_H q$) and Christodoulou–Ruffini irreducible mass [19], charged-scalar superradiance ($\omega < m\Omega_H + q\Phi_H$) [25], and separation plus horizon Frobenius exponents of the four-dimensional Kerr Teukolsky master equation [23;24].
2. **4D ADM constraints, evolution, Penrose rigidity, and asymptotic BMS_4/memory laws (Section 4).** On spatial hypersurfaces, we establish the exact four-dimensional ADM 3+1 decomposition [31], uniqueness of the three-dimensional Yamabe exponent $p = 4$, the Lichnerowicz–York conformal constraint system [32;33], exact n-body Brill–Lindquist initial data [34], spinning Bowen–York momentum constraints and global mass barriers $m \leq M_{\rm ADM} \leq m + 12|S|^2/m^3$ [35], the seven inhomogeneous four-dimensional Gauss–Codazzi–Mainardi and ADM evolution equations together with symmetric-hyperbolic constraint propagation and an explicit non-flat vacuum Kasner witness, the Schwarzschild J-cost throat area $A(r) = 16\pi M^2\big(1 + \frac{1}{2}J(2r/M)\big)^2$, spherical and inverse-mean-curvature-flow Riemannian Penrose inequalities with rigidity [36–38], and six gauge-invariant Bardeen cosmological observables together with exact bounce local non-Gaussianity $f_{\rm NL}^{\rm loc} = +\frac{5}{2}(1+w)$. At future null infinity, we establish pure-vacuum Christodoulou nonlinear memory ($\Delta M_{\rm Bondi} = -429/(350G)$ on an explicit C^2 burst) [41], the spin-2 E/B Hodge decomposition on S^2 and local Flanagan–Nichols superrotation balance ($k_{\rm sr}$) [44], and the classical BMS_4 supertranslation Ward identity linking permanent strain memory directly to Weinberg's leading soft-graviton pole [39;40;42;43].
3. **Nonsingular collapse bounces, Obstruction I (two-sided inhomogeneous LTB), and Obstruction II (supercritical no-exterior-echo) (Section 5).** Incorporating the effective capacity density ceiling $\rho_c = 3/(8\pi G\ell^2)$ linked to the canonical reciprocal cost $J(x) = \frac{1}{2}(x + x^{-1}) - 1$ [4;5] produces exact nonsingular FLRW bounces (cf. Ashtekar et al. [65]) and homogeneous Oppenheimer–Snyder bouncing dust stars [45] ($K_{\rm int} \leq 27/\ell^4$, uniquely forced exterior $f_{\rm ext}(r) = 1 - 2GM/r + 4\ell^2G^2M^2/r^4$ matching the polymerized exterior of Ref. [69], and exact critical horizon threshold $27G^2M^2 = 64\ell^2$). Extending to marginally bound inhomogeneous Lemaître–Tolman–Bondi (LTB) dust collapse [46–48] parameterized by dimensionless shell-shear margin $\eta_{\rm sh}$ yields a sharp *two-sided theorem*: for $m'(r) > 0$ and $\tau_0'(r) \geq 0$, no shell crossing occurs before turning; every sub-critical C^3 profile ($|\eta_{\rm sh}| < 1$) avoids shell crossings globally for all $\tau \in \mathbb{R}$ and obeys the exact closed-form Kretschmann bound $0 \leq K \leq C_{\rm LTB}(|\eta_{\rm sh}|)/\ell^4$ (witnessed at $\eta_{\rm sh} = \frac{1}{2}$ with $C_{\rm LTB}(\frac{1}{2}) = 5355/4$). Conversely, **Obstruction I** refutes unconstrained inhomogeneous boundedness via the

explicit super-critical C^3 profile $m(r) = r^3$, $\tau_0(r) = \frac{5}{2}\ell r$ ($\eta_{\rm sh} = \frac{5}{4}$), which develops a genuine *post-turn* shell-crossing curvature blow-up ($R' \to 0^+$, $K \to +\infty$) as $s = \tau - \tau_0(1) \to (+\ell/3)^-$ [49]. Within Section 5.3, matching the bouncing stellar surface onto an outgoing Eddington–Finkelstein chart yields $0 \le K_{\rm ext} \le 360/\ell^4$ and all 9+9 Israel–Darmois junction conditions [50], while **Obstruction II** proves that whenever $27G^2M^2 > 64\ell^2$, the advanced time $V(\tau)$ of the original ingoing exterior diverges ($\lim_{\tau\to\tau_-^-} V(\tau) = +\infty$) as the boundary reaches r_- with $R'(\tau_-) = +1$: every causal trajectory emerging from the bounce exits into a *second asymptotic exterior region* rather than returning to the original exterior observer, causally obstructing naive black-hole echo return signals in the matched bounce geometry [61;62].

4. **Geodesic completeness of bouncing collapse, static Hayward rain trajectories, and rotating Gürses–Gürsey core structure (Section 6).** Interior causal geodesics and the bouncing stellar surface extend globally for all affine or proper parameter ($\tau \in \mathbb{R}$). On the static Hayward capacity core [51;52], every unit-energy infalling radial "rain" timelike geodesic extends smoothly for all $\tau \in (-\infty, +\infty)$, obeying $r(\tau) \ge r_0\, e^{-\tau/\ell} > 0$ ($\tau \ge 0$) and $|K| \le 896/\ell^4$. On rotating regular black holes built via the Gürses–Gürsey construction [53–55] with the unique capacity mass profile $m_{\rm cap}(r) = GMr^3/(r^3 + 2GM\ell^2)$, ingoing principal null geodesics enter the core smoothly with uniform curvature cap $|K_{\rm GG}(r,\chi)| \le 896/\ell^4$ (approaching the de Sitter value $24/\ell^4$ along the equator while vanishing on the $r = 0$ disk, revealing a genuine bounded direction-dependence at the ring), explicitly contrasted against singular Kerr's equatorial ring blow-up $K_{\rm Kerr}(r,0) = 48M^2/r^6 \to +\infty$.
5. **Quantum horizon microstructure: universal 3/2 Crofton projection, forced $\gamma_{\log} = 3/2$ entropy law, and deterministic decoding (Section 7).** Integrating $|n \cdot u|$ over the curved Kruskal horizon 2-sphere proves a universal $SO(3)$-invariant three-dimensional Voronoi Crofton theorem [75]: raw face counting overcounts Bekenstein–Hawking area [72;73] by an exact factor $\mathcal{C}_{S^2} = \frac{3}{2}$ across simple cubic ($\mathbb{Z}^3$), face-centred cubic (D_3), and body-centred cubic (D_3^*) Voronoi tessellations, forcing the geometric projection factor 2/3 independently of lattice choice. On the $SU(2)$-intertwiner horizon Hilbert space, exact Weyl closure integrals and two-sided Gaussian character bounds establish a two-sided entropy-area window $S = A/(4\ell_{\rm P}^2) - \gamma_{\log}\ln(A/\ell_{\rm P}^2) + O(1)$ across arbitrary finite twice-spin ceilings $N_{\max} \ge 1$ and prove *forced uniqueness* of the logarithmic coefficient $\gamma_{\log} = \frac{3}{2}$ [76–80]. Finally, in finite-dimensional post-Page black-hole radiation models [81;82], we construct both a deterministic exterior-only Yoshida–Kitaev Grover decoder with zero post-selection ($F_{\rm det} \ge 1 - \frac{8}{\sqrt{3}}\sqrt{\eta}$, achieving $1 - \frac{8}{\sqrt{3}} d_M/d_T$ on unitary 2-designs) [83;84] and an explicit one-step Stinespring/Uhlmann recovery isometry obeying $1 - \|\Delta_{\rm dec}\|_1 \le F_{\rm Uhlmann} \le P_{\rm pair}$ (achieving $1 - d_M/d_T$ on unitary 2-designs) [85].

1.3 Scope boundaries and explicitly open questions

Keeping proved mathematics distinct from open physics requires stating exact scope boundaries up front. Every theorem, explicit witness, and obstruction summarized above is proved in full under its stated hypotheses; where a physical modelling relation is adopted as an effective closure rather than derived microscopically from discrete lattice dynamics (specifically the compact-phase collapse rate pricing, the Bianchi-I holonomy shear cap, the rotating capacity mass profile $m_{\rm cap}$, and the per-puncture area footprint $a_N = 4\ln(N+1)\,\ell_{\rm P}^2$), it is marked explicitly at the point of use. Five major strong-field and quantum-gravity questions remain *explicitly open* and are not claimed here:

1. *Generic asymmetric $(3+1)$-dimensional collapse:* Our collapse and bounce theorems cover homogeneous FLRW/Oppenheimer–Snyder dynamics, marginally bound inhomogeneous spherically symmetric LTB dust, and static/rotating regular cores; gravitational collapse with pressure and no spherical or axial symmetry remains open.
2. *Nonlinear inner-horizon dynamical stability and continuation past $r = 0$:* While regular rotating and charged cores obey uniform Kretschmann bounds and ingoing null completeness on $r \ge 0$, rotating timelike completeness, analytic extension into $r < 0$, and nonlinear Poisson–Israel mass-inflation stability of the inner Cauchy horizon [30;56;58] remain open.

3. *4D bulk Einstein derivation of asymptotic news laws:* Our BMS_4, Christodoulou memory, and superrotation balance theorems in Section 4 take the Bondi mass-aspect and angular-momentum-aspect evolution laws as explicit named hypotheses rather than deriving them here from bulk asymptotically flat four-dimensional Einstein evolution.
4. *Parameter-free microscopic derivation of* $S_{\mathrm{BH}} = A/(4\ell_{\mathrm{P}}^2)$*:* While the universal 3/2 Crofton projection and forced logarithmic coefficient $\gamma_{\log} = 3/2$ are proved unconditionally, deriving the leading area-per-puncture footprint microscopically without calibration remains open.
5. *Dynamical curved-spacetime Hawking evaporation and continuum UV quantum gravity:* Coupling Bogoliubov particle creation and metric backreaction dynamically to the bouncing spacetime, and constructing the nonperturbative $a_{\mathrm{lat}} \to 0$ continuum quantum-gravity measure, remain open.

1.4 Conventions and nomenclature

Throughout this paper we use Lorentzian metric signature $(-,+,+,+)$, matching our linearized lattice study[1] and standard black-hole conventions[10]. Spacetime indices run over $\mu,\nu,\cdots \in \{0,1,2,3\}$ and spatial hypersurface indices over $i,j,\cdots \in \{1,2,3\}$. The Levi–Civita connection, Riemann tensor, Ricci tensor, and Einstein tensor are defined by

$$\Gamma^{\rho}_{\mu\nu} = \frac{1}{2} g^{\rho\lambda}\big(\partial_\mu g_{\nu\lambda} + \partial_\nu g_{\mu\lambda} - \partial_\lambda g_{\mu\nu}\big), \tag{2}$$

$$R^{\rho}{}_{\sigma\mu\nu} = \partial_\mu \Gamma^{\rho}_{\nu\sigma} - \partial_\nu \Gamma^{\rho}_{\mu\sigma} + \Gamma^{\rho}_{\mu\lambda}\Gamma^{\lambda}_{\nu\sigma} - \Gamma^{\rho}_{\nu\lambda}\Gamma^{\lambda}_{\mu\sigma}, \tag{3}$$

$$R_{\mu\nu} = R^{\lambda}{}_{\mu\lambda\nu}, \qquad R = g^{\mu\nu}R_{\mu\nu}, \qquad G_{\mu\nu} = R_{\mu\nu} - \frac{1}{2}R g_{\mu\nu}. \tag{4}$$

In classical strong-field, ADM initial-data, and geodesic theorems (Sections 3, 4 and 6), we work in geometric units $G = c = 1$ unless G is retained explicitly (as in $\rho_c = 3/(8\pi G\ell^2)$ and BMS_4 memory fluxes in Sections 4 and 5). In Planck-scale calibration, horizon-entropy, and quantum-information sections (Sections 2 and 7), G, $\hbar$, and c are restored explicitly with $\ell_{\mathrm{P}} = \sqrt{\hbar G/c^3}$.

Because black-hole mechanics, inhomogeneous collapse, asymptotic symmetries, lattice geometry, and quantum horizon entropy traditionally reuse several Greek and Latin letters—most notably κ, a, J, K, Δ, and Σ—we enforce strictly disambiguated symbols across the entire manuscript, collected in Table 1. In particular, bare κ is never used: the lattice light-cone reach parameter is written κ_{cone}, the Killing horizon surface gravity is $\kappa_H = \kappa_+$ (with inner-horizon value κ_-), the dimensionless LTB shell-shear margin is η_{sh}, the logarithmic area-entropy coefficient is $\gamma_{\log}$, and the superrotation mode index is k_{sr}. Similarly, $J(x)$ is reserved for the canonical reciprocal cost, $J_{\mathrm{BH}} = Ma$ denotes black-hole angular momentum, $N_{\max}$ denotes the finite twice-spin ceiling in Section 7, and Δ_{dec} denotes the quantum decoupling defect (distinct from the Kerr–Newman horizon polynomial Δ).

2 Canonical reciprocal cost, strong-field D_4^* action, and formal methodology

Before presenting the strong-field black-hole, initial-data, collapse, geodesic, and quantum-horizon theorems of Sections 3 to 7, we state the three structural ingredients that organize them: the canonical reciprocal comparison cost $J(x)$ together with its compact phase branch and capacity ceiling at scale ℓ, the 104-hinge curvature action on the 24-bond D_4^* lattice and its local stationarity criterion across rotating horizons, and the Fréchet-derivative formal verification standard used throughout the paper.

2.1 Uniqueness, compact phase branch, and effective capacity saturation of the canonical reciprocal cost

In the recognition-ledger formulation of discrete spacetime[3–7], comparing two positive geometric or physical ratios $x \in \mathbb{R}_{>0}$ carries a unique real cost functional

$$J(x) = \frac{1}{2}\big(x + x^{-1}\big) - 1 = \frac{(x-1)^2}{2x}, \qquad x \in \mathbb{R}_{>0}. \tag{5}$$

Table 1 Nomenclature and conventions adopted throughout the manuscript to prevent symbol collisions across lattice geometry, classical black-hole mechanics, ADM/BMS_4 structure, inhomogeneous collapse, and quantum horizon physics.

Symbol	Meaning / Definition	Domain / Value
$(-,+,+,+)$	Lorentzian metric signature	All sections
$G = c = 1$	Geometric units (classical theorems); $G, \hbar, c$ restored where noted	$\ell_{\mathrm{P}} = \sqrt{\hbar G/c^3}$
$J(x)$, $J(\Omega)$	Canonical reciprocal cost $\frac{1}{2}(x + x^{-1}) - 1$; matrix $\frac{1}{2}(\operatorname{tr}\Omega + \operatorname{tr}\Omega^{-1}) - 4$	$x > 0$, $\det\Omega \neq 0$
$J_{\mathrm{phase}}(\theta)$	Compact phase branch $1 - \cos\theta = -\operatorname{Re} J_{\mathbb{C}}(e^{i\theta})$	$\theta \in \mathbb{R}$
ℓ, ρ_c	Fundamental recognition length and capacity density ceiling $\rho_c = 3/(8\pi G\ell^2)$	$\ell > 0$
λ_{rec}	One-bit horizon-area spacing under $\lambda_{\mathrm{rec}}^2/(4\ell_{\mathrm{P}}^2) = \ln 2$	$2\sqrt{\ln 2}\,\ell_{\mathrm{P}} \approx 1.665\,\ell_{\mathrm{P}}$
a_{lat}, b	Half-bond and nearest-neighbour bond length on D_4^* ($b = 2a_{\mathrm{lat}}$)	D_4^* lattice
κ_{cone}	Lattice light-cone reach parameter ($\kappa_{\mathrm{cone}} = \frac{1}{2}$ on double-entry D_4^*)	$\frac{1}{2}$ (D_4^*); $> \frac{1}{2}$ (Kuhn)
M, a, J_{BH}, Q	Black-hole mass, spin $a = J_{\mathrm{BH}}/M$, angular momentum, and electric charge	Kerr–Newman family
χ, W, $\bar{\varphi}$	Polar cosine $\chi = \cos\theta \in (-1,1)$, $W = 1 - \chi^2$, and ingoing azimuth $\bar{\varphi}$	Smooth rational charts
$r_\pm$, Δ, ϱ^2	$r_\pm = M \pm \sqrt{M^2 - a^2 - Q^2}$, $\Delta = r^2 - 2Mr + a^2 + Q^2$, $\varrho^2 = r^2 + a^2\chi^2$	$M^2 \geq a^2 + Q^2$
$\kappa_\pm$, κ_H, Ω_H, Φ_H	$\kappa_\pm = (r_\pm - M)/(r_\pm^2 + a^2)$, $\kappa_H = \kappa_+$, $\Omega_H = a/(r_+^2 + a^2)$, $\Phi_H = Qr_+/(r_+^2 + a^2)$	Constant on $r = r_+$
$a(t)$, $H(t)$	Spatially flat FLRW cosmological scale factor and Hubble rate $\dot{a}/a$	Cosmological bounce
η_{sh}	Dimensionless LTB bounce-time shell-shear margin	$\lvert\eta_{\mathrm{sh}}\rvert < 1$ vs. $\frac{5}{4}$
k_{sr}	BMS_4 superrotation vector-field mode index	$k_{\mathrm{sr}} \in \mathbb{Z}$
K	Four-dimensional Kretschmann curvature scalar $K = R_{abcd}R^{abcd}$	Curvature invariant
Σ, h_{ij}, K_{ij}	Three-dimensional hypersurface, induced 3-metric, and extrinsic curvature	ADM / Israel–Darmois
$\mathcal{C}_{S^2}$	Universal 3D Voronoi spherical Cauchy–Crofton projection factor	$\mathcal{C}_{S^2} = \frac{3}{2}$
$N_{\max}$, $\gamma_{\log}$	Twice-spin ceiling $N \leq N_{\max}$ and logarithmic area-entropy slope	Forced $\gamma_{\log} = \frac{3}{2}$
Δ_{dec}, η	Quantum decoupling defect $\rho_{NK} - \rho_N \otimes \rho_K$ and $\eta = d_M d_K \operatorname{Tr}(\Delta_{\mathrm{dec}}^2)$	Finite-dim. decoding

As proved previously[4–6], four elementary consistency requirements fix Eq. (5) uniquely: zero cost at equality ($J(1) = 0$), reciprocal inversion symmetry ($J(x) = J(x^{-1})$), unit quadratic calibration ($J''(1) = 1$), and multiplicative composition under the d'Alembert functional equation

$$J(xy) + J(xy^{-1}) = 2J(x)J(y) + 2J(x) + 2J(y) \qquad (x, y > 0). \tag{6}$$

Evaluating the analytic continuation $J_{\mathbb{C}}(z) = \frac{1}{2}(z + z^{-1}) - 1$ on the unit circle $z = e^{i\theta}$ defines the companion compact phase cost

$$J_{\mathrm{phase}}(\theta) = 1 - \cos\theta = -\operatorname{Re} J_{\mathbb{C}}\big(e^{i\theta}\big), \qquad \theta \in \mathbb{R}. \tag{7}$$

While the exact classical black-hole, ADM, BMS_4, Crofton, $SU(2)$-intertwiner, and quantum-decoding theorems of Sections 3, 4 and 7 stand independently of any phenomenological collapse ansatz,

the reciprocal functional Eq. (5)–Eq. (7) organizes three distinct strong-field structures across this paper:

1. *Weak-field strain norm and Schwarzschild throat inversion.* Near unit ratio, $J(1+\varepsilon) = \frac{1}{2}\varepsilon^2 - \frac{1}{2}\varepsilon^3 + \frac{1}{2}\varepsilon^4 + O(\varepsilon^5)$. Extending Eq. (5) to an invertible 4×4 relative metric $\Omega = g_0^{-1}(g_0+\varepsilon H)$ yields $J(\Omega) = \frac{1}{2}(\operatorname{tr}\Omega + \operatorname{tr}\Omega^{-1}) - 4$, which reduces at leading order in a symmetric metric perturbation εH to $\frac{1}{2}\varepsilon^2 \operatorname{tr}\big(g_0^{-1}Hg_0^{-1}H\big)$, providing the quadratic pointwise strain norm whose lattice difference stencil enters the linearized graviton operator[1]. On the isotropic Schwarzschild spatial slice (Section 4), the exact reciprocal symmetry $J(x) = J(x^{-1})$ appears directly in the Einstein–Rosen throat area $A(r) = 16\pi M^2\big(1 + \frac{1}{2}J(2r/M)\big)^2$ and the exact inversion isometry $r \mapsto M^2/(4r)$.
2. *Unbounded cost floor and effective capacity density ceiling.* Unlike a continuum quadratic potential $\frac{1}{2}(x-1)^2$, which stays finite as $x \to 0^+$, the reciprocal cost Eq. (5) diverges as $\frac{1}{2}x^{-1}$ when $x \to 0^+$: any finite cost budget $J(x) \le B$ enforces the strict positive lower bound $x \ge 1+B-\sqrt{B^2+2B} > 0$. Evaluating the compact phase branch Eq. (7) on a collapse rate variable b at scale $\ell > 0$ yields the bounded rate cost $C(b) = \frac{1-\cos(2\ell b)}{2\ell^2} = \sin^2(\ell b)/\ell^2$ and fixes the finite capacity energy-density ceiling
$$\rho_c = \frac{3}{8\pi G\ell^2}. \tag{8}$$
In homogeneous FLRW and Oppenheimer–Snyder collapse (Section 5), the resulting modified Friedmann rate law $H^2 = \frac{8\pi G}{3}\rho(1-\rho/\rho_c)$—structurally matching effective polymerized collapse dynamics[65;68;69]—admits the exact reciprocal-cost identity
$$\rho\left(1-\frac{\rho}{\rho_c}\right) = \frac{\rho_c}{4+2J\big((\rho_c-\rho)/\rho\big)} \qquad (0<\rho<\rho_c), \tag{9}$$
which recovers classical general relativity linearly when $\rho \ll \rho_c$ while driving the collapse rate smoothly to zero at $\rho = \rho_c$.
3. *Exterior general relativity vs. regular core separation ($r \gg \ell$ vs. $r \sim \ell$).* In static and rotating regular black holes (Section 6), the capacity mass function
$$m_{\mathrm{cap}}(r) = \frac{GMr^3}{r^3+2GM\ell^2}, \qquad m'_{\mathrm{cap}}(r) = \frac{3GM/r}{4+2J\big((r/R_{\min})^3\big)} \tag{10}$$
(with $R_{\min} = (2GM\ell^2)^{1/3}$) separates the macroscopic and core regimes sharply whenever $GM \gg \ell$. For $r \gg R_{\min}$, $m_{\mathrm{cap}}(r) = GM\big[1-(R_{\min}/r)^3+O((R_{\min}/r)^6)\big]$, leaving solar-system post-Newtonian parameters ($\beta=\gamma=1$) and macroscopic horizon geometry indistinguishable from exact vacuum Kerr up to $O(\ell^2r^{-6})$ Ricci curvature corrections. As $r \to 0^+$, $m_{\mathrm{cap}}(r) = r^3/(2\ell^2) + O(r^6/(GM\ell^4))$ replaces the singular $1/r$ divergence with a regular de Sitter core capping curvature invariants at $O(\ell^{-4})$.

Under the one-bit horizon area normalization $\lambda_{\mathrm{rec}}^2/(4\ell_{\mathrm{P}}^2) = \ln 2$[1;3], the microscopic spacing sits near the Planck scale at $\lambda_{\mathrm{rec}} = 2\sqrt{\ln 2}\,\ell_{\mathrm{P}} \approx 1.665\,\ell_{\mathrm{P}}$. Throughout Sections 5 and 6, however, we keep $\ell > 0$ as a general positive scale parameter so that every curvature cap ($27/\ell^4$, $360/\ell^4$, $896/\ell^4$, $C_{\mathrm{LTB}}(|\eta_{\mathrm{sh}}|)/\ell^4$) and critical horizon threshold $27G^2M^2 = 64\ell^2$ holds parametrically for any $\ell > 0$.

2.2 The 24-bond D_4^* lattice, 104-hinge curvature action, and local horizon stationarity

At the discrete geometric level, the double-entry recognition ledger lives on the four-dimensional body-centred hypercubic lattice D_4^*. In doubled integer coordinates $2D_4^*$, each lattice vertex connects to 24 nearest neighbours consisting of 8 axial bonds $\pm 2e_\mu$ and 16 diagonal bonds $(\pm1,\pm1,\pm1,\pm1)$, with nearest-neighbour bond length $b = 2a_{\mathrm{lat}}$ and full point-group symmetry F_4 of order 1,152[1;3]. Holding the diagonal time axis $(1,1,1,1)$ fixed selects $\kappa_{\mathrm{cone}} = \frac{1}{2}$ uniquely from equal pricing of closed four-posting cycles and fourth-order isotropy of the lattice light operator[1].

Curvature on a periodic $n \times n \times n \times n$ refinement of the unit four-torus $[0,1]^4$ tiled by n^4 cells of D_4^* is measured by the 104-hinge discrete curvature functional

$$\mathcal{C}_{104}(g,n) := \sum_{p \in (\mathbb{Z}/n\mathbb{Z})^4} \sum_{h=1}^{104} w_h \, \mathcal{A}_h(g;p,n) \, \delta_h(g;p,n), \tag{11}$$

where the inner sum runs over the 104 elementary triangular hinge classes per D_4^* cell (56 non-null hinges carrying signed area weights $\mathcal{A}_h$ and discrete deficit angles δ_h evaluated from squared edge lengths induced by g at lattice spacing $1/n$, together with 48 lightlike cone-hinge classes whose real-time area-deficit terms vanish at flat background and contribute smoothly at first order without an external regulator; exact weights w_h and hinge tables are given in Ref.[3]). Scaling $\mathcal{C}_{104}$ by $1/n^2$ accounts for the n^4 cells multiplied by the $O(n^{-2})$ area-times-deficit scaling per hinge. Three continuum properties of Eq. (11) anchor the strong-field black-hole theorems of Section 3[3]:

1. *Unconditional real-time first variation in both signatures.* For every C^6 symmetric periodic nondegenerate metric field $g : \mathbb{R}^4 \to \mathrm{Mat}_{4\times4}(\mathbb{R})$ (Euclidean or Lorentzian signature) and every C^6 symmetric periodic perturbation h, the fine-lattice continuum first variation of Eq. (11) satisfies

$$\lim_{n\to\infty} \frac{d}{ds}\bigg|_{s=0} \frac{1}{n^2} \mathcal{C}_{104}(g+sh,n) = \int_{[0,1]^4} 4 \, \mathrm{sgn}(\det g) \sqrt{|\det g|} \, G^{ab}(g) \, h_{ab} \, d^4x, \tag{12}$$

   so first-order stationarity is unconditionally equivalent to the weak vacuum Einstein equation. (Nonlinear second-order lightlike cone-hinge regularity and discrete gauge fixing for quantum loops are distinct open issues discussed in Section 8.3 and Refs.[1;3].)
2. *Sourced matter coupling and covariant conservation.* Coupling continuum real scalar and Maxwell actions on the periodic four-torus to Eq. (11) with the physical sign yields positive Minkowski energy densities $T^{00}_{\mathrm{scalar}} \geq 0$ (for $V \geq 0$) and $T^{00}_{\mathrm{Maxwell}} = \frac{1}{2}(|\mathbf{E}|^2 + |\mathbf{B}|^2) \geq 0$, forces the pointwise nonlinear field equations $G^{ab} + \Lambda g^{ab} = +8\pi G T^{ab}$, and enforces exact covariant conservation $\nabla_a G^{ab} = \nabla_a T^{ab} = 0$ via the four-dimensional contracted second Bianchi identity.
3. *Local periodic-patch stationarity across rotating black-hole horizons.* A black-hole exterior is noncompact and asymptotically flat, whereas $\mathcal{C}_{104}$ is summed over periodic cells. To test whether an exact rotating black-hole metric is stationary for the 104-hinge action directly *on* and *across* the event horizon $\Delta = 0$, one works in smooth ingoing Kerr coordinates $(v, r, \theta, \bar{\varphi})$, where $g_{\mathrm{Kerr}}(M,a)$ is real-analytic and nondegenerate across r_+, r_-, and extremality. Around every regular point x (including points directly on $\Delta = 0$), one constructs an open neighborhood $U \ni x$ and a C^6 symmetric unit-periodic nondegenerate metric field $\tilde{g}$ coinciding identically with $g_{\mathrm{Kerr}}(M,a)$ on U. By Eq. (12), the continuum first variation of $\mathcal{C}_{104}$ against every C^6 symmetric periodic perturbation h supported on integer translates of U vanishes identically whenever all 16 components of $\mathcal{G}^{ab} = \sqrt{-\det g}\, G^{ab}$ vanish on U.

The scope boundary of this local stationarity theorem is explicit: it proves exact local first-variation stationarity of the full 104-hinge action at every regular point of ingoing Kerr spacetime (including both horizons and extremality, excluding only the spherical coordinate poles $\theta \in \{0,\pi\}$), without constructing an asymptotically flat Gibbons–Hawking–York boundary functional or proving global Kerr uniqueness from discrete records.

2.3 Direct Fréchet curvature calculus and machine-verified formal methodology

Strong-field general relativity and regular-black-hole geometry are vulnerable to hidden coordinate singularities, omitted connection terms, subtle index-raising sign errors, and unstated regularity assumptions. To rule out those failure modes, every theorem, explicit witness, counterexample, and obstruction in Sections 3 to 7 is established under a three-layer verification standard:

1. *Direct four-dimensional Fréchet differentiation.* Rather than substituting tabulated formulas for Christoffel symbols or curvature scalars, every metric field $g : \mathbb{R}^4 \to \mathrm{Mat}_{4\times4}(\mathbb{R})$ is differentiated

directly via coordinate Fréchet derivatives to compute the exact matrix inverse $g^{\mu\nu}$, all 64 Levi–Civita components Eq. (2), all 256 Riemann and Weyl components Eq. (3), all 16 Ricci and Einstein components Eq. (4), and the complete 8-index Kretschmann contraction $K = R_{abcd}R^{abcd}$. For Israel–Darmois matching (Section 5.3), all 9 induced-metric components h_{ij} and all 9 extrinsic-curvature components K_{ij} are evaluated directly from the embedded boundary tangents and unit outward normals on both sides.

2. *Machine-checked Lean 4 proofs with zero unproven gaps.* Every theorem statement, analytic witness (such as the sub-critical LTB profile $\eta_{\rm sh} = \frac{1}{2}$ and the super-critical post-turn blow-up profile $\eta_{\rm sh} = \frac{5}{4}$), and obstruction is formally verified in the Lean 4 interactive theorem prover with zero unfinished proofs and resting strictly on standard mathematical foundations (classical logic, propositional extensionality, and quotient soundness), with no custom physical axioms inserted inside proofs.
3. *Independent symbolic–numerical cross-checks and isolated adversarial audit.* Alongside the formal proofs, an independent Python verification suite executes 30 symbolic and numerical cross-checks spanning Kerr–Newman horizons, Petrov Type D scalars, Komar and Gauss charges, and Teukolsky separation; 4D ADM constraints, Yamabe uniqueness, and Kasner blow-up; BMS_4 memory, Weinberg poles, and spin-2 Hodge balance; Oppenheimer–Snyder bounces, $9+9$ Israel–Darmois matching, $V(\tau)$ divergence, and two-sided LTB curvature; static Hayward and off-equator Gürses–Gürsey cores; 3D Voronoi Crofton integrals; $SU(2)$ Weyl closure integrals; and finite-register Grover and Uhlmann matrices. Every theorem statement has also cleared isolated adversarial review confirming that stated hypotheses match proved conclusions and that every negative obstruction carries a constructive witness. A complete reproducibility index mapping each theorem block and obstruction to its verified Lean 4 module appears in Section A.

With the canonical reciprocal cost, the 104-hinge D_4^* action, the disambiguated nomenclature of Table 1, and the formal verification standard established, we turn first to the exact nonlinear classical black-hole family in Section 3.

3 Exact nonlinear black holes across both horizons: Schwarzschild, Kerr, and Kerr–Newman

A discrete theory of gravity that passes flat-space dispersion and Cherenkov tests must next meet general relativity on its most demanding nonlinear ground: the exact rotating and charged black-hole family. The sharpest test is not whether asymptotic weak-field expansions reproduce $1/r$ potentials, but whether the full nonlinear vacuum Einstein and coupled Einstein–Maxwell equations hold directly *across* the outer event horizon r_+, the inner Cauchy horizon r_-, and the extremal limit $\Delta = 0$, without coordinate singularities or punctured radial limits.

Throughout this section we work in geometric units $G = c = 1$ with signature $(-,+,+,+)$, using the rational polar cosine coordinate $\chi := \cos\theta \in (-1,1)$ and $W := 1-\chi^2 = \sin^2\theta$, together with $\varrho^2 := r^2 + a^2\chi^2$ for the Kerr and Kerr–Newman radial-angular metric factor (reserving Σ strictly for three-dimensional hypersurfaces in Sections 4 and 5). Every curvature tensor, covariant derivative, and surface integral is evaluated directly by four-dimensional Fréchet differentiation from the metric field without importing tabulated textbook identities.

3.1 Maximally extended Schwarzschild, smooth ingoing Kerr, local D_4^* stationarity, and equatorial optics

Static and stationary vacuum black holes are tested first in global horizon-penetrating charts: Kruskal–Szekeres coordinates (T, X, θ, φ) for Schwarzschild [13;14], and rational ingoing Kerr coordinates $(v, r, \chi, \bar\varphi)$ for rotating Kerr [11]. In the ingoing Kerr chart with $\Delta(r) := r^2 - 2Mr + a^2$, the metric takes the rational form

$$\begin{aligned} ds^2 = &-\left(1 - \frac{2Mr}{\varrho^2}\right) dv^2 + 2\,dv\,dr - 2aW\,dr\,d\bar\varphi - \frac{4MraW}{\varrho^2}\,dv\,d\bar\varphi \\ &+ \frac{\varrho^2}{W}\,d\chi^2 + W\left(r^2 + a^2 + \frac{2Mra^2W}{\varrho^2}\right) d\bar\varphi^2, \end{aligned} \tag{13}$$

which contains no Δ^{-1} denominators anywhere. Because its determinant is $\det g = -\varrho^4 < 0$, the metric and its inverse remain real-analytic across both horizons $r_\pm = M \pm \sqrt{M^2 - a^2}$ and across extremality $a = M$, breaking down only on the classical ring $\varrho^2 = 0$ and the polar coordinate axes $W = 0$.

Theorem 3.1 (Maximally extended Schwarzschild, smooth ingoing Kerr, and local 104-hinge D_4^* stationarity)**.** *Let $M, a \in \mathbb{R}$.*

1. Kruskal–Szekeres Schwarzschild. *For every $M > 0$ and $u = X^2 - T^2 > -1$, there exists a unique $r = r(u) > 0$ solving $\left(\frac{r}{2M} - 1\right)e^{r/(2M)} = u$, defining a C^2 map on $(-1, \infty)$ with derivative $r'(u) = \frac{4M^2}{r} e^{-r/(2M)}$ that spans the exterior ($r > 2M$), horizon ($r = 2M$), and interior ($0 < r < 2M$). On the maximal domain $\{(T, X, \theta, \varphi) \in \mathbb{R}^4 : X^2 - T^2 > -1,\ \sin\theta \neq 0\}$, the Kruskal–Szekeres metric field is C^2, its Fréchet first and second jets match the exact analytic tables, and all 16 components of $R_{\mu\nu}$, R, and the Einstein tensor density $\mathcal{G}_{\mu\nu} = \sqrt{-\det g}\, G_{\mu\nu}$ vanish identically. (In isotropic Cartesian coordinates, the weak-field metric likewise satisfies exact vacuum Einstein equations with Eddington–Robertson post-Newtonian parameters $\beta = \gamma = 1$, photon sphere $r = 3M$, and equatorial ISCO $r = 6M$, $L^2 = 12M^2$.)*
2. Smooth ingoing rotating Kerr across both horizons. *On the open domain $\mathcal{U}_{\mathrm{Kerr}}(a) := \{(v, r, \chi, \bar{\varphi}) \in \mathbb{R}^4 : \varrho^2 \neq 0,\ W \neq 0\}$, the metric Eq. (13) is C^2, satisfies $\det g = -\varrho^4 < 0$ and $g \cdot g^{-1} = I_4$, matches all 64 first-jet and 256 second-jet Fréchet derivatives, and obeys $R_{\mu\nu} = 0$, $R = 0$, and $\mathcal{G}_{\mu\nu} = 0$ identically for all 16 components—including directly at $r = r_+$, $r = r_-$, and extremal $\Delta = 0$.*
3. Local 104-hinge D_4^* stationarity across the Kerr horizon. *For any C^6 symmetric unit-periodic nondegenerate metric field g (Euclidean or Lorentzian signature), the fine-lattice continuum first variation of the full 104-hinge D_4^* recognition curvature cost $\mathcal{C}_{104}$ (including all 48 lightlike cone hinges without regulator) satisfies unconditionally*

$$\lim_{n\to\infty} \frac{d}{ds}\bigg|_{s=0} \frac{1}{n^2}\, \mathcal{C}_{104}(g + sh, n) = \int_{[0,1]^4} 4\ \mathrm{sgn}(\det g) \sqrt{|\det g|}\, G^{ab} h_{ab}. \tag{14}$$

Consequently, at every regular point x of the ingoing Kerr chart ($r > 0$, $0 < \theta < \pi$, including points directly on $r = r_+$, $r = r_-$, and $\Delta = 0$), there exist an open neighborhood $U \ni x$ and a C^6 symmetric unit-periodic nondegenerate metric field $\tilde{g}$ coinciding identically with $g_{\mathrm{Kerr}}(M, a)$ on U such that for every C^6 symmetric periodic perturbation h supported on integer translates of U,

$$\lim_{n\to\infty} \frac{d}{ds}\bigg|_{s=0} \frac{1}{n^2}\, \mathcal{C}_{104}(\tilde{g} + sh, n) = 0. \tag{15}$$

Proof structure. In Part 1, strict monotonicity of $f(r) = (\frac{r}{2M} - 1)e^{r/(2M)}$ on $(0, \infty)$ with range $(-1, \infty)$ yields the unique C^2 inverse $r(u)$ and its exact derivative by the inverse-function theorem; differentiating the resulting 4×4 Kruskal metric twice via coordinate Fréchet derivatives reduces all 16 Ricci components to exact rational-exponential identities vanishing identically on $X^2 - T^2 > -1$. In Part 2, the rational ingoing metric Eq. (13) is smooth on $\mathcal{U}_{\mathrm{Kerr}}(a)$ with explicit rational inverse g^{-1}; verifying all 64 first and 256 second Fréchet jets collapses all 16 Ricci and Einstein-density components algebraically to zero without ever dividing by Δ. In Part 3, the unconditional real-time D_4^* variational formula Eq. (14) equates stationarity of $\mathcal{C}_{104}$ to weak vanishing of $\mathcal{G}^{ab}$. Because g_{Kerr} is smooth and nondegenerate at x, a smooth bump-function cutoff on a small ball $U \ni x$ embedded in $[0, 1]^4$ yields a C^6 unit-periodic nondegenerate extension $\tilde{g}$ agreeing with g_{Kerr} on U; for any periodic h supported inside $U + \mathbb{Z}^4$, the integrand of Eq. (14) evaluates $\mathcal{G}^{ab}(g_{\mathrm{Kerr}})$ solely on U, where Part 2 forces it to vanish identically. □

Remark 3.2 (Scope of local D_4^* stationarity). Equation Eq. (15) establishes exact local bulk stationarity of the full 104-hinge D_4^* action across rotating horizons without constructing an asymptotically flat Gibbons–Hawking–York boundary term. Higher-order second-variation and discrete one-loop tensor-structure obstructions of the lattice action are catalogued in Section 2 and Ref.[3] and do not affect the unconditional first-variation theorem Eq. (14).

On the exact ingoing Kerr geometry of Theorem 3.1, the stationary and axial Killing symmetries, horizon thermodynamics, Komar charges[28], and ergosphere energetics[17;19] follow directly from the four-dimensional Levi–Civita connection.

Proposition 3.3 (Kerr Killing horizon, exact Komar charges, ergosphere, and Penrose energetics)**.** *Let $M > 0$ and $a^2 \le M^2$, with outer horizon $r_+ = M + \sqrt{M^2 - a^2}$ and horizon angular velocity $\Omega_H = \frac{a}{2Mr_+} = \frac{a}{r_+^2 + a^2}$.*

1. Killing horizon, area, and 4D Zeroth Law. *Every constant combination $\xi = c_v \partial_v + c_{\bar\varphi} \partial_{\bar\varphi}$ solves all* 16 *Killing equations $\nabla_\mu \xi_\nu + \nabla_\nu \xi_\mu = 0$. On $r = r_+$, $\xi_H = \partial_v + \Omega_H \partial_{\bar\varphi}$ is null ($\xi_H^\top g \xi_H = 0$), direct two-dimensional surface integration yields*

$$A_H = \int_{-1}^{1} \int_0^{2\pi} \sqrt{g_{\chi\chi} g_{\bar\varphi\bar\varphi}}\, d\bar\varphi\, d\chi = 8\pi M r_+ = 4\pi(r_+^2 + a^2), \tag{16}$$

and direct evaluation of all 64 *Christoffel symbols at $r = r_+$ ($W \neq 0$) gives $\xi_H^\nu \nabla_\nu \xi_H^\mu = \kappa_H \xi_H^\mu$ with surface gravity*

$$\kappa_H = \frac{\sqrt{M^2 - a^2}}{2Mr_+}, \tag{17}$$

strictly independent of polar latitude χ (reducing to $\kappa_H = \frac{1}{4M}$ at $a = 0$ and $\kappa_H = 0$ at $a = \pm M$).

2. Exact Komar mass and angular momentum (Boyer–Lindquist chart). *On the Boyer–Lindquist chart (t, r, θ, φ)* [15] *(distinct from the horizon-penetrating ingoing chart $(v, r, \chi, \bar\varphi)$), for every $M, a \in \mathbb{R}$ and every coordinate sphere $r > 0$ with $\Delta(r) \neq 0$ (in particular all $r > r_+$ when $M > 0$, $a^2 \le M^2$), direct evaluation of the covariant Komar surface integrals yields*

$$\begin{aligned} M_{\mathrm{Komar}}(r) &= -\frac{1}{4\pi} \int_0^{\pi} \int_0^{2\pi} \sqrt{-g}\, \nabla^t \xi^r_{(t)}\, d\varphi\, d\theta = M, \\ J_{\mathrm{Komar}}(r) &= \frac{1}{8\pi} \int_0^{\pi} \int_0^{2\pi} \sqrt{-g}\, \nabla^t \xi^r_{(\varphi)}\, d\varphi\, d\theta = Ma, \end{aligned} \tag{18}$$

and hence $J_{\mathrm{Komar}}/M_{\mathrm{Komar}} = a$.

3. Ergosphere, mandatory co-rotation, and negative-energy states. *The static limit $r_{\mathrm{erg}}(\chi) := M + \sqrt{M^2 - a^2\chi^2}$ satisfies $r_+ \le r_{\mathrm{erg}}(\chi) \le 2M$ ($r_{\mathrm{erg}}(0) = 2M$, $r_{\mathrm{erg}}(\pm 1) = r_+$), with $g_{vv} < 0$ for $r > r_{\mathrm{erg}}$, $g_{vv} = 0$ on $r = r_{\mathrm{erg}}$, and $g_{vv} > 0$ for $r_+ < r < r_{\mathrm{erg}}$. Whenever $0 < a \le M$, $\chi^2 < 1$, and $r_+ < r < r_{\mathrm{erg}}(\chi)$, every timelike stationary worldline $w = \partial_v + \Omega \partial_{\bar\varphi}$ ($w^\top g w < 0$) must co-rotate ($\Omega > 0$), and there exists an explicit future-directed timelike four-velocity U ($U^v > 0$, $U^\top g U < 0$) carrying strictly negative Killing energy $E = -(gU)_v < 0$.*

4. Christodoulou–Ruffini mass formula and extraction bound. *With angular momentum $J_{\mathrm{BH}} := Ma$ and irreducible mass $M_{\mathrm{irr}} := \sqrt{A_H/(16\pi)} = \sqrt{Mr_+/2}$, one has $M^2 = M_{\mathrm{irr}}^2 + J_{\mathrm{BH}}^2/(4M_{\mathrm{irr}}^2)$ and $M/\sqrt{2} \le M_{\mathrm{irr}} \le M$. Under the First Law and $dM - \Omega_H dJ_{\mathrm{BH}} \ge 0$ ($a^2 < M^2$), horizon area is non-decreasing ($dA_H \ge 0$); at $a = 0$ no energy can be extracted ($dM \ge 0$), while for $a > 0$ and $dM < 0$ extraction requires $dJ_{\mathrm{BH}} < 0$ and $(-dM)/(-dJ_{\mathrm{BH}}) \le \Omega_H$.*

Strong-field observables of rotating black holes—equatorial photon rings, the Bardeen–Press–Teukolsky (BPT) innermost stable circular orbit [20], and the two-dimensional shadow contour [26]—are governed by the radial geodesic potentials. To avoid colliding with the polar cosine $\chi = \cos\theta$, we write $a_* := a/M \in [-1, 1]$ for the dimensionless spin parameter in the BPT expressions below.

Theorem 3.4 (Unconditional Kerr light rings, BPT ISCOs, and exact shadow contours)**.** *Let $M > 0$ and $|a| \le M$, with orbit orientation $s \in \{+1, -1\}$ ($s = +1$ prograde, $s = -1$ retrograde).*

1. Equatorial photon spheres. *The closed-form radius*

$$r_{\mathrm{ph}} = 2M\left[1 + \cos\left(\frac{2}{3}\arccos(-s a_*)\right)\right] \tag{19}$$

solves $r(r - 3M)^2 = 4Ma^2$, satisfies $R(r_{\mathrm{ph}}) = R'(r_{\mathrm{ph}}) = 0$ for the equatorial null radial potential $R(r)$, and carries the universal spin-independent instability $R''(r_{\mathrm{ph}}) = 6E^2 r_{\mathrm{ph}}^2 > 0$. Special values: $a = 0 \Rightarrow r_{\mathrm{ph}} = 3M$ (impact parameter $b = 3\sqrt{3}M$); $a = M, s = +1 \Rightarrow r_{\mathrm{ph}}^+ = M$ ($b_+ = 2M$); $a = M, s = -1 \Rightarrow r_{\mathrm{ph}}^- = 4M$ ($b_- = -7M$).

2. Closed-form BPT ISCO and unconditional sub-extremal existence. *Setting* $Z_1(a_*) := 1 + (1 - a_*^2)^{1/3}\big[(1+a_*)^{1/3} + (1-a_*)^{1/3}\big]$ *and* $Z_2(a_*) := \sqrt{3a_*^2 + Z_1(a_*)^2}$*, the BPT radius*

$$r_{\mathrm{ISCO}} = M\left[3 + Z_2(a_*) - s\sqrt{\big(3 - Z_1(a_*)\big)\big(3 + Z_1(a_*) + 2Z_2(a_*)\big)}\right] \tag{20}$$

solves $r^2 - 6Mr + 8sa\sqrt{Mr} - 3a^2 = 0$ *and obeys* $M \le r^+_{\mathrm{ISCO}} \le 6M \le r^-_{\mathrm{ISCO}} \le 9M$*, with specific binding energies* $E_{\mathrm{ISCO}}(a=0) = \frac{2\sqrt{2}}{3}$*,* $\lim_{r\to M^+} E^+_{\mathrm{ISCO}}(a=M) = \frac{1}{\sqrt{3}}$*, and* $E^-_{\mathrm{ISCO}}(a = M, 9M) = \frac{5}{3\sqrt{3}}$*. Moreover, in the sub-extremal regime* $a^2 < M^2$ *(writing* $M = m^2 > 0$*,* $\rho = \sqrt{r}$*, and adopting the radial-equation sign convention* $\dot r^2 = V(r)$ *so that* $V'' < 0$ *characterizes radial stability of circular orbits), there exist* unconditionally *a unique light ring* $\rho_{\mathrm{ph}} \ge m$ *satisfying* $\Delta(\rho^2_{\mathrm{ph}}) = (m\rho_{\mathrm{ph}} - sa)^2 > 0$ *and a unique ISCO* $\rho_I \ge \rho_{\mathrm{ph}}$*, with the exact effective-potential trichotomy* $V'' > 0$ *for* $\rho_{\mathrm{ph}} < \rho < \rho_I$*,* $V'' = 0$ *at* $\rho = \rho_I$*, and* $V'' < 0$ *for* $\rho > \rho_I$*. (Here* $V'' < 0$ *is the effective-potential stability criterion for circular geodesics, not nonlinear dynamical stability.)*

3. Spherical photon orbits and exact Kerr shadow. *For general spin* $a \neq 0$*, constant-r spherical photon orbits have conserved impact parameters*

$$\xi(r) = \frac{r^2(3M - r) - a^2(r + M)}{a(r - M)}, \qquad \eta(r) = \frac{r^3\big(4a^2M - r(r-3M)^2\big)}{a^2(r-M)^2}, \tag{21}$$

and, normalized to unit photon energy $E = 1$*, strict radial instability* $R''(r_0) = 8r_0\big[(r_0 - M)^3 + M(M^2 - a^2)\big]/(r_0 - M)^2 > 0$*. For an asymptotic observer in the equatorial plane* ($\theta_0 = \frac{\pi}{2}$)*, Bardeen's celestial shadow coordinates are* $\alpha = -\xi$ *and* $\beta^2 = \eta$ [21]*. For* $a = 0$*, the shadow is the exact circle* $\alpha^2 + \beta^2 = 27M^2$ *(*$R_{\mathrm{sh}} = 3\sqrt{3}M$*). For extremal Kerr (*$a = M$*), the equatorial shadow is strictly D-shaped with vertical prograde edge at* $\alpha(M) = -2M$ *(*$\beta^2 = 3M^2$*), vertical maximum at* $r = 3M$ *(*$\alpha = 2M$*,* $\beta^2 = 27M^2$*), retrograde edge at* $\alpha(4M) = +7M$ *(*$\beta = 0$*), and horizontal diameter* $9M$*.*

3.2 Horizon-penetrating Kerr–Newman Einstein–Maxwell geometry, direct on-horizon surface gravity, and thermodynamic laws

Adding electric charge Q yields the rotating charged Kerr–Newman spacetime [12]. In smooth ingoing coordinates $(v, r, \chi, \bar\varphi)$ with $\varrho^2 = r^2 + a^2\chi^2$, $W = 1 - \chi^2$, $\Delta = r^2 - 2Mr + a^2 + Q^2$, and $w_Q := 2Mr - Q^2$, the metric and horizon-regular electromagnetic 4-potential are

$$\begin{aligned} ds^2 = &-\left(1 - \frac{w_Q}{\varrho^2}\right) dv^2 + 2\,dv\,dr - 2aW\,dr\,d\bar\varphi - \frac{2w_Q aW}{\varrho^2}\,dv\,d\bar\varphi \\ &+ \frac{\varrho^2}{W}\,d\chi^2 + W\left(r^2 + a^2 + \frac{w_Q a^2 W}{\varrho^2}\right) d\bar\varphi^2, \end{aligned} \tag{22}$$

$$A_\mu\,dx^\mu = -\frac{Qr}{\varrho^2}\big(dv - aW\,d\bar\varphi\big). \tag{23}$$

The metric determinant remains $\det g = -\varrho^4 < 0$, and the contravariant radial component is $g^{rr} = \Delta/\varrho^2$, which vanishes smoothly on $\Delta = 0$ with zero Δ^{-1} denominators anywhere in $g_{\mu\nu}$, $g^{\mu\nu}$, or A_μ. Consequently, both the field equations and the surface-gravity equation can be evaluated directly *on* the horizon $\Delta = 0$ without taking a punctured limit $r \to r_+^+$.

Theorem 3.5 (Horizon-penetrating Kerr–Newman Einstein–Maxwell)**.** *For all* $M, a, Q \in \mathbb{R}$ *and every point* $y = (v, r, \chi, \bar\varphi) \in \mathbb{R}^4$ *with* $\varrho^2 \neq 0$ *and* $W \neq 0$ *(spanning the exterior, outer horizon* r_+*, inner Cauchy horizon* r_-*, extremal horizon* $\Delta = 0$*, and interior), the metric Eq.* (22) *and electromagnetic potential Eq.* (23) *with* $F_{\mu\nu} = \partial_\mu A_\nu - \partial_\nu A_\mu$ *and*

$$T^{\mathrm{EM}}_{\mu\nu} = \frac{1}{4\pi}\left(F_{\mu\alpha}F_\nu{}^\alpha - \frac{1}{4}\,g_{\mu\nu}F_{\alpha\beta}F^{\alpha\beta}\right) \tag{24}$$

satisfy identically:

1. *vanishing curvature and stress traces,* $R = 0$ *and* $g^{\mu\nu}T^{\mathrm{EM}}_{\mu\nu} = 0$*;*
2. *all* 16 *nonlinear Einstein–Maxwell equations* $R_{\mu\nu} = 8\pi T^{\mathrm{EM}}_{\mu\nu}$ *and* $G_{\mu\nu} = 8\pi T^{\mathrm{EM}}_{\mu\nu}$*;*
3. *all* 4 *source-free covariant Maxwell equations* $\nabla_\mu F^{\mu\nu} = 0$*;*
4. *all* 64 *Maxwell Bianchi identities* $\partial_\lambda F_{\mu\nu} + \partial_\mu F_{\nu\lambda} + \partial_\nu F_{\lambda\mu} = 0$.

Theorem 3.6 (Direct on-horizon surface gravity, both 4D Zeroth Laws, Smarr and First Laws, and Gauss's Law)**.** *Consider the ingoing Kerr–Newman geometry Eq.* (22) *and Eq.* (23)*.*

1. Direct on-horizon surface gravity (zero punctured limit). *For every constant* $\Omega \in \mathbb{R}$, $\xi = \partial_v + \Omega\partial_{\bar\varphi}$ *is a Killing vector. At any horizon root* $\Delta(r) = 0$ *with* $\varrho^2 \neq 0$ *and* $W \neq 0$*, setting* $\Omega = \frac{a}{r^2+a^2}$ *makes* ξ *null with covector* $\xi_\mu = \frac{\varrho^2}{r^2+a^2}\,\delta^r_\mu$*, and direct evaluation of the four-dimensional connection on* $\Delta(r) = 0$ *yields* $\xi^\nu\nabla_\nu\xi^\mu = \kappa_H\,\xi^\mu$ *with*

$$\kappa_H = \frac{r - M}{r^2 + a^2}. \tag{25}$$

For $M > 0$ *and* $a^2 + Q^2 < M^2$*, the outer and inner horizons* $r_\pm = M \pm \sqrt{M^2 - a^2 - Q^2}$ *carry*

$$\kappa_+ = \frac{\sqrt{M^2 - a^2 - Q^2}}{r_+^2 + a^2} > 0 > \kappa_- = -\frac{\sqrt{M^2 - a^2 - Q^2}}{r_-^2 + a^2}, \qquad \kappa_{\mathrm{ext}} = 0 \;\; (a^2 + Q^2 = M^2). \tag{26}$$

2. Both 4D Zeroth Laws. *Across all polar latitudes* $\chi \in (-1, 1)$ *on* $r = r_+$*, both the surface gravity* $\kappa_H = \kappa_+$ *and the corotating electric potential*

$$\Phi_H := -\xi^\mu_H A_\mu = \frac{Qr_+}{r_+^2 + a^2} \tag{27}$$

are strictly independent of χ*.*

3. Smarr formula, 3-parameter First Law, and special limits. *With* $A_H = 4\pi(r_+^2 + a^2)$, $J_{\mathrm{BH}} = Ma$*, and* $\Omega_H = \frac{a}{r_+^2+a^2}$*, the Kerr–Newman family obeys the exact Smarr identity and exact three-parameter Fréchet-differentiable First Law*[22]*,*

$$M = \frac{\kappa_H}{4\pi}A_H + 2\Omega_H J_{\mathrm{BH}} + \Phi_H Q, \qquad dM = \frac{\kappa_H}{8\pi}\,dA_H + \Omega_H\,dJ_{\mathrm{BH}} + \Phi_H\,dQ. \tag{28}$$

Setting $Q = 0$ *recovers Kerr identically, and setting* $a = 0$ *recovers Reissner–Nordström identically (with photon sphere* $r_{\mathrm{ph}} = \frac{3M+\sqrt{9M^2-8Q^2}}{2} \in [2M, 3M]$ *and extremal ISCO* $r = 4M$*,* $E^2 = 27/32$*).*

4. Exact Gauss's Law electric charge (Boyer–Lindquist chart). *On the Boyer–Lindquist chart* (t, r, θ, φ) *(distinct from the ingoing chart* $(v, r, \chi, \bar\varphi)$*), for every coordinate sphere* $r > 0$ *with* $\Delta(r) \neq 0$ *(in particular every* $r > r_+$*), direct covariant surface integration gives*

$$Q_{\mathrm{Gauss}}(r) = \frac{1}{4\pi}\int_0^\pi\int_0^{2\pi} \sqrt{-g}\,F^{tr}\,d\varphi\,d\theta = Q. \tag{29}$$

Remark 3.7 (Scope note on finite-r Kerr–Newman Komar integrals). While Eq. (18) evaluates the exact vacuum Kerr Komar charges (M, Ma) on every finite sphere $r > r_+$ and Eq. (29) evaluates the exact Kerr–Newman Gauss charge Q, finite-r Kerr–Newman Komar integrals—which receive an additional electromagnetic bulk-stress volume contribution—are not separately formalized in this theorem block.

3.3 256-component Weyl tensor, Petrov Type D, and exact 8-index Kretschmann scalar

Because the Kerr–Newman Ricci tensor is nonzero ($R_{\mu\nu} = 8\pi T^{\mathrm{EM}}_{\mu\nu}$), verifying its algebraic Petrov classification[27] and exact Kretschmann invariant[29] directly from the metric requires constructing all 256 Riemann components, subtracting the Ricci trace part to assemble all 256 Weyl components $C_{\mu\nu\rho\sigma}$,

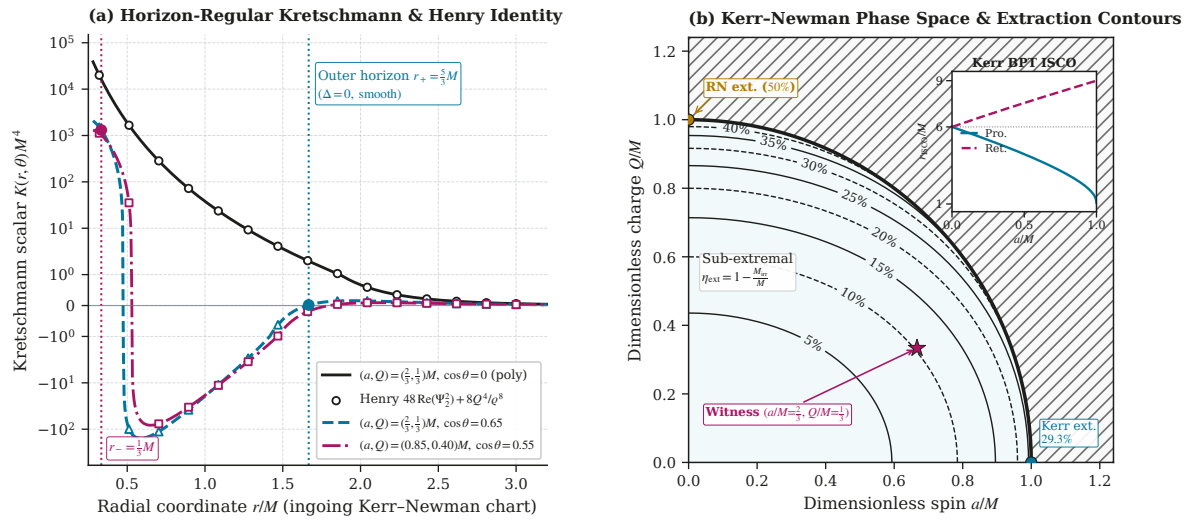

Fig. 1 Exact Kerr–Newman curvature and phase-space structure (Theorems 3.4, 3.8 and 3.10). **(a)** Horizon-regular 8-index Kretschmann scalar $K_{\mathrm{KN}}(r,\theta)M^4$ across outer ($r_+ = \frac{5}{3}M$) and inner ($r_- = \frac{1}{3}M$) horizons for $(a,Q) = (\frac{2}{3}, \frac{1}{3})M$ and $(0.85, 0.40)M$, matching Henry's algebraic identity $48\,\mathrm{Re}(\Psi_2^2) + 8Q^4/\varrho^8$ point-by-point. **(b)** Sub-extremal $(a/M, Q/M)$ phase space showing Christodoulou–Ruffini extractable-energy contours $\eta_{\mathrm{ext}} = 1 - M_{\mathrm{irr}}/M$, the explicit witness $(\frac{2}{3}, \frac{1}{3})M$, and inset prograde/retrograde Kerr BPT ISCO radii.

contracting against a horizon-regular null tetrad, and evaluating the literal 8-index contraction $K_{\mathrm{KN}} = R_{\mu\nu\rho\sigma}R^{\mu\nu\rho\sigma}$.

In the ingoing chart Eq. (22), we adopt the horizon-regular boosted Kinnersley null tetrad

$$\begin{aligned} L &= \big(2(r^2+a^2),\ \Delta,\ 0,\ 2a\big), \qquad N = \left(0,\ -\frac{1}{2\varrho^2},\ 0,\ 0\right), \\ m &= \frac{\sqrt{W}}{\sqrt{2}}(\mu_R + i\mu_I), \quad \mu_R = \frac{1}{\varrho^2}\left(a^2\chi,\ 0,\ -r,\ \frac{a\chi}{W}\right), \quad \mu_I = \frac{1}{\varrho^2}\left(ar,\ 0,\ a\chi,\ \frac{r}{W}\right), \end{aligned} \tag{30}$$

which remains finite and nondegenerate directly on both horizons $\Delta = 0$ ($\varrho^2 \neq 0$, $W > 0$) and satisfies $L \cdot N = -1$, $m \cdot \bar{m} = 1$, with all other inner products vanishing.

Theorem 3.8 (256-component Weyl tensor, Petrov Type D, and exact 8-index Kretschmann scalar)**.** *For all $M, a, Q \in \mathbb{R}$ and every point $y = (v, r, \chi, \bar{\varphi}) \in \mathbb{R}^4$ with $\varrho^2 \neq 0$ and $W > 0$ (across both horizons $\Delta = 0$), let $C_{\mu\nu\rho\sigma}$ be the full 256-component Weyl tensor obtained from the Fréchet Riemann tensor of Eq. (22) by subtracting the non-vanishing Einstein–Maxwell Ricci tensor $R_{\mu\nu} = 8\pi T^{\mathrm{EM}}_{\mu\nu}$, and write $A := a^2\chi^2$.*

1. Newman–Penrose Weyl scalars and exact Petrov Type D locus. *Contracted on the horizon-regular null tetrad Eq. (30), the five complex Weyl scalars are*

$$\Psi_0 = \Psi_1 = \Psi_3 = \Psi_4 = 0, \qquad \Psi_2 = -\frac{M - \dfrac{Q^2}{r + ia\chi}}{(r - ia\chi)^3}. \tag{31}$$

Moreover, Ψ_2 vanishes if and only if

$$\Psi_2 = 0 \iff Mr - Q^2 = 0 \ \wedge\ Ma\chi = 0. \tag{32}$$

Consequently, Kerr–Newman is strictly Petrov Type D at every point with $Mr - Q^2 \neq 0$ or $Ma\chi \neq 0$ (in particular every $r > M$ whenever $M > 0$ and $a^2 + Q^2 \leq M^2$), while at the equatorial circle $r = Q^2/M$, $\chi = 0$ ($M, Q \neq 0$) all five Weyl scalars vanish simultaneously. (Full Type O tensor reconstruction $C_{\mu\nu\rho\sigma} = 0$ at that single equatorial circle is not separately formalized.)

2. Exact 8-index Kretschmann scalar. *The literal 8-index contraction* $K_{\mathrm{KN}} = R_{\mu\nu\rho\sigma}R^{\mu\nu\rho\sigma}$ *equals*

$$K_{\mathrm{KN}} = \frac{8}{\varrho^{12}}\Big[6M^2\big(r^6 - 15r^4A + 15r^2A^2 - A^3\big) - 12MQ^2r\big(r^4 - 10r^2A + 5A^2\big) + Q^4\big(7r^4 - 34r^2A + 7A^2\big)\Big]. \tag{33}$$

At $Q = 0$*, Eq.* (33) *reduces identically to the vacuum Kerr Kretschmann scalar, which satisfies the directly proved identity*

$$K_{\mathrm{Kerr}} = 48\,\mathrm{Re}\big(\Psi_2^2\big) = \frac{48M^2(r^2 - a^2\chi^2)(\varrho^4 - 16r^2a^2\chi^2)}{\varrho^{12}}. \tag{34}$$

On the equatorial plane ($a\chi = 0$)*, Eq.* (33) *collapses to*

$$K_{\mathrm{KN}}\big|_{a\chi=0} = \frac{8\big[6(Mr - Q^2)^2 + Q^4\big]}{r^8}, \tag{35}$$

which is strictly positive for all $(M, Q) \neq (0, 0)$ *and diverges unboundedly as* $r \to 0^+$.

Remark 3.9 (Algebraic relation to Henry (2000)). Comparing the two independently proved closed forms Eq. (31) and Eq. (33) exhibits the exact algebraic identity $K_{\mathrm{KN}} = 48\,\mathrm{Re}(\Psi_2^2) + 8Q^4/\varrho^8$, reproducing Henry's curvature decomposition[29]. In our formal theorem ledger, $K_{\mathrm{Kerr}} = 48\,\mathrm{Re}(\Psi_2^2)$ (Eq. (34)) is proved directly as a named Kerr theorem, while Eq. (31) and Eq. (33) are each proved independently from the 256-component Kerr–Newman Riemann and Weyl tensors. Notice from Eq. (35) that even at the equatorial point $r = Q^2/M$ where $\Psi_2 = 0$, the electromagnetic Ricci contribution keeps $K_{\mathrm{KN}} = 8M^8/Q^{12} > 0$ strictly positive (Fig. 1).

3.4 Kerr–Newman Penrose extraction, charged-scalar superradiance, and 4D Kerr Teukolsky separation

The smooth ingoing Kerr–Newman chart also governs classical energy extraction by charged particles, superradiant scattering of charged scalar fields, and the Teukolsky master perturbation equation[23;24].

Theorem 3.10 (Kerr–Newman Penrose extraction bound and Christodoulou–Ruffini mass formula)**.** *Let* $M > 0$ *and* $a^2 + Q^2 \le M^2$*, with outer horizon* $r_+ = M + \sqrt{M^2 - a^2 - Q^2}$*,* $\Omega_H = \frac{a}{r_+^2 + a^2}$*, and* $\Phi_H = \frac{Qr_+}{r_+^2 + a^2}$.

1. Horizon extraction identity and causal bound. *At any root* $\Delta(r) = 0$ *with* $\varrho^2 \neq 0$*, for any kinetic four-momentum* p^μ *and electric charge* q *with Killing energy* $E := -(p_v + qA_v)$ *and axial angular momentum* $L := p_{\bar\varphi} + qA_{\bar\varphi}$*,*

$$E - \Omega L - \Phi q = -\frac{\varrho^2}{r^2 + a^2}\,p^r. \tag{36}$$

Time-orienting the horizon by $T := \partial_v - \partial_r + \Omega_H\partial_{\bar\varphi}$ *(which is strictly timelike,* $g(T,T) = -\frac{2\varrho^2}{r_+^2 + a^2} < 0$*), every future-directed causal momentum* ($g(p,p) \le 0$*,* $g(p,T) < 0$) *at* $r = r_+$ ($W > 0$) *satisfies* $p^r \le 0$ *and*

$$E \ge \Omega_H L + \Phi_H q, \tag{37}$$

with equality if and only if p *is aligned with the null horizon generator* ($p^r = 0$*,* $p^\chi = 0$*, and* $(r_+^2 + a^2)p^{\bar\varphi} = ap^v$*).*

2. Irreducible mass and monotonicity. *Defining* $J_{\mathrm{BH}} := Ma$ *and* $M_{\mathrm{irr}} := \frac{1}{2}\sqrt{r_+^2 + a^2}$ ($A_H = 16\pi M_{\mathrm{irr}}^2$)*, the black-hole parameters obey the Christodoulou–Ruffini identity*[19]

$$M^2 = \left(M_{\mathrm{irr}} + \frac{Q^2}{4M_{\mathrm{irr}}}\right)^2 + \frac{J_{\mathrm{BH}}^2}{4M_{\mathrm{irr}}^2}, \qquad \frac{M}{2} \le M_{\mathrm{irr}} \le M \quad \Big(\frac{M}{\sqrt{2}} \le M_{\mathrm{irr}} \text{ when } Q = 0\Big). \tag{38}$$

Along any differentiable family $(M(s), a(s), Q(s))$ of non-extremal Kerr–Newman holes satisfying $M' \geq \Omega_H J'_{\mathrm{BH}} + \Phi_H Q'$, both horizon area and irreducible mass are non-decreasing: $A'_H \geq 0$ and $M'_{\mathrm{irr}} = A'_H/(32\pi M_{\mathrm{irr}}) \geq 0$.

3. Explicit witness. *For $M = \frac{3}{2}$, $a = 1$, $Q = \frac{1}{2}$, one has $r_+ = \frac{5}{2}$, $\Omega_H = \frac{4}{29}$, and $\Phi_H = \frac{5}{29}$; evaluating the explicit future-directed horizon momentum $p = T = \partial_v - \partial_r + \Omega_H \partial_{\bar{\varphi}}$ at the equator $\chi = 0$ yields $E - \Omega_H L - \Phi_H q = \frac{25}{29} > 0$.*

Remark 3.11 (Scope of test-particle absorption). In Theorem 3.10, identifying the black-hole parameter changes $(\Delta M, \Delta J_{\mathrm{BH}}, \Delta Q)$ with test-particle (E, L, q) enters as an explicit hypothesis of the monotonicity statement; nonlinear gravitational-electromagnetic back-reaction and the dynamical Hawking area theorem are not formalized here.

Theorem 3.12 (Charged-scalar superradiance at the Kerr–Newman horizon and radial Wronskian)**.** *Consider a complex scalar mode $\psi(v, r, \chi, \bar{\varphi}) = e^{-i\omega v + im\bar{\varphi}} S(\chi) R(r)$ of charge q and mass μ on the ingoing Kerr–Newman background Eq. (22) and Eq. (23), with gauge-covariant derivative $D_\mu \psi := \partial_\mu \psi - iqA_\mu \psi$, stress-energy tensor*

$$T_{\mu\nu} := \frac{1}{2}\big[(D_\mu\psi)^* D_\nu\psi + (D_\nu\psi)^* D_\mu\psi\big] - \frac{1}{2} g_{\mu\nu}\big(g^{\alpha\beta}(D_\alpha\psi)^* D_\beta\psi + \mu^2|\psi|^2\big), \tag{39}$$

particle-number current $j^\mu := g^{\mu\nu}\,\mathrm{Im}(\bar{\psi} D_\nu \psi)$, and canonical energy current $J^\mu_E := -(g^{\mu\alpha} T_{\alpha v} + qA_v j^\mu)$ (cf. [25;72]).

1. Exact energy-to-number flux ratio. *At every regular point ($\varrho^2 \neq 0$, $W \neq 0$), $J^r_E = \omega j^r$.*
2. Horizon superradiance equivalence. *Directly on the outer horizon $r = r_+$ ($\Delta = 0$, $W \neq 0$), the inward energy flux into the black hole is*

$$-J^r_E = \frac{r_+^2 + a^2}{\varrho^2}\,\omega\,\big(\omega - m\Omega_H - q\Phi_H\big)\,|\psi|^2. \tag{40}$$

For every non-vanishing mode ($\psi \neq 0$) with $\omega > 0$, net energy is extracted from the black hole ($-J^r_E < 0$) if and only if

$$\omega < m\Omega_H + q\Phi_H, \tag{41}$$

with zero flux if and only if $\omega = m\Omega_H + q\Phi_H$.

3. Explicit witness. *At $M = \frac{3}{2}$, $a = 1$, $Q = \frac{1}{2}$, $m = 2$, $q = 1$, $S = R = 1$, evaluated at $(v, r, \chi, \bar{\varphi}) = (0, \frac{5}{2}, 0, 0)$, the superradiant threshold is $m\Omega_H + q\Phi_H = \frac{13}{29}$: choosing $\omega = \frac{1}{29}$ gives $-J^r_E = -\frac{12}{725} < 0$ (superradiant extraction), while $\omega = 1$ gives $-J^r_E = +\frac{16}{25} > 0$ (absorption).*
4. Radial Wronskian conservation. *For real parameters $\omega, m, q, Q, \lambda, \mu \in \mathbb{R}$, every solution $R(r)$ of the charged radial wave equation $(\Delta R')' + \big(\frac{K^2}{\Delta} - \lambda - \mu^2 r^2\big)R = 0$ with $K(r) = (r^2 + a^2)\omega - am - qQr$ obeys exact Sturm–Liouville Wronskian conservation, $\frac{d}{dr}\big[\Delta\,\mathrm{Im}(\bar{R}R')\big] = 0$.*

Remark 3.13 (Scope of local superradiance flux). Theorem 3.12 establishes the exact local horizon energy flux, the sharp iff condition Eq. (41), and radial Wronskian conservation; global covariant conservation $\nabla_\mu J^\mu_E = 0$ and asymptotic reflection-coefficient matching at $\mathscr{I}^\pm$ are outside its scope.

Finally, we turn to spin-s perturbations on rotating Kerr spacetime governed by the Teukolsky master operator $\mathcal{T}_{M,a,s}$ [23]. For $s = 0$, $\mathcal{T}_{M,a,0}$ is derived directly from the four-dimensional Boyer–Lindquist Kerr d'Alembertian $\Box_g$ via coordinate Fréchet derivatives; for $s \neq 0$, $\mathcal{T}_{M,a,s}$ is Teukolsky's master PDE (Eq. (4.7) of Ref. [23]), whose derivation from the Maxwell and Newman–Penrose Bianchi identities is explicitly noted as outside the scope of the theorem below.

Theorem 3.14 (4D Kerr Teukolsky separation, five static solutions, and horizon Frobenius exponents)**.** *Let $M, a \in \mathbb{R}$ with $\Delta = r^2 - 2Mr + a^2$ and $\varrho^2 = r^2 + a^2\cos^2\theta$.*

1. Direct $s = 0$ d'Alembertian derivation. *At every point with $\varrho^2 \neq 0$, $\Delta \neq 0$, and $\sin\theta \neq 0$, the Boyer–Lindquist Kerr scalar wave operator satisfies identically $\varrho^2\,\Box_g\psi = -\mathcal{T}_{M,a,0}[\psi]$.*
2. Exact master PDE separation. *For all $s, \omega, m \in \mathbb{R}$, $A \in \mathbb{C}$, C^2 functions $S, R : \mathbb{R} \to \mathbb{C}$, $\Delta \neq 0$, and $\sin\theta \neq 0$,*

$$\mathcal{T}_{M,a,s}\big[e^{i(-\omega t + m\varphi)} S(\theta) R(r)\big] = -e^{i(-\omega t + m\varphi)}\Big(S(\theta)\,\mathcal{R}[R](r) + R(r)\,\mathcal{S}[S](\theta)\Big), \tag{42}$$

where $K(r) := (r^2+a^2)\omega - am$, $\lambda := A + a^2\omega^2 - 2am\omega$, *and*

$$\mathcal{R}[R](r) = \Delta R'' + (s+1)(2r-2M)R' + \left(\frac{K^2 - 2is(r-M)K}{\Delta} + 4is\omega r - \lambda\right) R, \tag{43}$$

$$\mathcal{S}[S](\theta) = S'' + \cot\theta\, S' + \left(a^2\omega^2\cos^2\theta - \frac{m^2}{\sin^2\theta} - 2a\omega s\cos\theta - \frac{2ms\cos\theta}{\sin^2\theta} - s^2\cot^2\theta + s + A\right) S. \tag{44}$$

3. Five explicit nonzero static ($\omega = m = 0$) solutions. *The master PDE* $\mathcal{T}_{M,a,s}[\psi] = 0$ *admits exact closed-form static solutions across all five physical spin weights:*
   - $s = 0$*:* $\psi = (r-M)\cos\theta$ *(*$A = 2$*, also solving* $\Box_g\psi = 0$ *identically);*
   - $s = +1$*:* $\psi = \sin\theta$ *(*$A = 0$*);* $\quad s = -1$*:* $\psi = \Delta\sin\theta$ *(*$A = 2$*);*
   - $s = +2$*:* $\psi = \sin^2\theta$ *(*$A = 0$*);* $\quad s = -2$*:* $\psi = \Delta^2\sin^2\theta$ *(*$A = 4$*).*
4. Exact horizon Frobenius indicial limit. *For every sub-extremal Kerr black hole (*$M > 0$, $a^2 < M^2$*) and every complex exponent* $\alpha \in \mathbb{C}$*,*

$$\lim_{r\to r_+^+} \frac{\mathcal{R}\big[(r-r_+)^\alpha\big](r)}{(r-r_+)^{\alpha-1}} = (r_+ - r_-)\big(\alpha - i\beta\big)\big(\alpha + s + i\beta\big), \qquad \beta := \frac{\omega - m\Omega_H}{2\kappa_H}. \tag{45}$$

Hence the exact horizon Frobenius exponents are $\alpha = i\beta$ *and* $\alpha = -s - i\beta$*.*

4 Four-dimensional ADM geometry, Penrose rigidity, and asymptotic BMS$_4$ memory

Stationary black holes test Einstein's equations on isolated equilibrium geometries; dynamical gravity is governed by the $(3+1)$ initial-value formulation[31–33] on spatial hypersurfaces Σ and by asymptotic radiation balance at future null infinity $\mathscr{I}^+$[39–41;44]. In this section we establish the nonlinear ADM constraint and evolution algebra, exact multi-black-hole initial data and global mass brackets, the Schwarzschild reciprocal-cost throat and Riemannian Penrose rigidity, exact anisotropic vacuum curvature blow-up alongside bounce cosmology, and the asymptotic BMS$_4$ memory, superrotation, and soft-graviton identities. We keep $G = 1$ in the geometric constraint theorems of Sections 4.1 and 4.2 (restoring G explicitly in the cosmology and asymptotic BMS$_4$ balance formulas where mass and flux dimensions appear directly).

4.1 Exact 4D ADM $3+1$ decomposition, unique $D = 3$ Yamabe exponent, and multi-black-hole initial data

Splitting a four-dimensional Lorentzian metric $g_{\mu\nu}$ into lapse N, shift vector β^i, and spatial 3-metric γ_{ij} on a spatial slice Σ yields exact algebraic and elliptic constraint structures whose conformal exponent is uniquely selected by three spatial dimensions.

Theorem 4.1 (4D ADM $3+1$ algebra, unique $D = 3$ Yamabe exponent $p = 4$, and Lichnerowicz–York constraints)**.** *Let* $(N, \beta^i, \gamma_{ij})$ *be smooth ADM variables on a spatial slice* Σ *with* $N > 0$ *and symmetric positive-definite* γ_{ij}*.*

1. Exact $3+1$ LDU factorization, determinant, and projector. *The four-dimensional ADM metric admits the exact block LDU factorization* $g = S_\beta^\top \operatorname{diag}(-N^2, \gamma)\, S_\beta$*, obeys* $g \cdot g^{-1} = g^{-1} \cdot g = I_4$*, has determinant* $\det g = -N^2 \det\gamma$ *and volume element* $\sqrt{|\det g|} = N\sqrt{\det\gamma}$*, and defines the unit timelike normal* $n^\mu = (1/N, -\beta^i/N)$ *(*$g_{\mu\nu}n^\mu n^\nu = -1$*) together with the idempotent, normal-orthogonal spatial projector* $h^\mu_\nu = \delta^\mu_\nu + n^\mu n_\nu$*.*
2. Unique $D = 3$ Yamabe exponent $p = 4$. *For any positive* C^2 *conformal factor* $\psi > 0$ *and exponent* $p \in \mathbb{R}$*, the spatial Ricci scalar of the conformally flat 3-metric* $\gamma_{ij} = \psi^p\delta_{ij}$ *is*

$$R^{(3)}\big[\psi^p\delta\big] = \psi^{-p}\left(-\frac{2p\,\Delta\psi}{\psi} + \frac{p(4-p)}{2}\,\frac{|\nabla\psi|^2}{\psi^2}\right). \tag{46}$$

The nonlinear gradient-squared term vanishes identically for nonzero p if and only if $p = 4$, leaving the linear Laplacian identity

$$R^{(3)}\left[\psi^4\delta\right] = -8\,\psi^{-5}\Delta\psi. \tag{47}$$

3. Exact Lichnerowicz–York Hamiltonian and momentum constraints. *Setting $\gamma_{ij} = \psi^4\delta_{ij}$ and decomposing the extrinsic curvature as $K_{ij} = \psi^{-2}\hat{A}_{ij} + \frac{1}{3}\tau\psi^4\delta_{ij}$ with $\operatorname{tr}\hat{A} = 0$ yields $\operatorname{tr}K = \tau$, $K_{ij}K^{ij} = \psi^{-12}|\hat{A}|^2 + \frac{1}{3}\tau^2$, the exact Hamiltonian constraint equivalence*

$$R^{(3)} + K^2 - K_{ij}K^{ij} = 16\pi\rho \iff 8\Delta\psi + \psi^5\left(16\pi\rho - \frac{2}{3}\tau^2\right) + \psi^{-7}|\hat{A}|^2 = 0, \tag{48}$$

and the exact curved conformal momentum constraint

$$D_j\left(K^{ij} - \gamma^{ij}K\right) = \psi^{-10}\,\partial_j\hat{A}_{ij} - \frac{2}{3}\psi^{-4}\,\partial_i\tau. \tag{49}$$

The elliptic structure of Eq. (48) and Eq. (49) admits exact n-body time-symmetric Brill–Lindquist initial data[34], exact spinning Bowen–York extrinsic-curvature solutions[35], and global two-sided analytic barriers trapping the ADM mass of a spinning puncture.

Theorem 4.2 (n-body Brill–Lindquist data, spinning Bowen–York data, and global ADM mass bracket)**.**

1. n-body Brill–Lindquist initial data. *For any n punctures $x_1, \dots, x_n \in \mathbb{R}^3$ and bare masses $m_1, \dots, m_n \geq 0$, the conformal factor $\psi_{\mathrm{BL}}(x) := 1 + \sum_{a=1}^{n} \frac{m_a}{2|x-x_a|}$ satisfies $\psi_{\mathrm{BL}} > 0$, $\Delta\psi_{\mathrm{BL}} = 0$, and $R^{(3)} = 0$ on $\mathbb{R}^3 \setminus \{x_1, \dots, x_n\}$, with exact ADM surface-flux limit $M_{\mathrm{ADM}} = \sum_{a=1}^{n} m_a$.*
2. Spinning Bowen–York momentum solution. *For any spin vector $S \in \mathbb{R}^3$ and $x \in \mathbb{R}^3 \setminus \{0\}$, the tensor*

$$\hat{A}_{ij}(x) := \frac{3}{|x|^5}\left[(x \times S)_i x_j + (x \times S)_j x_i\right] \tag{50}$$

is symmetric, traceless, and divergence-free ($\partial_j\hat{A}_{ij} = 0$), solving the curved 3-dimensional maximal ($\tau = 0$) momentum constraint Eq. (49) identically for every conformal factor $\psi > 0$, with nonnegative Hamiltonian source

$$|\hat{A}(x)|^2 = \frac{18}{|x|^8}\left(|x|^2|S|^2 - (x \cdot S)^2\right) \geq 0. \tag{51}$$

3. Maximum-principle comparison and global Bowen–York mass bracket. *On any bounded open domain $U \subset \mathbb{R}^3$ with conformal background scalar curvature $\bar{R} \geq 0$ ($\bar{R} = 0$ for the flat background $\bar{\gamma} = \delta$) and $\frac{2}{3}\tau^2 - 16\pi\rho \geq 0$, the three-dimensional elliptic maximum principle enforces sub-/supersolution comparison and uniqueness for the Lichnerowicz equation $8\Delta\psi - \bar{R}\psi + |\hat{A}|^2\psi^{-7} - (\frac{2}{3}\tau^2 - 16\pi\rho)\psi^5 = 0$. On $\mathbb{R}^3 \setminus \{0\}$ with bare mass $m > 0$ and spin $S \in \mathbb{R}^3$, for every regular Bowen–York solution of the form $\psi(x) = 1 + \frac{m}{2r} + u(x)$ ($r = |x|$) with u bounded as $r \to 0^+$ and $u(x) \to 0$ as $r \to \infty$, the explicit global analytic barriers*

$$\psi_{\mathrm{sub}}(x) = 1 + \frac{m}{2r}, \qquad \psi_{\mathrm{sup}}(x) = 1 + \frac{m}{2r} + \frac{6|S|^2}{m^3}\left(r^2 + \frac{m^2}{4}\right)^{-1/2} \quad (r = |x|) \tag{52}$$

bracket $\psi_{\mathrm{sub}} \leq \psi \leq \psi_{\mathrm{sup}}$ globally and trap its ADM mass in the exact two-sided interval

$$m \leq M_{\mathrm{ADM}} \leq m + \frac{12|S|^2}{m^3}. \tag{53}$$

4.2 Schwarzschild J-cost throat, Penrose rigidity, ADM evolution, Kasner singularity, and bounce cosmology

The canonical reciprocal cost $J(x) = \frac{1}{2}(x + x^{-1}) - 1$ appears directly in the classical geometry of the Einstein–Rosen bridge, linking the Schwarzschild throat area and inversion symmetry to the Riemannian Penrose inequality[36–38]. To avoid collision with the polar cosine $\chi = \cos\theta$, we denote the Euler characteristic of a closed 2-surface in the inverse mean curvature flow (IMCF) by χ_{E}.

Theorem 4.3 (Schwarzschild J-cost throat, inversion isometry, and spherical & IMCF Penrose rigidity)**.**

1. Schwarzschild J-cost throat and inversion isometry. *On the time-symmetric isotropic Schwarzschild slice $\gamma = \left(1 + \frac{M}{2r}\right)^4 \delta$ ($M > 0$, $r = |x| > 0$), the coordinate-sphere area is an exact function of the canonical reciprocal cost:*

$$A(r) = 4\pi r^2 \left(1 + \frac{M}{2r}\right)^4 = 16\pi M^2 \left(1 + \frac{1}{2} J\left(\frac{2r}{M}\right)\right)^2 . \tag{54}$$

   It attains its unique minimal surface at $r = M/2$ with $A_{\min} = 16\pi M^2$ ($M = \sqrt{A_{\min}/(16\pi)}$). The spatial inversion $\Phi(x) := \frac{M^2}{4|x|^2} x$ is an exact three-dimensional metric isometry, $J_\Phi^\top \gamma(\Phi(x)) J_\Phi = \gamma(x)$, directly realizing the reciprocal symmetry $J(x) = J(1/x)$.
2. Spherically symmetric Riemannian Penrose inequality and rigidity. *For any spherically symmetric metric $\gamma = \left(1 - \frac{2m(r)}{r}\right)^{-1} dr^2 + r^2 d\Omega^2$, the scalar curvature is $R^{(3)} = 4m'(r)/r^2$. If $r_H > 0$ satisfies $2m(r_H) = r_H$, $2m(r) < r$ and $R^{(3)} \geq 0$ for all $r > r_H$, and $\lim_{r\to\infty} m(r) = M_{\mathrm{ADM}}$, then*

$$M_{\mathrm{ADM}} \geq \sqrt{\frac{A_{\min}}{16\pi}}, \qquad A_{\min} = 4\pi r_H^2, \tag{55}$$

   with equality if and only if $m(r) = M_{\mathrm{ADM}}$ *and $m'(r) = 0$ for all $r \geq r_H$ (exact Schwarzschild rigidity). For two-body Brill–Lindquist data ($m_1, m_2 > 0$, puncture separation $d > 2(m_1 + m_2)$), letting $A_{1,\mathrm{up}}, A_{2,\mathrm{up}}$ denote the analytic coordinate-sphere upper bounds on the minimal apparent-horizon neck areas surrounding punctures x_1 and x_2, the inequality is strictly satisfied: $\sqrt{(A_{1,\mathrm{up}} + A_{2,\mathrm{up}})/(16\pi)} < m_1 + m_2 = M_{\mathrm{ADM}}$.*
3. Non-spherical IMCF Hawking-mass monotonicity and rigidity. *Along any smooth inverse mean curvature flow[36;37] whose area $A(t) > 0$ and Willmore energy $W(t)$ satisfy $A' = A$ and $W' = 4\pi\chi_{\mathrm{E}} - \frac{1}{2}W - Q$ with $\chi_{\mathrm{E}} \leq 2$ and $Q(t) \geq 0$, the Hawking mass $m_H(t) := \sqrt{\frac{A}{16\pi}}\left(1 - \frac{W}{16\pi}\right)$ obeys*

$$\frac{dm_H}{dt} = \frac{\sqrt{A/(16\pi)}}{16\pi}\left(8\pi - 4\pi\chi_{\mathrm{E}} + Q\right) \geq 0. \tag{56}$$

   Whenever $W(0) = 0$ and $\lim_{t\to\infty} m_H(t) = M_{\mathrm{ADM}}$, this yields $M_{\mathrm{ADM}} \geq \sqrt{A(0)/(16\pi)}$, with equality forcing leaf-wise rigidity $8\pi - 4\pi\chi_{\mathrm{E}} + Q(t) = 0$. (General weak-IMCF existence on non-spherical 3-manifolds is outside the scope of this theorem.)

Turning from constraints on a single slice to four-dimensional evolution, direct coordinate Fréchet differentiation establishes the contracted Bianchi identity, symmetric-hyperbolic constraint propagation, and all seven inhomogeneous Gauss–Codazzi–Mainardi and ADM evolution equations.

Theorem 4.4 (4D contracted Bianchi, symmetric-hyperbolic constraint propagation, and the 7 inhomogeneous ADM evolution equations)**.**

1. 4D Bianchi identities and contracted conservation. *For every C^3 symmetric nondegenerate four-dimensional metric g (C^2 inverse), the Fréchet Riemann tensor satisfies the first and second Bianchi identities and exact contracted conservation $\nabla_\mu G^{\mu\nu} = 0$.*
2. Symmetric-hyperbolic ADM constraint propagation. *Let $\mathcal{H} := 2G_{\mu\nu}n^\mu n^\nu$ and $\mathcal{M}_i := -G_{\mu i}n^\mu$ denote the vacuum Hamiltonian and momentum constraint residuals, and $E_{ij} := G_{ij}$ the spatial Einstein defect. The spatial Ricci evolution vanishes if and only if $E_{ij} = \frac{1}{2}\gamma_{ij}\mathcal{H}$ (with coefficient $\frac{1}{2(D-2)} = \frac{1}{2}$ unique to $D = 3$). The resulting constraint-propagation PDE system for $(\mathcal{H}, \mathcal{M}_i)$*

has explicit background-only coefficients, exact Friedrichs symmetrizer $P = \operatorname{diag}\left(\frac{1}{2}, 2\gamma\right)$*, exact lightcone characteristic speeds* $-\beta\cdot\xi \pm N\sqrt{\gamma^{ij}\xi_i\xi_j}$ *together with transverse speeds* $-\beta\cdot\xi$*, exact pointwise causal energy-flux bound* $|F\cdot\nu| \le (N + |\beta\cdot\nu|)e$ *(where* $e := \frac{1}{2}\mathcal{H}^2 + 2\gamma^{ij}\mathcal{M}_i\mathcal{M}_j$ *is the symmetrized constraint energy density and* F *its spatial energy-flux vector), and Grönwall preservation* $E(0) = 0 \implies E(t) = 0$ *for the integrated constraint energy* $E(t) := \int_\Sigma e\sqrt{\det\gamma}\, d^3x$*.*

3. Seven inhomogeneous 4D Gauss–Codazzi–Mainardi and ADM evolution equations. *For any zero-shift* C^2 *ADM metric* $g = \operatorname{diag}(-N^2, \gamma)$ *(*$N \neq 0$*,* γ *symmetric invertible) with* $K_{ij} = -\frac{1}{2N}\partial_0\gamma_{ij}$*, direct four-dimensional differentiation proves identically:*

$$R^{l\,(4)}_{\ ijk} = R^{l\,(3)}_{\ ijk} + K^l_j K_{ki} - K^l_k K_{ji} \qquad \textit{(Gauss)}, \tag{57}$$

$$R^{0\,(4)}_{\ ijk} = -\frac{1}{N}\left(D_j K_{ki} - D_k K_{ji}\right) \qquad \textit{(Codazzi–Mainardi)}, \tag{58}$$

$$-\frac{1}{N}G_{0i} = D_k K^k_i - \partial_i K \qquad \textit{(Momentum constraint)}, \tag{59}$$

$$\partial_0 K_{ij} = -D_i D_j N + N\left(R^{(3)}_{ij} + K K_{ij} - 2K_{im}K^m_j - R^{(4)}_{ij}\right) \qquad \textit{(ADM evolution)}, \tag{60}$$

$$R^{(4)}_{00} = N\partial_0 K + N\Delta_\gamma N - N^2 K_{ij}K^{ij} \qquad \textit{(Raychaudhuri trace)}, \tag{61}$$

$$R^{(4)} = R^{(3)} + K^2 + K_{ij}K^{ij} - \frac{2}{N}\partial_0 K - \frac{2}{N}\Delta_\gamma N \qquad \textit{(4D Ricci scalar)}, \tag{62}$$

$$2G_{\mu\nu}n^\mu n^\nu = R^{(3)} + K^2 - K_{ij}K^{ij} \qquad \textit{(Gauss–Hamiltonian)}. \tag{63}$$

(For general non-zero shift β^i*, the shifted extrinsic-curvature and metric-evolution relation* $\partial_0\gamma_{ij} = -2NK_{ij} + D_i\beta_j + D_j\beta_i$ *is likewise established directly.)*

The ADM equations Eqs. (57) to (63) sharpen the contrast between classical anisotropic vacuum singularities and regular bounce cosmology: classical vacuum evolution admits genuine curvature blow-up in the exact Kasner family, whereas introducing the capacity density ceiling $\rho_c = \frac{3}{8\pi G\ell^2}$ resolves homogeneous bounces globally and yields exact perturbation and non-Gaussianity benchmarks.

Proposition 4.5 (Exact non-flat Kasner singularity, Bianchi-I holonomy shear cap, Bardeen invariants, and bounce $f_{\mathrm{NL}}^{\mathrm{loc}}$)**.**

1. Exact non-flat Kasner vacuum witness. *For* $N = 1$ *and* $\gamma = \operatorname{diag}(t^{2p_1}, t^{2p_2}, t^{2p_3})$ *(*$t > 0$*) with* 1*-based Kasner exponents* $\sum_{i=1}^3 p_i = \sum_{i=1}^3 p_i^2 = 1$*:* $\det g = -t^2$*,* $K = -1/t$*,* $K_{ij}K^{ij} = 1/t^2$*, shear* $K_{ij}K^{ij} - \frac{1}{3}K^2 = \frac{2}{3t^2}$*, all* 16 *components of* $R_{\mu\nu}$ *and* $G_{\mu\nu}$ *vanish identically, and* $R^i{}_{0i0} = p_i(1-p_i)/t^2$ *(*$i \in \{1,2,3\}$*). At the explicit non-flat witness* $p^* = (-\frac{1}{3}, \frac{2}{3}, \frac{2}{3})$ *(*$p_1 = -\frac{1}{3}$*),* $R_{\mu\nu} = 0$ *identically while* $R^1{}_{010} = -\frac{4}{9t^2}$ *and* $|R^1{}_{010}| = \frac{4}{9t^2} \to +\infty$ *as* $t \to 0^+$*.*
2. Bianchi-I holonomy shear cap (working ansatz). *Under the working Bianchi-I holonomy constraint ansatz* $h_1h_2 + h_2h_3 + h_3h_1 = 8\pi G\rho$ *with* $h_i = \sin(\ell H_i)/\ell$ *(*$|h_i| \le 1/\ell$*,* $i \in \{1,2,3\}$*), the energy density is bounded by* $\rho \le \rho_c := \frac{3}{8\pi G\ell^2}$*; saturation* $\rho = \rho_c$ *forces exact Planck-ceiling isotropization* $h_1 = h_2 = h_3 = \pm 1/\ell$ *(*$\sigma^2_{\mathrm{hol}} = 0$*). Adopting the unhalved shear-squared normalization* $\sigma^2_{\mathrm{hol}} := \sum_{i=1}^3 (h_i - \bar{h})^2$ *with* $\bar{h} := \frac{1}{3}(h_1 + h_2 + h_3)$ *(twice the* $\frac{1}{2}\sum_i (h_i - \bar{h})^2$ *convention), for all* $\rho \ge 0$ *the holonomy shear satisfies the sharp bound*

$$\sigma^2_{\mathrm{hol}} \le \frac{3}{2\ell^2} = 4\pi G\rho_c, \tag{64}$$

attained at $(h_1, h_2, h_3) = (1/\ell, 1/\ell, -1/(2\ell))$*.*
3. Six exact Bardeen gauge-invariant observables. *Under general scalar cosmological gauge transformations, all six Bardeen variables* $(\Phi_B, \Psi_B, \Delta_m, \zeta, \mathcal{R}_c, V_s)$ *are exactly gauge-invariant; longitudinal gauge fixing recovers* Φ_B, Ψ_B *directly; vanishing anisotropic stress* $\Pi = 0$ *forces* $\Phi_B = \Psi_B$*; and the comoving and uniform-density curvature perturbations obey the exact identities*

$$\mathcal{R}_c = \Psi_B + \frac{2}{3(1+w)}\left(\frac{\Psi_B'}{\mathcal{H}} + \Phi_B\right), \qquad \zeta - \mathcal{R}_c = \frac{2}{9(1+w)}\left(\frac{k}{\mathcal{H}}\right)^2 \Psi_B. \tag{65}$$

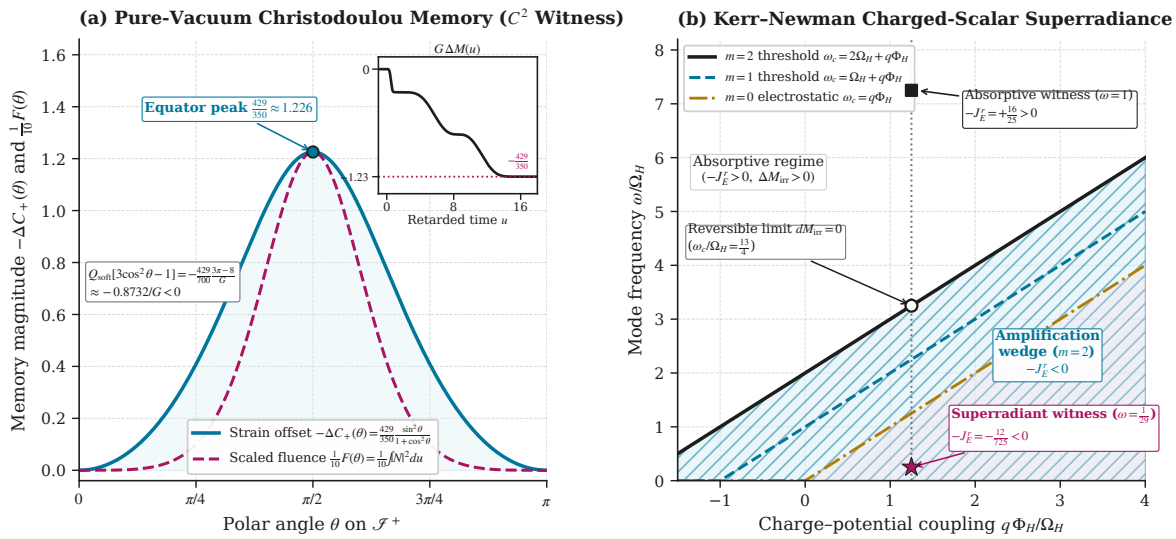

Fig. 2 Asymptotic BMS_4 radiation memory and charged horizon extraction benchmarks. **(a)** Explicit C^2 pure-vacuum Christodoulou memory witness (Theorem 4.7): angular strain offset $-\Delta C_+(\theta) = \frac{429}{350}\frac{\sin^2\theta}{1+\cos^2\theta}$ (peaking at $\frac{429}{350}$ on the equator), scaled news fluence $\frac{1}{10}F(\theta)$, quadrupole soft charge $Q_{\rm soft}[3\cos^2\theta - 1] = -\frac{429}{700}\frac{3\pi-8}{G} < 0$, and inset Bondi mass drop $G\Delta M(u) \to -\frac{429}{350}$. **(b)** Kerr–Newman charged-scalar superradiance phase diagram (Theorem 3.12): amplification wedge $-J_E^r < 0$ below $\omega = m\Omega_H + q\Phi_H$, reversible thresholds ($m = 0, 1, 2$), and explicit superradiant ($\omega = \frac{1}{29}$, $-J_E^r = -\frac{12}{725}$) versus absorptive ($\omega = 1$, $-J_E^r = +\frac{16}{25}$) witnesses.

4. Exact 9/4 bounce Friedmann solution and local non-Gaussianity. *For any $G, \ell > 0$ and equation of state $w > -1$, setting $u(t) := 1 + \frac{9}{4}(1+w)^2 t^2/\ell^2$, $\rho(t) = \rho_c/u(t)$, $a(t)/a_0 = u(t)^{1/(3(1+w))}$, and $H(t) = \frac{3}{2}(1+w)t/(\ell^2 u(t))$ solves both the modified Friedmann equation $H^2 = \frac{8\pi G}{3}\rho(1-\rho/\rho_c)$ (cf.* [65] *) and continuity $\dot{\rho} = -3(1+w)H\rho$ smoothly on all of $\mathbb{R}$. Because the barotropic conservation law $\rho\, a^{3(1+w)} = \text{const}$ holds globally through $t = 0$ independently of ℓ, the nonlinear e-folding shift δN under $\rho \mapsto \rho e^{\delta}$ is exactly conserved across the bounce, preserving the standard barotropic δN local non-Gaussianity (with respect to Gaussian $\delta\rho$):*

$$f_{\rm NL}^{\rm loc} = \frac{5}{6}\frac{N''}{(N')^2} = +\frac{5}{2}(1+w). \tag{66}$$

4.3 Pure-vacuum Christodoulou memory, S^2 spin-2 Hodge balance, and the 4D BMS_4 Ward identity

Isolated gravitating systems radiate energy and angular momentum to future null infinity $\mathscr{I}^+$, where the asymptotic symmetry algebra is the infinite-dimensional Bondi–Metzner–Sachs group BMS_4 [39;40;43]. Here we establish three exact asymptotic theorems: pure-vacuum Christodoulou nonlinear gravitational-wave memory [41], the spin-2 electric/magnetic Hodge decomposition on S^2 with local Flanagan–Nichols superrotation balance [44], and the exact BMS_4 supertranslation Ward identity matching Weinberg's leading soft-graviton pole [42].

Remark 4.6 (Explicit conditional scope of asymptotic evolution laws). Every calculus, Hodge, balance, and Ward identity in Theorems 4.7 to 4.9 is proved unconditionally *given* the standard Bondi mass-aspect evolution equation and the Bondi angular-momentum-aspect evolution equation as explicit named hypotheses on $\mathscr{I}^+$. Deriving the Bondi mass-aspect evolution law directly from an asymptotic expansion of the four-dimensional interior Einstein equations is explicitly excluded from the claims of this section.

Theorem 4.7 (Pure-vacuum Christodoulou nonlinear gravitational-wave memory)**.** *Suppose a regular Bondi radiative dataset on $[u_1, u_2] \times S^2$ obeys the Bondi mass-aspect evolution law in pure vacuum ($L_m \equiv 0$) with uniform initial and final mass aspects $M(u_1) = m_1$ and $M(u_2) = m_2$.*

1. Supertranslation soft-charge balance. *For every regular supertranslation generator $T : S^2 \to \mathbb{R}$, the soft memory charge satisfies*

$$Q_{\mathrm{soft}}[T] = (m_2 - m_1)\,\frac{1}{4\pi}\int_{S^2} T\,d\Omega + \frac{1}{16\pi G}\int_{S^2} T\left(\int_{u_1}^{u_2}\left(N_+^2 + N_\times^2\right)du\right)d\Omega. \tag{67}$$

2. Explicit C^2 pure-vacuum radiative witness. *For any $G > 0$ and initial mass M_0, there exists an explicit C^2 pure-vacuum radiative pulse with non-polynomial rational angular profile $w(\theta) = 1+\cos^2\theta$ (smoothly ramped on $u \in [0,1]$, radiating on $u \in [1,16]$, and returning to a uniform final mass aspect) satisfying all hypotheses with exact fluence*

$$\int_0^{16}\left(N_+^2 + N_\times^2\right)du = \frac{429}{175}\,\frac{\sin^4\theta\,(5+\cos^2\theta)}{(1+\cos^2\theta)^3}, \tag{68}$$

exact Bondi mass loss and permanent memory strain offset (Fig. 2),

$$\begin{aligned} \Delta M_{\mathrm{Bondi}} &= -\frac{429}{350\,G}, \qquad \Delta C_\times = 0, \\ \Delta C_+(\theta) &= -\frac{429}{350}\,\frac{\sin^2\theta}{1+\cos^2\theta} \qquad \left(\Delta C_+\left(\tfrac{\pi}{2}\right) = -\frac{429}{350}\right), \end{aligned} \tag{69}$$

dual-verified quadrupole soft charge for $T(\theta) = 3\cos^2\theta - 1$ (computed independently from the balance law Eq. (67) and directly from ΔC_+)

$$Q_{\mathrm{soft}}\left[3\cos^2\theta - 1\right] = -\frac{429}{700}\,\frac{3\pi - 8}{G} < 0, \tag{70}$$

and strictly positive reciprocal comparison cost J on the retained permanent offset.

Theorem 4.8 (S^2 spin-2 E/B Hodge decomposition and local Flanagan–Nichols superrotation balance)**.** *On the unit 2-sphere S^2 ($\sin\theta \neq 0$), denote the electric and magnetic symmetric trace-free tensor operators built from a scalar potential Ψ by $E[\Psi]^{AB}$ and $B[\Psi]^{AB}$, and let Δ be the S^2 Laplacian.*

1. Exact E/B orthogonality and $\ell \leq 1$ kernel. *For every separated C^4 potential $\Psi(\theta,\varphi) = g(\theta)h(\varphi)$ with $h'' = -n^2 h$,*

$$\begin{aligned} D_A D_B E[\Psi]^{AB} &= \frac{1}{2}\Delta(\Delta+2)\Psi, \qquad & D_A D_B B[\Psi]^{AB} &= 0, \\ \epsilon^{AC} D_C D_B E[\Psi]^{B}{}_{A} &= 0, & \epsilon^{AC} D_C D_B B[\Psi]^{B}{}_{A} &= \frac{1}{2}\Delta(\Delta+2)\Psi. \end{aligned} \tag{71}$$

   For any spherical-harmonic eigenmode $\Delta\Psi = -\lambda\Psi$, $D_A D_B E[\Psi]^{AB} = \frac{1}{2}\lambda(\lambda-2)\Psi$, which annihilates $\ell \leq 1$ ($\lambda \in \{0,2\}$) and is injective mode-by-mode for all $\ell \geq 2$.
2. Circular-binary electric strain and superrotation generators. *The gravitational strain of a circular binary is purely electric $\ell = 2$ with potential $\Psi = Q\sin^2\theta\cos 2(\varphi - \omega u)$, giving $D_A D_B E[\Psi]^{AB} = 12Q\sin^2\theta\cos 2(\varphi-\omega u)$ and vanishing magnetic divergence. For meromorphic superrotation vector fields $Y_{k_{\mathrm{sr}}}$ labeled by mode index $k_{\mathrm{sr}} \in \mathbb{Z}$, the electric tensor of $D \cdot Y_{k_{\mathrm{sr}}}$ carries the prefactor $2k_{\mathrm{sr}}(k_{\mathrm{sr}}^2 - 1)\rho^{k_{\mathrm{sr}}}/\sin^2\theta$ (with stereographic radial coordinate ρ), which vanishes identically on the six global Lorentz fields ($k_{\mathrm{sr}} \in \{0, \pm 1\}$) and equals 12 at the equator for $k_{\mathrm{sr}} = 2$.*
3. Local Flanagan–Nichols balance and binary axial flux witness. *Under the angular-momentum-aspect evolution hypothesis, the pointwise Flanagan–Nichols superrotation balance law holds on $0 < \theta < \pi$ and is jointly witnessed by the radiating circular binary with total integrated axial angular-momentum flux $\frac{8}{5}\omega Q^2/G$. (Global S^2 harmonic completeness and integrated global balance for singular $|k_{\mathrm{sr}}| \geq 2$ vector fields are not claimed.)*

Theorem 4.9 (4D BMS_4 supertranslation Ward identity and Weinberg leading soft-graviton pole)**.** *Consider a finite collection of timelike massive scattering bodies with four-momenta $p_k = (E_k, \mathbf{p}_k)$, masses $\mu_k^2 = E_k^2 - |\mathbf{p}_k|^2 > 0$, Doppler factors $\sigma_k(\hat{n}) := E_k - \mathbf{p}_k \cdot \hat{n} \neq 0$, and incoming/outgoing signs*

$\eta_k \in \{+1,-1\}$ *satisfying four-momentum conservation* $\sum_k \eta_k p_k = 0$. *Let* $S(p)^{AB}$ *denote the single-body memory tensor on* S^2.

1. Exact cancellation of $\ell \le 1$ moments and Ward identity. *Each single-body tensor obeys* $D_A D_B S(p)^{AB} = \mu^4/\sigma^3 - E - 3\mathbf{p}\cdot\hat{n}$. *Under four-momentum conservation, the* $\ell = 0,1$ *pieces cancel identically, giving* $D_A D_B \sum_k \eta_k S(p_k)^{AB} = \sum_k \eta_k \mu_k^4/\sigma_k^3$. *Consequently, with total memory tensor* $\Delta C := 4G\sum_k \eta_k S(p_k)$, *every regular supertranslation* $T : S^2 \to \mathbb{R}$ *obeys the exact* BMS_4 *Ward identity*

$$\frac{1}{16\pi G}\int_{S^2} \Delta C^{AB}\, D_A D_B T\, d\Omega = \sum_k \eta_k Q_T[p_k], \qquad Q_T[p] := \frac{1}{4\pi}\int_{S^2} T\,\frac{\mu^4}{\sigma^3}\, d\Omega, \tag{72}$$

where on global translations $T_a(\hat{n}) = a_0 + \mathbf{a}\cdot\hat{n}$ *the body charge reduces exactly to* $Q_{T_a}[p] = a_0 E + \mathbf{a}\cdot\mathbf{p}$.

2. Equivalence with Weinberg's leading soft-graviton pole. *For a null soft momentum* $k = \omega(1,\hat{n})$ *(*$\omega \neq 0$*) and transverse-traceless polarization tensors* $e^{+}_{\mu\nu}, e^{\times}_{\mu\nu}$, *the permanent memory polarizations equal Weinberg's leading soft factor*[42] *identically:*

$$\Delta C_{+,\times}(\hat{n}) = -4G\,\omega \sum_i \eta_i \frac{p_i^\mu p_i^\nu e^{+,\times}_{\mu\nu}}{p_i \cdot k}. \tag{73}$$

3. Explicit axisymmetric and non-axisymmetric scattering witnesses.
   - Symmetric two-body decay: $(10,0,0,0) \to (5,0,0,3) + (5,0,0,-3)$ *gives* $\Delta C_+ = \frac{180G\sin^2\theta}{25-9\cos^2\theta}$, $\Delta C_\times = 0$, *and dual-verified supertranslation charge for* $T = \cos^2\theta$ *equal to* $-\frac{100}{9} + \frac{512}{27}\ln 2 > 0$.
   - Non-axisymmetric three-body decay: $(16,0,0,0) \to (5,3,0,0) + (5,0,0,4) + (6,-3,0,-4)$ *produces a strictly non-vanishing cross-polarization memory offset* $\Delta C_\times(\frac{\pi}{2},\frac{\pi}{2}) = 8G \neq 0$.

Remark 4.10 (Scope of the classical BMS_4 Ward identity). Theorem 4.9 establishes the exact classical equivalence between Weinberg's leading soft-graviton pole, permanent gravitational-wave memory, and the BMS_4 supertranslation Ward identity for massive timelike bodies ($\sigma_k \neq 0$); quantum S-matrix amplitudes and massless null bodies ($\sigma_k = 0$) lie outside its scope.

5 Nonsingular gravitational collapse, two-sided LTB bounds, and the no-exterior-echo obstruction

Classical general relativity predicts that pressureless spherical collapse drives the Kretschmann scalar to infinity in finite proper time[16;45]. When a microscopic length scale $\ell > 0$ caps the local energy density, three sharp questions determine whether singularity resolution is mathematically genuine rather than a homogeneous artifact:

1. Does the bounded collapse interior join smoothly—across all $9+9$ Israel–Darmois conditions[50] with uniformly bounded four-dimensional curvature—to a uniquely forced exterior metric?
2. When homogeneity is relaxed to inhomogeneous Lemaître–Tolman–Bondi (LTB) dust collapse[46–48], where is the exact boundary between global curvature boundedness and genuine shell-crossing divergence[49]?
3. When a supercritical collapsing star bounces behind its trapped horizon, can causal signals from the bounce return as late-time echoes to the original exterior observer[60–62], or does the global horizon geometry strictly forbid return?

Throughout this section we keep $G > 0$ and $\ell > 0$ explicit so that every curvature cap and mass threshold displays its exact scaling, and we use the rational polar coordinate $\chi = \cos\theta \in (-1,1)$ with Σ denoting the moving stellar boundary hypersurface.

5.1 Canonical cost rate law, Oppenheimer–Snyder bounce, and $9+9$ outgoing Israel–Darmois junction

The mechanism that prevents zero-volume collapse is the divergence of the canonical reciprocal cost $J(x) = \frac{1}{2}(x + x^{-1}) - 1$ as $x \to 0^+$. Whenever a positive scale ratio $x > 0$ obeys a finite cost budget

$J(x) \le B$, it is bounded strictly away from zero by the exact floor

$$x \ge 1 + B - \sqrt{B^2 + 2B} > 0, \qquad \lim_{x \to 0^+} J(x) = +\infty. \tag{74}$$

On the unit circle, the complex analytic continuation of J yields the compact phase cost $J_{\text{phase}}(\theta) := 1 - \cos\theta = -\operatorname{Re} J_{\mathbb{C}}(e^{i\theta})$. Under the *working physical identification* pricing the collapse rate variable b through the compact phase branch $C(b) := \frac{1-\cos(2\ell b)}{2\ell^2} = \frac{\sin^2(\ell b)}{\ell^2}$ with capacity density ceiling

$$\rho_c := \frac{3}{8\pi G \ell^2}, \tag{75}$$

the homogeneous collapse dynamics closes in exact analytic form and uniquely fixes the matched exterior spacetime.

Theorem 5.1 (Canonical cost rate law, Oppenheimer–Snyder bounce, uniquely forced exterior, and $9+9$ Israel–Darmois junction)**.** *Let $G, M, \ell > 0$ and $\rho_c = \frac{3}{8\pi G\ell^2}$.*

1. Modified collapse rate law and J-cost balance. *Under the compact-phase rate cost $C(b) = \sin^2(\ell b)/\ell^2$ (working identification), the collapse rate obeys $H^2 = \frac{8\pi G}{3}\rho(1-\rho/\rho_c)$ (whose quadratic germ recovers classical $H^2 = \frac{8\pi G}{3}\rho$), with exact algebraic reciprocal-cost identity for all $0 < \rho < \rho_c$:*

$$\rho\left(1 - \frac{\rho}{\rho_c}\right) = \frac{\rho_c}{4 + 2\,J\left(\dfrac{\rho_c - \rho}{\rho}\right)}. \tag{76}$$

   The cell equations admit the exact global solution $\ell b(\tau) = \frac{\pi}{2} - \arctan\left(\frac{3\tau}{2\ell}\right)$ and cell volume $v_{\text{cell}}(\tau) = v_{\text{cell,min}}\left(1 + \frac{9\tau^2}{4\ell^2}\right)$ for all $\tau \in \mathbb{R}$.

2. Oppenheimer–Snyder bouncing dust ball and interior curvature cap. *The comoving stellar boundary radius*

$$R(\tau) = \left(2GM\ell^2 + \frac{9}{2}GM\tau^2\right)^{1/3}, \qquad R_{\min} := R(0) = \left(2GM\ell^2\right)^{1/3} = \left(\frac{3M}{4\pi\rho_c}\right)^{1/3}, \tag{77}$$

   is smooth on all of $\mathbb{R}$, attains its strict global minimum $R(\tau) \ge R_{\min} > 0$ uniquely at $\tau = 0$ with $R'(0) = 0$ and $R''(0) = \frac{3GM}{R_{\min}^2} = \frac{3R_{\min}}{2\ell^2} > 0$, obeys $\rho(\tau) \le \rho_c$ (equality iff $\tau = 0$) and $R'(\tau)^2 = \frac{2GM}{R(\tau)}(1-\rho(\tau)/\rho_c)$, and carries the uniform interior four-dimensional Kretschmann bound

$$0 \le K_{\text{int}}(\tau) \le \frac{27}{\ell^4} \qquad (\forall \tau \in \mathbb{R}). \tag{78}$$

3. Uniquely forced exterior metric and exact critical horizon mass. *Matching $h_{\tau\tau}$ and $K_{\chi\chi}$ across the collapsing branch $\tau \le 0$ in ingoing Eddington–Finkelstein coordinates (v, r, χ, φ)* uniquely forces *the static exterior lapse function and advanced-time trajectory*

$$f_{\text{ext}}(r) = 1 - \frac{2GM}{r} + \frac{4\ell^2 G^2 M^2}{r^4}, \qquad V'(\tau) = \frac{1}{1 - R'(\tau)}, \tag{79}$$

   satisfying $1 - R'(\tau)^2 = f_{\text{ext}}(R(\tau))$ and $R''(\tau) = -\frac{1}{2}f'_{\text{ext}}(R(\tau))$ identically. Horizon formation is governed by the exact critical mass threshold

$$27\,(GM)^2 = 64\,\ell^2 \qquad \Longleftrightarrow \qquad GM = \frac{8}{3\sqrt{3}}\,\ell. \tag{80}$$

   In the subcritical regime $27(GM)^2 < 64\ell^2$, $f_{\text{ext}}(r) > 0$ and $R'(\tau)^2 < 1$ for all $\tau \in \mathbb{R}$ (horizonless bounce). In the supercritical regime $27(GM)^2 > 64\ell^2$ (witnessed explicitly by $G = 1$, $M = 2$, $\ell = 1$,

where $64 < 108$*),* $f_{\rm ext}$ *possesses exactly two distinct horizon roots satisfying*

$$R_{\min} < r_- < \frac{3}{2}GM < r_+ < 2GM. \tag{81}$$

4. Smooth outgoing Eddington–Finkelstein chart, universal exterior curvature cap, and $9+9$ Israel–Darmois junction. *In the outgoing Eddington–Finkelstein chart* (u, r, χ, φ)*,*

$$ds^2 = -f_{\rm ext}(r)\,du^2 - 2\,du\,dr + r^2\left(\frac{d\chi^2}{1-\chi^2} + (1-\chi^2)\,d\varphi^2\right), \qquad U'(\tau) = \frac{1}{1+R'(\tau)}, \tag{82}$$

direct four-dimensional Fréchet differentiation yields $K_{\rm ext}(r) = (f''_{\rm ext})^2 + 4(f'_{\rm ext})^2/r^2 + 4(1 - f_{\rm ext})^2/r^4$ *identically in both ingoing and outgoing charts, obeying the universal mass-independent curvature cap*

$$0 \le K_{\rm ext}(r) \le \frac{360}{\ell^4} \qquad (\forall r \ge R_{\min},\ \forall G, M, \ell > 0). \tag{83}$$

For every $G, M, \ell > 0$ *and comoving boundary radius* $r_b > 0$*, all* 9 *induced-metric components* $h_{ij} = \mathrm{diag}\big(-1,\ R^2/(1-\chi^2),\ R^2(1-\chi^2)\big)$ *and all* 9 *extrinsic-curvature components* $K_{ij} = \mathrm{diag}\big(0,\ R/(1-\chi^2),\ R(1-\chi^2)\big)$ *match identically across the moving stellar boundary* Σ *in both ingoing* $(\tau < \tau_-)$ *and outgoing* $(\tau > -\tau_-)$ *charts with unit, tangent-annihilating, outward-pointing* $(n^r > 0)$ *normals on both sides.*

Remark 5.2 (Relation to loop-quantum Oppenheimer–Snyder collapse). The exact matched exterior metric Eq. (79), its critical horizon mass threshold Eq. (80), and the resulting black-to-white-hole bounce topology were derived earlier in effective loop-quantum Oppenheimer–Snyder collapse models[66;67;69–71]. What Theorem 5.1 and Theorem 5.6 contribute within the canonical reciprocal-cost framework is the algebraic identification Eq. (76) with $J(x)$, exact mass-independent four-dimensional Kretschmann ceilings ($K_{\rm int} \le 27/\ell^4$ and $K_{\rm ext} \le 360/\ell^4$), machine-verified $9+9$ Israel–Darmois matching in both ingoing and outgoing charts, and a formal proof that advanced-time divergence $V(\tau) \to +\infty$ obstructs causal return to Exterior I.

5.2 Sharp two-sided inhomogeneous LTB dust-collapse theorem

Homogeneous dust forces every radial shell to bounce simultaneously, hiding a central instability of realistic collapse: differential turning times between adjacent radial shells can drive the radial metric coefficient $\partial_r R$ to zero, creating a shell-crossing curvature singularity[49] even when every individual shell has finite minimum radius. To test whether the bounce ceiling ℓ resolves inhomogeneous collapse unconditionally or only below a sharp shear threshold, we examine marginally bound inhomogeneous LTB dust collapse in comoving coordinates (τ, r, χ, φ),

$$ds^2 = -d\tau^2 + \big(\partial_r R(\tau, r)\big)^2 dr^2 + R(\tau, r)^2\left(\frac{d\chi^2}{1-\chi^2} + (1-\chi^2)\,d\varphi^2\right), \tag{84}$$

with smooth mass profile $m(r) > 0$, shell turning-time profile $\tau_0(r)$, shifted proper time $s := \tau - \tau_0(r)$, and bounce areal radius

$$R(\tau, r) = \Big(G\,m(r)\,D(\ell, s)\Big)^{1/3}, \qquad D(\ell, s) := 2\ell^2 + \frac{9}{2}s^2. \tag{85}$$

(For a general LTB metric with arbitrary energy function $E(r)$, direct Fréchet differentiation proves the exact non-negative four-dimensional Kretschmann identity $K = 4(R_{\tau\tau r}/R_r)^2 + 8(R_{\tau\tau}/R)^2 + 8((R_{\tau r}R_\tau - E')/(R_r R))^2 + 4((R_\tau^2 - 2E)/R^2)^2 \ge 0$.)

To quantify radial turning-time shear across shells without overloading surface gravity κ_H, we introduce the dimensionless LTB shell-shear parameter $\eta_{\rm sh}$ via the uniform margin condition

$$9\,m(r)^2\,\tau_0'(r)^2 \le \eta_{\rm sh}^2\left(4\ell^2\,m'(r)^2\right) \qquad \Longleftrightarrow \qquad |\tau_0'(r)| \le |\eta_{\rm sh}|\,\frac{2\ell}{3}\,\frac{m'(r)}{m(r)}. \tag{86}$$

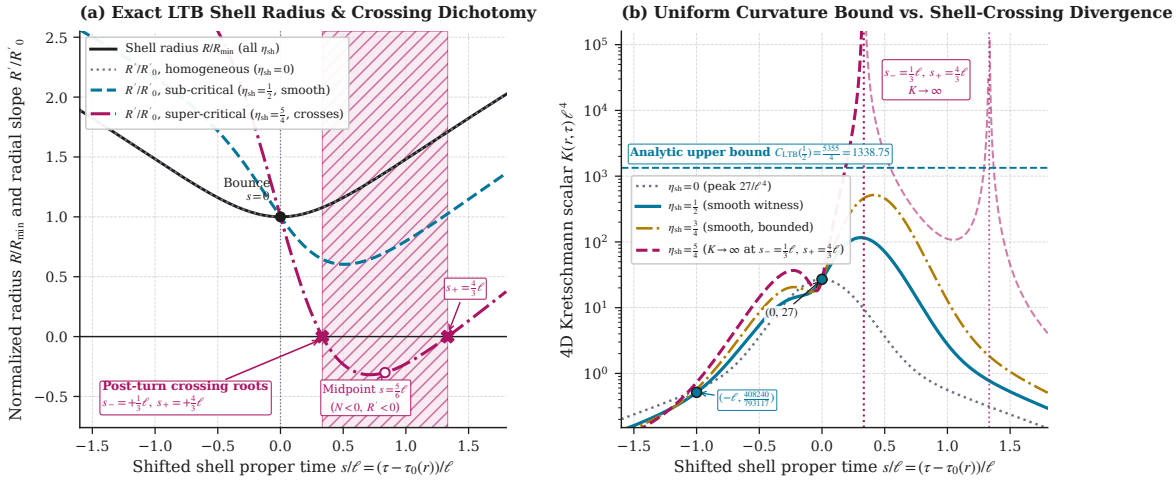

Fig. 3 Sharp two-sided inhomogeneous LTB dust-collapse dichotomy (Theorems 5.3 and 5.4). **(a)** Normalized shell radius $R/R_{\min}$ and radial slope R'/R'_0 versus shifted proper time $s/\ell = (\tau - \tau_0(r))/\ell$, contrasting smooth sub-critical bounces ($\eta_{\rm sh} = 0, \frac{1}{2}$) with the super-critical profile $m(r) = r^3$, $\tau_0(r) = \frac{5}{2}\ell r$ ($\eta_{\rm sh}(1) = \frac{5}{4}$), whose radial slope vanishes at the genuine *post-turn* shell crossing $s_- = +\frac{1}{3}\ell$ ($\tau = \frac{17}{6}\ell > \tau_0(1)$). **(b)** Four-dimensional Kretschmann scalar $K(r,\tau)\ell^4$ obeying the uniform bound $K \le C_{\rm LTB}(\frac{1}{2})/\ell^4 = \frac{5355}{4\ell^4}$ for the inhomogeneous witness $m(r) = e^r$, $\tau_0(r) = \frac{\ell}{3}r$ (marking the $\tau = 0$ slice values at $r = 0$, $s = 0$, $(0, 27)$ and at $r = 3$, $s = -\ell$, $(-\ell, \frac{408\,240}{793\,117})$), while diverging unboundedly ($K \to +\infty$) as $s \to (\frac{1}{3}\ell)^-$ at $\eta_{\rm sh}(1) = \frac{5}{4}$.

This single dimensionless parameter separates global regularity from genuine post-turn shell-crossing blow-up sharply at $|\eta_{\rm sh}| = 1$ (Fig. 3).

Theorem 5.3 (Positive inhomogeneous LTB dust-collapse theorem ($|\eta_{\rm sh}| < 1$))**.** *Let $G, \ell > 0$, and consider the marginally bound inhomogeneous LTB bounce geometry Eq. (84) and Eq. (85) generated by C^3 profiles $m, \tau_0 : \mathbb{R} \to \mathbb{R}$ with $m(r) > 0$ and $m'(r) > 0$. Define $N(\tau, r) := m'(r)D(\ell, s) - 9m(r)s\tau_0'(r)$.*

1. Exact shell-crossing criterion and crossing roots. *For every fixed shell r, the radial metric coefficient remains strictly positive ($\partial_r R(\tau, r) > 0$) for all $\tau \in \mathbb{R}$* if and only if

$$9\,m(r)^2\,\tau_0'(r)^2 < 4\ell^2\,m'(r)^2 \qquad \Longleftrightarrow \qquad |\tau_0'(r)| < \frac{2\ell}{3}\,\frac{m'(r)}{m(r)}. \tag{87}$$

Whenever $m'(r) > 0$ and $\tau_0'(r) \ge 0$, no shell crossing occurs before turning ($\tau \le \tau_0(r)$). Whenever Eq. (87) fails strictly ($9m^2(\tau_0')^2 > 4\ell^2(m')^2$), the exact shell-crossing roots where $N(s, r) = 0$ ($\partial_r R = 0$) are

$$s_\pm(r) = \frac{m(r)\tau_0'(r)}{m'(r)} \pm \frac{\sqrt{9m(r)^2\tau_0'(r)^2 - 4\ell^2 m'(r)^2}}{3m'(r)}, \tag{88}$$

both strictly positive (post-turn) whenever $\tau_0'(r) > 0$; at the midpoint $s_{\rm mid}(r) := \frac{m(r)\tau_0'(r)}{m'(r)}$ inside (s_-, s_+), one has $N(s_{\rm mid}, r) = \frac{4\ell^2(m')^2 - 9m^2(\tau_0')^2}{2m'} < 0$, witnessing failure of $\partial_r R > 0$. In the classical limit ($\ell = 0$), every profile with $\tau_0'(r) \ne 0$ suffers a shell crossing (witnessed at $r = 1$ by $m(r) = r^3$, $\tau_0(r) = r$, whose crossing roots are $\tau = 1$ ($s = 0$) and $\tau = \frac{5}{3}$ ($s = \frac{2}{3}$), with midpoint $\tau = \frac{4}{3}$ where $N = -\frac{3}{2} < 0$).

2. Exact G-independent 4D Kretschmann scalar. *Wherever $N(\tau, r) \ne 0$, Newton's constant G cancels identically and the four-dimensional Kretschmann invariant equals*

$$K = 4\big(b - 2fug_1 + 9ug_2\big)^2 + 8b^2 + 8\big((f - ug_1)f\big)^2 + 4f^4, \tag{89}$$

where $f := \frac{3s}{D}$, $b := \frac{3}{D} - \frac{18s^2}{D^2}$, $g_1 := \frac{2\ell^2 - \frac{9}{2}s^2}{D}$, $g_2 := \frac{s(6\ell^2 - \frac{9}{2}s^2)}{D^2}$, and $u := \frac{9m\tau_0'}{N}$.

3. Positive uniform bound (sub-critical regime $|\eta_{\rm sh}| < 1$). *If m, τ_0 satisfy the shear-margin bound Eq. (86) globally on $\mathbb{R}$ with $|\eta_{\rm sh}| < 1$, then no shell crossing occurs anywhere ($\partial_r R > 0$ everywhere)*

and the four-dimensional Kretschmann scalar obeys the uniform global bound

$$0 \le K(\tau, r, \chi, \varphi) \le \frac{C_{\mathrm{LTB}}(|\eta_{\mathrm{sh}}|)}{\ell^4} \qquad (\forall(\tau, r, \chi, \varphi) \text{ with } |\chi| < 1), \tag{90}$$

with the exact closed-form constant (setting $c := \frac{k}{1-k}$ *for* $k = |\eta_{\mathrm{sh}}| \in [0, 1)$*)*

$$C_{\mathrm{LTB}}(k) = (3 + 33c)^2 + 18 + \frac{(1 + 6c)^2}{2} + \frac{1}{4}, \tag{91}$$

yielding exact benchmarks $C_{\mathrm{LTB}}(0) = \frac{111}{4}$ *and* $C_{\mathrm{LTB}}(\frac{1}{2}) = \frac{5355}{4}$. Explicit inhomogeneous global witness: *The smooth profile* $m(r) = e^r$, $\tau_0(r) = \frac{\ell}{3} r$ *satisfies every hypothesis globally on* $\mathbb{R}$ *with* $\eta_{\mathrm{sh}} = \frac{1}{2}$, *obeys* $0 \le K \le \frac{5355}{4\ell^4}$ *everywhere, and is genuinely inhomogeneous on the* $\tau = 0$ *slice (*$s = 0$ *at* $r = 0$, $s = -\ell$ *at* $r = 3$*):*

$$K(0, 0) = \frac{27}{\ell^4} \neq K(0, 3) = \frac{408\,240}{793\,117\,\ell^4}. \tag{92}$$

The sharp threshold $|\eta_{\mathrm{sh}}| = 1$ in Theorem 5.3 cannot be relaxed: exceeding it produces a genuine post-turn curvature singularity, establishing our first strong-field obstruction.

Obstruction 5.4 (Post-turn shell-crossing curvature blow-up at $\eta_{\mathrm{sh}} = 5/4$)**.** *The uniform curvature-boundedness property of Theorem 5.3 fails strictly above* $|\eta_{\mathrm{sh}}| = 1$. *For the explicit smooth* C^3 *super-critical dust profile*

$$m(r) = r^3, \qquad \tau_0(r) = \frac{5}{2}\ell r \qquad \left(\eta_{\mathrm{sh}}(r) := \frac{3m(r)\tau_0'(r)}{2\ell m'(r)} = \frac{5}{4} r, \;\; \eta_{\mathrm{sh}}(1) = \frac{5}{4}\right), \tag{93}$$

shell $r = 1$ *passes smoothly through its own turning point at* $\tau_0(1) = \frac{5}{2}\ell$ *(*$s = 0$*) and then encounters two exact* post-turn *shell-crossing roots* $s_- = +\frac{\ell}{3}$ *and* $s_+ = +\frac{4\ell}{3}$ *(first crossing at proper time* $\tau = \tau_0(1) + \frac{\ell}{3} = \frac{17}{6}\ell > \tau_0(1)$*). Along regular spacetime points approaching the first crossing as* $s \to (\ell/3)^-$, *the radial metric factor vanishes (*$N \to 0^+$, $\partial_r R \to 0^+$*) and the four-dimensional Kretschmann scalar Eq. (89) diverges unboundedly (*$K \to +\infty$*).*

Proof structure for Theorem 5.3 and Theorem 5.4. Differentiating Eq. (85) with respect to r gives $\partial_r R = \frac{G^{1/3}}{3}(mD)^{-2/3} N(\tau, r)$, where $N(\tau, r) = \frac{9}{2} m' s^2 - 9 m \tau_0' s + 2\ell^2 m'$ is a quadratic in s with leading coefficient $\frac{9}{2} m' > 0$. Its discriminant is $81 m^2 (\tau_0')^2 - 36\ell^2 (m')^2 = 9\big[9 m^2 (\tau_0')^2 - 4\ell^2 (m')^2\big]$, which is strictly negative if and only if Eq. (87) holds, proving Part 1 and giving the exact roots Eq. (88) (both strictly positive when $\tau_0' > 0$) whenever the criterion fails. Direct four-dimensional Fréchet differentiation of Eq. (84) cancels G identically and yields Eq. (89). For $|\eta_{\mathrm{sh}}| = k < 1$, Cauchy–Schwarz bounds $|9ms\tau_0'| \le k\, m' D$, forcing $N \ge (1-k) m' D > 0$ and $|u| \le \frac{3c}{\ell D^{1/2}}$ uniformly; inserting sharp rational maxima of f, b, g_1, g_2 into Eq. (89) produces the closed constant Eq. (91). Conversely, for Eq. (93) at $r = 1$, $N(s, 1) = \frac{3}{2}(3s - \ell)(3s - 4\ell)$ vanishes linearly at the post-turn instant $s_- = \ell/3$ while the numerator of u remains strictly nonzero, driving the leading u^2 terms in Eq. (89) to $+\infty$ as $s \to (\ell/3)^-$. □

Remark 5.5 (Physical meaning, post-bounce LTB shocks, and open collapse boundary). Theorem 5.3 and Theorem 5.4 show that a finite microscopic density ceiling $\rho_c \propto \ell^{-2}$ is *not* a blanket guarantee against every curvature singularity in inhomogeneous dust: it opens a sharp, finite stability window $|\eta_{\mathrm{sh}}| < 1$ (which collapses to measure zero in classical GR, $\ell \to 0$) while still allowing genuine post-turn shell-crossing singularities whenever differential turning-time shear exceeds the ℓ-scale threshold. This complements numerical studies of post-bounce shock-wave formation in loop-quantum LTB collapse[68] by supplying an exact analytic two-sided Kretschmann threshold $C_{\mathrm{LTB}}(|\eta_{\mathrm{sh}}|)/\ell^4$ together with a constructive blow-up refutation. Extending this two-sided classification beyond marginally bound C^3 spherical dust to generic (3+1)-dimensional asymmetric collapse with pressure remains explicitly open.

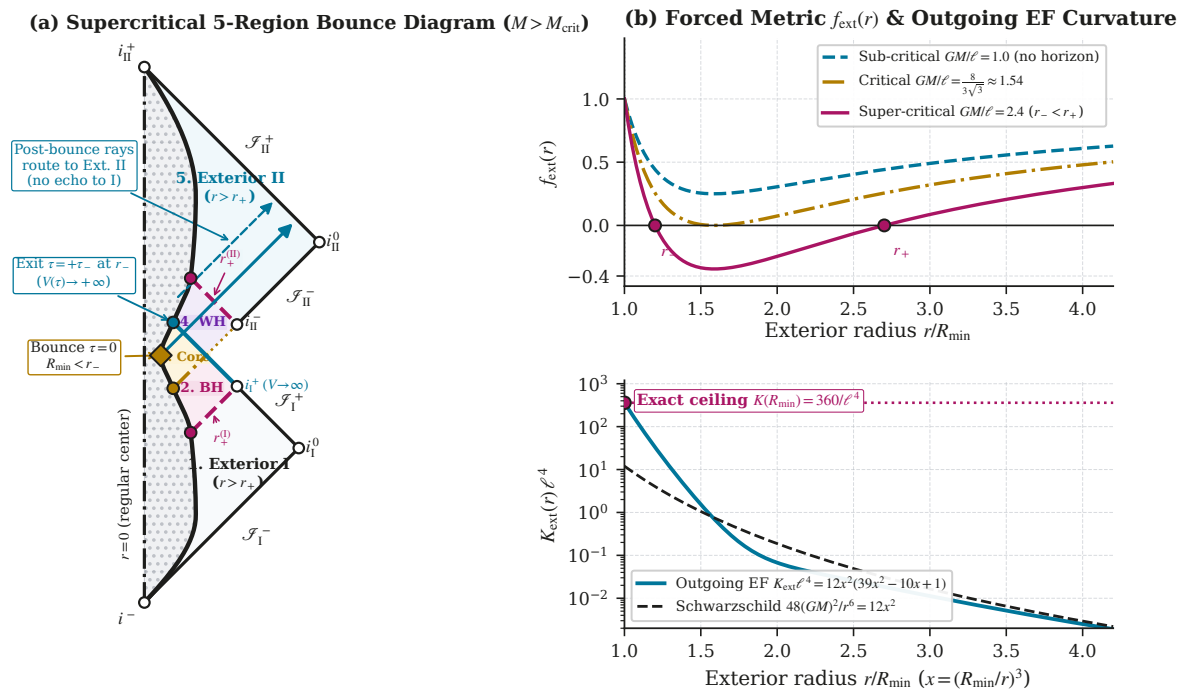

Fig. 4 Supercritical matched Oppenheimer–Snyder bounce and the no-exterior-echo obstruction (Theorems 5.1 and 5.6). **(a)** Conformal causal diagram for $27(GM)^2 > 64\ell^2$ displaying all five causal regions: the collapsing star enters from Exterior I through the trapped black-hole region into the untrapped bounce core, bounces smoothly at $R_{\min} < r_-$ across the $9+9$ Israel–Darmois junction, hits r_- at τ_- with $R'(\tau_-) = +1$ and $V(\tau) \to +\infty$, and passes through the anti-trapped white-hole region into a second asymptotic exterior (Exterior II) covered by the outgoing chart, strictly obstructing causal echoes back to Exterior I. **(b)** Uniquely forced exterior lapse $f_{\rm ext}(r)$ across sub-critical, critical ($GM/\ell = \frac{8}{3\sqrt{3}}$), and supercritical ($r_- < r_+$) regimes (top), and the universal outgoing Eddington–Finkelstein Kretschmann bound $K_{\rm ext}(R_{\min}) = 360/\ell^4$ contrasted against singular Schwarzschild $48(GM)^2/r^6$ (bottom).

5.3 Obstruction II: supercritical two-exterior geometry and the no-exterior-echo theorem

Regular bounce models of gravitational collapse are frequently invoked as a physical source of late-time gravitational-wave echoes returning to detectors in the original collapsing exterior[60–62]. Checking the global causal matching of Theorem 5.1 in the supercritical black-hole regime $27(GM)^2 > 64\ell^2$ yields a sharp negative result consistent with the two-exterior effective loop-quantum bounce topology[69–71]: the post-bounce expansion cannot re-enter the original ingoing exterior chart at all.

Obstruction 5.6 (Supercritical two-exterior / no-exterior-echo horizon obstruction)**.** *Let $G, M, \ell > 0$ lie in the supercritical black-hole regime $27(GM)^2 > 64\ell^2$ (witnessed explicitly by $G = 1$, $M = 2$, $\ell = 1$), so that $f_{\rm ext}(r)$ in Eq. (79) has two distinct horizons $R_{\min} < r_- < \frac{3}{2}GM < r_+ < 2GM$ with $f_{\rm ext}(r) > 0$ on $(0, r_-)$.*

1. Exact horizon-crossing times. *Along the bouncing stellar boundary Eq. (77), define the infalling outer-horizon crossing time and the re-expanding inner-horizon exit time by*

$$\tau_+^{\rm in} := -\sqrt{\frac{r_+^3 - 2GM\ell^2}{\frac{9}{2}GM}} < -\tau_- < 0, \qquad \tau_- := +\sqrt{\frac{r_-^3 - 2GM\ell^2}{\frac{9}{2}GM}} > 0. \tag{94}$$

At $\tau = \tau_-$, the expanding surface reaches r_- with $R'(\tau_-) = +1$; moreover $R(\tau) < r_-$ for all $|\tau| < \tau_-$ and $R(\tau) < r_+$ strictly throughout the nonempty interval $\tau_+^{\rm in} < \tau < \tau_-$ (indeed for all $|\tau| < |\tau_+^{\rm in}|$).

2. Divergence of ingoing advanced time and failure of ingoing matching. *For every* $\tau < \tau_-$, $R'(\tau) < 1$. *Because* $R''(\tau) \le \frac{3GM}{R_{\min}^2} =: L$, *the mean-value bound* $1 - R'(\tau) \le L(\tau_- - \tau)$ *forces* every *advanced-time trajectory obeying* $V'(\tau) = \frac{1}{1-R'(\tau)}$ *to diverge at the inner horizon:*

$$\lim_{\tau \to \tau_-^-} V(\tau) = +\infty. \tag{95}$$

Directly at $\tau = \tau_-$, *where* $R'(\tau_-) = +1$, *the ingoing Israel–Darmois matching equations become algebraically contradictory.*

3. Routing into a second asymptotic exterior and causal obstruction to echoes. *Symmetrically, the outgoing Eddington–Finkelstein chart Eq.* (82) *begins at* $-\tau_-$ *with* $\lim_{\tau \to (-\tau_-)^+} U(\tau) = -\infty$ *and smoothly covers the entire post-bounce expansion* $\tau > -\tau_-$ *(including all* $\tau \ge \tau_-$ *outside the ingoing chart). On the causal structure of surface events covered by the ingoing chart* ($\tau < \tau_-$), no *causal chain of surface events leads from the original exterior through the bounce turning point* $\tau = 0$ *back to the original exterior: post-bounce expansion beyond* τ_- *passes through the anti-trapped white-hole region into a* second asymptotic exterior region *covered by the outgoing chart (Fig. 4).*

Proof structure. Since $R(\tau)^3 = 2GM\ell^2 + \frac{9}{2}GM\tau^2$ is even and strictly increasing on $\tau > 0$ with $R(0) = R_{\min} < r_- < r_+$, solving $R(\tau) = r_+$ ($\tau < 0$) and $R(\tau) = r_-$ ($\tau > 0$) yields the exact crossing times Eq. (94) with $\tau_+^{\text{in}} < -\tau_- < 0 < \tau_-$. Inserting $f_{\text{ext}}(r_-) = 0$ into $1 - R'(\tau_-)^2 = f_{\text{ext}}(R(\tau_-))$ with $R'(\tau_-) > 0$ forces $R'(\tau_-) = +1$. On $\tau < \tau_-$, $R''(\tau) \le 3GM/R_{\min}^2 = L$ implies $0 < 1 - R'(\tau) \le L(\tau_- - \tau)$, so integrating $V'(\tau) = (1 - R'(\tau))^{-1} \ge L^{-1}(\tau_- - \tau)^{-1}$ proves Eq. (95) logarithmically, while $1 - R'(\tau_-) = 0$ renders the ingoing junction denominator identically zero. By time-reversal symmetry $R(-\tau) = R(\tau)$, $U'(\tau) = (1 + R'(\tau))^{-1}$ diverges as $\tau \to (-\tau_-)^+$ and remains smooth for all $\tau > -\tau_-$, carrying the expanding boundary into a second asymptotic exterior disjoint from the ingoing chart. Finally, because $R(\tau) < r_+$ for every $\tau \in (\tau_+^{\text{in}}, \tau_-)$, any causal model built on surface events inside the ingoing chart ($\tau < \tau_-$) cannot return to $r > r_+$ after crossing $\tau = 0$, proving the causal no-return obstruction. □

Remark 5.7 (Observational implication for gravitational-wave echoes). Theorem 5.6 does not claim that quantum gravity forbids all deviations from classical ringdown; rather, it proves that within the exact smooth matched bounce spacetime of Theorem 5.1, classical causal propagation cannot bounce off the core and re-emerge as an echo into Exterior I. Generating observable echoes in Exterior I therefore requires either horizonless subcritical compactness ($27(GM)^2 < 64\ell^2$) or a genuinely non-classical transition mechanism outside the smooth matched bounce geometry (such as quantum black-to-white-hole tunneling outside the trapping region[64]).

6 Geodesic completeness of bouncing collapse, static Hayward rain trajectories, and rotating Gürses–Gürsey core structure

Bounded curvature invariants do not by themselves establish that a spacetime is nonsingular. A geometry whose Kretschmann scalar $K = R_{abcd}R^{abcd}$ stays finite everywhere on a coordinate chart can still terminate freely falling observers or light rays at finite proper time or finite affine parameter if the chart ends prematurely, if metric components degenerate, or if directional discontinuities obstruct extension across a core[10;16;18;57]. Determining whether the capacity ceiling $\rho_c = 3/(8\pi G\ell^2)$ genuinely resolves strong-field collapse singularities therefore requires solving the four-dimensional geodesic equation directly and checking completeness across both dynamical bounce charts and static or rotating regular cores.

In this section we prove three global geodesic theorems together with their exact curvature bounds and honest geometric limits: (i) global causal geodesic completeness of the bouncing dust interior and global proper-time completeness of the bouncing stellar surface across overlapping ingoing and outgoing charts (Section 6.1); (ii) global proper-time completeness and an explicit exponential radial floor for unit-energy radial "rain" geodesics on the static Hayward capacity core (Section 6.2); and (iii) a complete characterization of the rotating Gürses–Gürsey capacity core, including its J-cost mass law, uniform curvature bound $|K_{\text{GG}}| \le 896/\ell^4$, honest directional discontinuity at the $r = 0$ equatorial ring,

and complete ingoing principal null rays contrasted directly against singular Kerr's $48M_g^2/r^6$ equatorial blow-up (Section 6.3).

6.1 Causal completeness of the bouncing dust interior and stellar surface

Consider the spatially flat bouncing dust interior

$$ds^2 = -d\tau^2 + a(\tau)^2\big(dx^2 + dy^2 + dz^2\big), \tag{96}$$

where $a : \mathbb{R} \to \mathbb{R}$ is smooth and strictly bounded below by a positive floor $a(\tau) \geq a_{\min} > 0$ for all $\tau \in \mathbb{R}$. In the homogeneous Oppenheimer–Snyder bounce driven by the compact-phase cost rate law, $a(\tau) = a_{\min}\big(1 + \frac{9\tau^2}{4\ell^2}\big)^{1/3}$ and the stellar boundary radius $R(\tau) = r_b a(\tau)$ satisfies

$$R(\tau) = \left(2GM\ell^2 + \frac{9}{2}GM\tau^2\right)^{1/3} \geq R_{\min} := (2GM\ell^2)^{1/3} > 0 \tag{97}$$

for all $\tau \in \mathbb{R}$ and every $G, M, \ell, r_b > 0$.

Theorem 6.1 (Global causal geodesic completeness of the bouncing interior)**.** *Let $a : \mathbb{R} \to \mathbb{R}$ be smooth with $a(\tau) \geq a_{\min} > 0$ for all $\tau \in \mathbb{R}$ (in particular, the homogeneous bouncing dust interior for any $G, M, \ell, r_b > 0$). Through every initial event $x_0 = (\tau_0, x_0^1, x_0^2, x_0^3) \in \mathbb{R}^4$ and for every future-directed causal initial velocity satisfying $g(\dot\gamma_0, \dot\gamma_0) = -\varepsilon \leq 0$ and $(\varepsilon, \mathbf{p}) \neq (0, \mathbf{0})$—where $p_i := a(\tau_0)^2 \dot x_0^i$ denotes the conserved spatial momentum—there exists a smooth global affine geodesic $\gamma : \mathbb{R} \to \mathbb{R}^4$ solving*

$$\ddot\gamma^\mu(\lambda) + \Gamma^\mu_{\nu\rho}\big(\gamma(\lambda)\big)\dot\gamma^\nu(\lambda)\dot\gamma^\rho(\lambda) = 0, \qquad g\big(\dot\gamma(\lambda), \dot\gamma(\lambda)\big) = -\varepsilon \tag{98}$$

for all affine parameter values $\lambda \in (-\infty, +\infty)$.

Mechanism and proof summary. Spatial translation invariance of Eq. (96) yields three exact first integrals $a(\tau)^2\dot x^i = p_i = \text{const}$ $(i = 1, 2, 3)$. Substituting these into the normalization condition $-\dot\tau^2 + a(\tau)^2\delta_{ij}\dot x^i\dot x^j = -\varepsilon$ reduces the geodesic system to a single autonomous differential equation for the comoving time $\tau(\lambda)$:

$$\dot\tau(\lambda) = \sqrt{\varepsilon + \frac{|\mathbf{p}|^2}{a\big(\tau(\lambda)\big)^2}}. \tag{99}$$

Because $a(\tau) \geq a_{\min} > 0$ uniformly on $\mathbb{R}$, the right-hand side of Eq. (99) is smooth, strictly positive, and uniformly bounded above by $\sqrt{\varepsilon + |\mathbf{p}|^2/a_{\min}^2}$ without requiring any global Lipschitz assumption on a. A global flow therefore exists for all $\lambda \in (-\infty, +\infty)$, and the spatial coordinates $x^i(\lambda) = x_0^i + p_i \int_0^\lambda a(\tau(s))^{-2}\, ds$ extend smoothly across the entire real line. Direct differentiation confirms all four components of Eq. (98) and preservation of $g(\dot\gamma, \dot\gamma) = -\varepsilon$. □

At the moving boundary of the collapsing dust star, completeness must also survive the horizon crossing where the ingoing Eddington–Finkelstein coordinate v diverges in the supercritical regime $(27G^2M^2 > 64\ell^2)$. Overlapping the ingoing chart (v, r, χ, φ) with the outgoing chart (u, r, χ, φ) resolves this coordinate boundary cleanly.

Theorem 6.2 (Global proper-time completeness of the bouncing stellar surface)**.** *For every $G, M, \ell, r_b > 0$ (setting $M_g := GM$), the bouncing stellar surface Eq. (97) is a complete proper-time timelike geodesic on $\tau \in (-\infty, +\infty)$ covered by overlapping ingoing $(\tau < \tau_m)$ and outgoing $(\tau > -\tau_m)$ Eddington–Finkelstein charts across all three horizon regimes:*

1. Subcritical $(27M_g^2 < 64\ell^2)$: *$f_{\text{ext}}(r) > 0$ everywhere and $\tau_m = +\infty$, so both charts cover all $\tau \in \mathbb{R}$;*
2. Critical $(27M_g^2 = 64\ell^2)$: *$f_{\text{ext}}(r)$ has a single double-root extremal horizon at $r_* = \frac{3}{2}M_g > R_{\min}$, with finite overlap half-width $\tau_m = \sqrt{(r_*^3 - 2M_g\ell^2)/(\frac{9}{2}M_g)} > 0$;*
3. Supercritical $(27M_g^2 > 64\ell^2)$: *$f_{\text{ext}}(r)$ has two simple horizons $R_{\min} < r_- < \frac{3}{2}M_g < r_+ < 2M_g$, with overlap half-width $\tau_m = \tau_- = \sqrt{(r_-^3 - 2M_g\ell^2)/(\frac{9}{2}M_g)} > 0$.*

On every region where $f_{\rm ext}(r) = 1 - \frac{2M_g}{r} + \frac{4\ell^2 M_g^2}{r^4} \neq 0$*, the two charts are glued smoothly by the exact Jacobian pullback*

$$dv = du + \frac{2}{f_{\rm ext}(r)}\, dr, \tag{100}$$

which leaves the four-dimensional exterior metric invariant identically. Everywhere along the surface trajectory, the areal radius and four-dimensional Kretschmann scalar obey

$$R(\tau) \geq R_{\min} = (2M_g\ell^2)^{1/3} > 0, \qquad 0 \leq K\big(\gamma_{\rm surf}(\tau)\big) \leq \frac{360}{\ell^4} \qquad (\forall \tau \in \mathbb{R}). \tag{101}$$

Together, Theorems 6.1 and 6.2 establish that neither the interior matter nor the collapsing stellar boundary encounters a geodesic endpoint at finite proper time: every worldline passes smoothly through the bounce at $\tau = 0$ with curvature capped at $O(\ell^{-4})$.

6.2 Global proper-time completeness on the static Hayward capacity core

Turning from dynamical dust collapse to an eternal static regular black hole, we examine the Hayward capacity metric[51] in smooth ingoing Eddington–Finkelstein coordinates (v, r, χ, φ) ($\chi = \cos\theta \in (-1, 1)$, $W := 1 - \chi^2$):

$$ds^2 = -f_{\rm Hay}(r)\, dv^2 + 2\, dv\, dr + r^2 \left(\frac{d\chi^2}{W} + W\, d\varphi^2 \right), \tag{102}$$

with lapse and capacity mass profile ($M_g := GM > 0$, $\ell > 0$)

$$f_{\rm Hay}(r) = 1 - \frac{2m_{\rm cap}(r)}{r}, \qquad m_{\rm cap}(r) = \frac{M_g r^3}{r^3 + 2M_g\ell^2}. \tag{103}$$

In classical Schwarzschild spacetime ($\ell = 0$), a freely falling radial observer released from rest at infinity (unit Killing energy $E = 1$, a "rain" geodesic) satisfies $r'(\tau) = -\sqrt{2M_g/r}$ and crashes into $r = 0$ in finite proper time $\Delta\tau = \frac{2}{3} r_0^{3/2}/\sqrt{2M_g}$. On the Hayward capacity core, the de Sitter softening $m_{\rm cap}(r) \simeq r^3/(2\ell^2)$ changes the infall law qualitatively.

Define the radial infall speed

$$w_{\rm rain}(r) := \sqrt{1 - f_{\rm Hay}(r)} = r\sqrt{\frac{2M_g}{r^3 + 2M_g\ell^2}} > 0 \qquad (r > 0), \tag{104}$$

and consider the first-order radial system

$$r'(\tau) = -w_{\rm rain}\big(r(\tau)\big), \qquad v'(\tau) = \frac{1}{1 + w_{\rm rain}\big(r(\tau)\big)}, \qquad \chi(\tau) = \chi_0, \qquad \varphi(\tau) = \varphi_0. \tag{105}$$

Because $1 - f_{\rm Hay} = w_{\rm rain}^2$, any solution of Eq. (105) automatically satisfies

$$g(\dot\gamma, \dot\gamma) = -f_{\rm Hay}(v')^2 + 2v'r' = -1, \qquad E := f_{\rm Hay} v' - r' = 1, \tag{106}$$

and solves all four components of the geodesic equation $\ddot\gamma^\mu + \Gamma^\mu_{\nu\rho}\dot\gamma^\nu\dot\gamma^\rho = 0$ identically.

Theorem 6.3 (Global completeness and exponential radial floor on the Hayward core)**.** *For every* $M_g > 0$*,* $\ell > 0$*, and every initial event* $(v_0, r_0, \chi_0, \varphi_0)$ *with* $r_0 > 0$ *and* $\chi_0 \in (-1, 1)$*, there exist smooth global functions* $v, r : \mathbb{R} \to \mathbb{R}$ *solving the full four-dimensional geodesic equation on Eq.* (102) *via Eq.* (105) *for all proper time* $\tau \in (-\infty, +\infty)$*. Every such unit-energy radial rain geodesic is future-directed* ($v'(\tau) > 0$)*, strictly infalling* ($r'(\tau) < 0$)*, and remains strictly at positive radius* $r(\tau) > 0$ *for all* $\tau \in \mathbb{R}$*, obeying the explicit exponential radial floor and uniform Kretschmann bound*

$$r(\tau) \geq r_0\, e^{-\tau/\ell} > 0 \quad (\forall \tau \geq 0), \qquad |K\big(\gamma(\tau)\big)| \leq \frac{896}{\ell^4} \quad (\forall \tau \in \mathbb{R}). \tag{107}$$

Moreover, the static curvature bound $|K(r,\chi)| \le 896/\ell^4$ *holds at every chart point with* $r > 0$ *and* $\chi \in (-1,1)$.

Mechanism and proof summary. Introducing the logarithmic radius $x(\tau) := -\ln r(\tau)$ converts the radial equation in Eq. (105) into

$$x'(\tau) = \frac{w_{\text{rain}}\big(r(\tau)\big)}{r(\tau)} = \sqrt{\frac{2M_g}{r(\tau)^3 + 2M_g\ell^2}} \le \frac{1}{\ell}. \tag{108}$$

The upper bound $0 < x'(\tau) \le 1/\ell$ holds uniformly for all $r > 0$ and all $M_g > 0$ because $r^3 > 0$ strictly enlarges the denominator. Therefore $x(\tau)$ cannot blow up in finite forward or backward proper time, yielding global smooth existence on $(-\infty, +\infty)$ for $x(\tau)$, $r(\tau) = e^{-x(\tau)} > 0$, and $v(\tau) = v_0 + \int_0^\tau [1 + w_{\text{rain}}(r(s))]^{-1}\, ds$. Integrating Eq. (108) over $[0,\tau]$ gives $x(\tau) - x(0) \le \tau/\ell$, which exponentiates directly to $r(\tau) \ge r_0 e^{-\tau/\ell}$ for all $\tau \ge 0$. The uniform curvature bound $|K| \le 896/\ell^4$ is the $a = 0$ specialization of Theorem 6.6 below. □

Remark 6.4 (Scope boundary for higher-energy radial trajectories). Theorem 6.3 proves global completeness specifically for the unit-energy ($E = 1$) radial rain family, whose turning energy matches the de Sitter core's zero potential at $r = 0$ so that $r(\tau) \to 0^+$ only as $\tau \to +\infty$. Strictly higher-energy radial timelike geodesics ($E > 1$) satisfy $(r')^2 = E^2 - f_{\text{Hay}}(r) \to E^2 - 1 > 0$ as $r \to 0^+$, reach the regular origin $r = 0$ in finite proper time, and require continuation across the center into an antipodal chart; those trajectories lie outside the scope of Theorem 6.3.

6.3 Rotating Gürses–Gürsey capacity core: mass law, directional ring geometry, and complete principal null rays

Astrophysical black holes spin, and classical Kerr spacetime concentrates its curvature blow-up on an equatorial ring singularity ($\varrho^2 = r^2 + a^2\chi^2 = 0$) rather than a central point[11;15]. To test whether the capacity ceiling tames the Kerr ring without obscuring geometric subtleties, we embed the radial mass function $m_{\text{cap}}(r)$ into the rotating Gürses–Gürsey metric[53–55;59] in smooth ingoing Kerr-form coordinates $(v, r, \chi, \bar\varphi)$ ($\chi = \cos\theta \in (-1,1)$, $W = 1 - \chi^2$, $\varrho^2 = r^2 + a^2\chi^2$):

$$ds^2 = -\left(1 - \frac{2m_{\text{cap}}(r)\, r}{\varrho^2}\right) dv^2 + 2\, dv\, dr - 2aW\, dr\, d\bar\varphi - \frac{4m_{\text{cap}}(r)\, raW}{\varrho^2}\, dv\, d\bar\varphi + \frac{\varrho^2}{W}\, d\chi^2 + W\left(r^2 + a^2 + \frac{2m_{\text{cap}}(r)\, ra^2W}{\varrho^2}\right) d\bar\varphi^2. \tag{109}$$

We treat the choice $m(r) = m_{\text{cap}}(r)$ inside Eq. (109) explicitly as a working structural ansatz (*Working Input*), while establishing three exact algebraic characterizations linking $m_{\text{cap}}(r)$ directly to the capacity ceiling $\rho_c = 3/(8\pi G\ell^2)$, the canonical reciprocal cost $J(x)$, and the forced collapse exterior $m_{\text{ext}}(r) = M_g\big(1 - (R_{\min}/r)^3\big)$.

Proposition 6.5 (Harmonic, differential, and J-cost characterizations of m_{cap})**.** *Let* $M_g > 0$, $\ell > 0$, *and* $R_{\min} = (2M_g\ell^2)^{1/3}$. *For all* $r > 0$, *the capacity mass function* $m_{\text{cap}}(r) = M_g r^3/(r^3 + 2M_g\ell^2)$ *satisfies:*

1. Harmonic capacity sum:

$$\frac{1}{m_{\text{cap}}(r)} = \frac{1}{M_g} + \frac{1}{r^3/(2\ell^2)}, \qquad \frac{r^3}{2\ell^2} = G\rho_c \cdot \frac{4\pi}{3} r^3. \tag{110}$$

2. Uniqueness of the local differential law: m_{cap} *is the unique strictly positive differentiable profile on* $(0,\infty)$ *satisfying*

$$m'(r) = \frac{6\ell^2 m(r)^2}{r^4}, \qquad \lim_{r\to\infty} m(r) = M_g. \tag{111}$$

3. Exact reciprocal-cost gradient and exterior agreement:

$$m'_{\mathrm{cap}}(r) = \frac{3M_g/r}{4 + 2\,J\big((r/R_{\min})^3\big)}, \tag{112}$$

and $m_{\mathrm{cap}}(r) - m_{\mathrm{ext}}(r) = M_g(R_{\min}/r)^6/\big(1+(R_{\min}/r)^3\big)$*, agreeing with the matched collapse exterior through first order in* $(R_{\min}/r)^3$*.*

Mechanism. Identity Eq. (110) is immediate upon inverting $m_{\mathrm{cap}}(r) = M_g/(1+2M_g\ell^2/r^3)$. Differentiating $1/m(r)$ converts Eq. (111) into $(1/m)' = -6\ell^2/r^4$, whose unique solution with $\lim_{r\to\infty} 1/m(r) = 1/M_g$ is $1/m(r) = 1/M_g + 2\ell^2/r^3$. Writing $x := (r/R_{\min})^3 = r^3/(2M_g\ell^2)$ gives $4+2J(x) = x + x^{-1} + 2 = (x+1)^2/x$, so $3M_g/[r(4+2J(x))] = 3M_g x/[r(x+1)^2] = 6M_g^2\ell^2 r^2/(r^3+2M_g\ell^2)^2 = m'_{\mathrm{cap}}(r)$. □

Direct four-dimensional Fréchet computation of the Riemann, Ricci, and Kretschmann tensors of Eq. (109) reveals both a strong positive regularization theorem and an essential geometric subtlety on the $r = 0$ disk.

Theorem 6.6 (Curvature structure, directional ring discontinuity, and horizons of the rotating capacity core)**.** *For all* $M_g > 0$*,* $\ell > 0$*, and arbitrary spin parameter* $a \in \mathbb{R}$*, the rotating Gürses–Gürsey capacity metric Eq.* (109) *satisfies:*

1. Global uniform Kretschmann bound: *At every chart point with* $r \geq 0$*,* $\varrho^2 = r^2 + a^2\chi^2 \neq 0$*, and* $W = 1 - \chi^2 \neq 0$*,*

$$|K_{\mathrm{GG}}(r,\chi)| \leq \frac{896}{\ell^4}. \tag{113}$$

2. Exact equatorial closed form and de Sitter limit: *On the equatorial plane* $\chi = 0$ *(*$r > 0$*),*

$$K_{\mathrm{GG}}(r,0) = \frac{48M_g^2\big(32M_g^4\ell^8 - 16M_g^3\ell^6 r^3 + 72M_g^2\ell^4 r^6 - 8M_g\ell^2 r^9 + r^{12}\big)}{(r^3+2M_g\ell^2)^6}, \tag{114}$$

which approaches the exact de Sitter curvature invariant as $r \to 0^+$*,*

$$\lim_{r\to 0^+} K_{\mathrm{GG}}(r,0) = \frac{24}{\ell^4}, \tag{115}$$

while both effective Ricci eigenvalues tend simultaneously to $3/\ell^2 = 8\pi G\rho_c$*.*

3. Flat $r = 0$ disk and direction-dependent ring limit: *Whenever* $a \neq 0$*, at every interior point of the* $r = 0$ *disk (*$\chi \neq 0$*,* $W \neq 0$*), the Kretschmann scalar and both Ricci eigenvalues vanish identically:*

$$K_{\mathrm{GG}}(0,\chi) = 0 \qquad (a \neq 0,\ \chi \in (-1,1)\setminus\{0\}). \tag{116}$$

Consequently, although K_{GG} *is globally bounded by* $896/\ell^4$ *throughout* $r \geq 0$*,* $\varrho^2 \neq 0$*, it is* direction-dependent *at the equatorial ring* $r = \chi = 0$ *(*0 *along the disk* $r = 0, \chi \to 0$ *versus* $24/\ell^4$ *along the equator* $\chi = 0, r \to 0^+$*) and admits no continuous extension across the ring itself.*

4. Far-field decay to vacuum Kerr and horizon trichotomy: *For all* $r > 0$*, the Ricci scalar and Ricci eigenvalues obey*

$$|R(r,\chi)| \leq \frac{72M_g^2\ell^2}{r^6}, \qquad |\lambda_i(r,\chi)| \leq \frac{36M_g^2\ell^2}{r^6}, \tag{117}$$

so every curvature departure from vacuum Kerr decays as $O(\ell^2 r^{-6})$*. Defining* $\Delta_{\mathrm{GG}}(r) := r^2 - 2m_{\mathrm{cap}}(r)r + a^2$*: if* $M_g^2 < a^2$*, then* $\Delta_{\mathrm{GG}}(r) > 0$ *for all* $r \geq 0$ *(horizonless fast-spin core); if* $a \neq 0$ *and* $a^2M_g^2 + 2\ell^2M_g^2 + 2\ell^2a^2 < M_g^4$*, then* Δ_{GG} *has two distinct horizon roots* $0 < r_- < M_g < r_+ < 2M_g$*.*

The directional discrepancy between Eq. (115) and Eq. (116) is a genuine geometric feature of rotating Hayward/Gürses–Gürsey metrics, not an artifact of coordinates: replacing a constant mass M_g by $m_{\mathrm{cap}}(r) = O(r^3)$ eliminates the r^{-6} blow-up along the equator while forcing $m_{\mathrm{cap}}(0) = m'_{\mathrm{cap}}(0) = m''_{\mathrm{cap}}(0) = 0$ on the disk $r = 0, \chi \neq 0$ (where $\varrho^2 = a^2\chi^2 > 0$ remains strictly positive). Reporting this 0 vs. $24/\ell^4$ jump openly avoids misrepresenting a bounded rotating core as everywhere smooth across the ring.

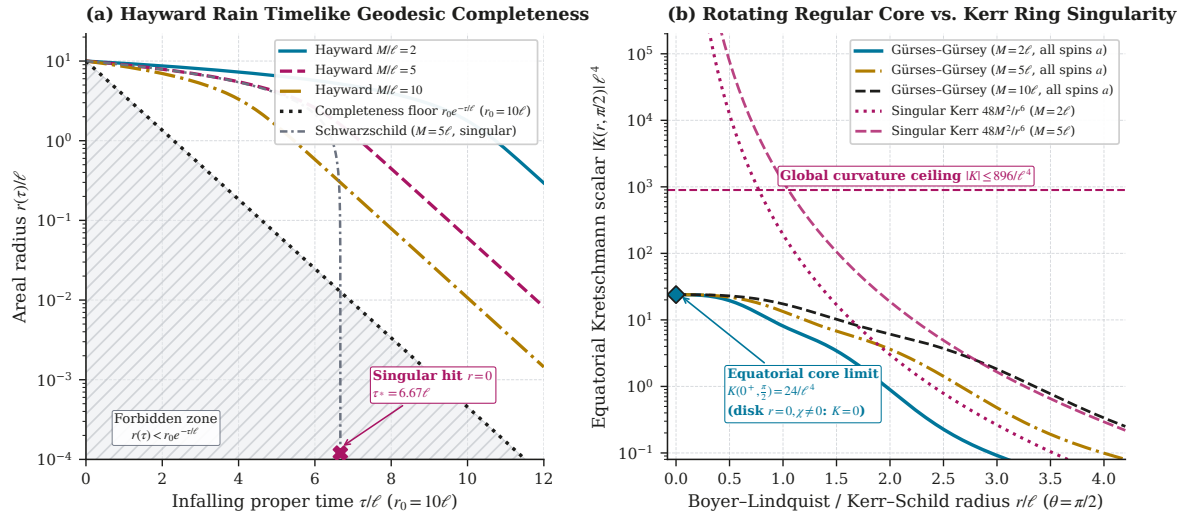

Fig. 5 Geodesic and curvature structure of the static Hayward and rotating Gürses–Gürsey capacity cores. (a) Unit-energy radial rain geodesics released from $r_0 = 10\,\ell$ on the static Hayward core ($M_g/\ell \in \{2, 5, 10\}$) obey the exponential completeness floor $r(\tau) \geq r_0 e^{-\tau/\ell} > 0$ for all forward proper time (Theorem 6.3), avoiding the finite-time classical Schwarzschild crash ($r = 0$ at $\tau_* = \frac{2}{3} r_0^{3/2}/\sqrt{2M_g} \approx 6.67\,\ell$ for $M_g = 5\,\ell$). (b) Equatorial Kretschmann curvature along ingoing principal null geodesics contrasts the singular Kerr blow-up $K_{\rm Kerr}(r, 0) = 48M_g^2/r^6 \to +\infty$ against the globally bounded rotating capacity core ($|K_{\rm GG}| \leq 896/\ell^4$ for all spins a, approaching the de Sitter value $24/\ell^4$ along the equator while vanishing on the $r = 0$ disk for $\chi \neq 0$; Theorems 6.6 and 6.7).

Finally, we compare ingoing principal null geodesics on the rotating capacity core directly against the same rays in singular vacuum Kerr spacetime.

Theorem 6.7 (Ingoing principal null geodesics: regular capacity core vs. singular Kerr)**.** *For any C^2 radial mass function $m(r)$ and any spin $a \in \mathbb{R}$, the Levi–Civita connection of the ingoing Gürses–Gürsey metric Eq. (109) satisfies $\Gamma^{\mu}_{rr} = 0$ identically for all $\mu \in \{0, 1, 2, 3\}$. Hence for every initial event $(v_0, r_0, \chi_0, \bar{\varphi}_0)$ with $r_0 > 0$ and $\chi_0 \in (-1, 1)$, the radial curve*

$$\gamma(\lambda) = (v_0,\, r_0 - \lambda,\, \chi_0,\, \bar{\varphi}_0) \tag{118}$$

is an affinely parametrized ingoing principal null geodesic. Specifically:

1. Rotating capacity core ($m = m_{\rm cap}$): *The ray Eq. (118) propagates smoothly for all $\lambda < r_0$ with $|K_{\rm GG}(\gamma(\lambda))| \leq 896/\ell^4$ everywhere along it. Along the equator ($\chi_0 = 0$), $K_{\rm GG}(\gamma(\lambda)) \to 24/\ell^4$ as $\lambda \to r_0^-$. Off the equator ($a \neq 0, \chi_0 \neq 0$), the ray reaches the regular $r = 0$ disk at $\lambda = r_0$ with $K_{\rm GG}(\gamma(r_0)) = 0$.*
2. Singular vacuum Kerr contrast ($m \equiv M_g > 0$): *On exact vacuum Kerr spacetime, the Kretschmann scalar evaluates to*

$$K_{\rm Kerr}(r, \chi) = \frac{48M_g^2\big(r^2 - a^2\chi^2\big)\big(\varrho^4 - 16r^2a^2\chi^2\big)}{\varrho^{12}}, \tag{119}$$

so along the exact same equatorial principal null geodesic ($\chi_0 = 0$),

$$K_{\rm Kerr}\big(\gamma(\lambda)\big) = \frac{48M_g^2}{(r_0 - \lambda)^6} \longrightarrow +\infty \qquad (\lambda \to r_0^-). \tag{120}$$

Figure 5 summarizes this contrast between classical finite-time collapse and capacity-regularized trajectories. Three explicit boundaries mark where the proved theorems of Section 6.3 stop: (i) analytic continuation through the flat $r = 0$ disk into the $r < 0$ region is not formalized; (ii) general non-radial rotating timelike geodesics on Eq. (109) remain open; and (iii) nonlinear dynamical stability of the inner Cauchy horizon r_- against Poisson–Israel mass-inflation perturbations[30;56;58] and scalar/gravitational perturbation stability of rotating regular cores[59] are not resolved by static curvature bounds and remain open problems (Section 8.3).

7 Quantum horizon microstructure: universal Crofton area projection, arbitrary-spin logarithmic entropy, and deterministic information decoding

Classical black-hole mechanics fixes horizon thermodynamics up to an overall microstate normalization, leaving three structural quantum questions open[72–74]. First, when a curved black-hole horizon is embedded in a three-dimensional discrete lattice, why does raw face counting overcount the Bekenstein–Hawking entropy $S_{\mathrm{BH}} = c^3 A_H/(4G\hbar) = A_H/(4\ell_{\mathrm{P}}^2)$ by exactly 50%, and can choosing a more isotropic lattice remove that mismatch? Second, in $SU(2)$ gauge-closed horizon microstate counting, does the universal logarithmic correction $-\gamma_{\log} \ln(A/\ell_{\mathrm{P}}^2)$ depend on restricting punctures to spin-1/2, or is $\gamma_{\log} = 3/2$ forced across arbitrary finite spin ceilings[76–80]? Third, after the Page time[81], can an outside observer recover a message dropped into an old black hole deterministically—without probabilistic post-selection—using strictly exterior operations[82–85]?

Throughout this section we restore G, $\hbar$, and c explicitly where horizon areas are measured in Planck units $\ell_{\mathrm{P}}^2 = \hbar G/c^3$, and we use $m := |L|$ for the number of horizon punctures and $N_{\max}$ for the finite twice-spin ceiling so that the microscopic length ℓ, Planck length ℓ_{P}, and reciprocal cost $J(x)$ remain strictly unambiguous.

7.1 Universal 3/2 three-dimensional Voronoi Crofton projection and exact $SO(3)$ horizon integral

On the curved Kruskal–Szekeres Schwarzschild horizon two-sphere S^2_{2M} of radius $2M$ and area $A_H = 16\pi M^2$ [13;14], a family of parallel lattice planes with unit normal $u \in S^2$ intercepts a surface element dA with unit normal $n(\theta,\varphi)$ at density proportional to $|n(\theta,\varphi)\cdot u|$ [75]. Integrating this projection directly over the curved horizon yields a strictly orientation-independent identity.

Theorem 7.1 (Exact $SO(3)$-invariant spherical projection integral)**.** *For every $M > 0$ and every unit vector $u = (u_x, u_y, u_z) \in S^2$ ($u_x^2 + u_y^2 + u_z^2 = 1$), direct integration over the Kruskal horizon two-sphere S^2_{2M} yields*

$$\iint_{S^2_{2M}} |n(\theta,\varphi)\cdot u|\, dA = 8\pi M^2 = \frac{1}{2} A_H, \tag{121}$$

strictly independent of the direction of u.

Now let $\mathcal{V} \subset \mathbb{R}^3$ be the Voronoi cell of any three-dimensional Bravais lattice, bounded by antipodal pairs of faces indexed by k, with face areas $a_k > 0$, apothems (perpendicular half-spacings from the cell center to the face) $h_k > 0$, and outward unit face normals $\pm u_k \in S^2$. Decomposing $\mathcal{V}$ into pyramids from the origin to every face yields the exact cell volume $V = \frac{2}{3}\sum_k a_k h_k > 0$. Because dual lattice bonds crossing the k-th face pair have spacing $2h_k$ and transverse area a_k, their contribution to the raw flux of Voronoi faces cutting a surface with unit normal n is $\frac{2a_k h_k}{V}|n\cdot u_k|$ per unit area. Combining the pyramidal volume identity with Theorem 7.1 establishes a lattice-independent universality theorem.

Theorem 7.2 (Universal 3/2 three-dimensional Voronoi Crofton projection)**.** *For every three-dimensional Voronoi polyhedron of volume $V = \frac{2}{3}\sum_k a_k h_k > 0$, the face-density weights obey the universal normalization*

$$\sum_k \frac{2a_k h_k}{V} = 3, \tag{122}$$

and the total raw face count crossing the curved Kruskal horizon S^2_{2M} evaluates identically to

$$\iint_{S^2_{2M}} \left(\sum_k \frac{2a_k h_k}{V} |n(\theta,\varphi)\cdot u_k| \right) dA = 24\pi M^2 = \frac{3}{2} A_H. \tag{123}$$

Table 2 summarizes the explicit evaluation of Eq. (122) and Eq. (123) on three canonical lattices: simple cubic $\mathbb{Z}^3$, the FCC D_3 rhombic dodecahedron (spatial slice of D_4), and the BCC D_3^* truncated octahedron (spatial slice of the D_4^* recognition lattice[1]). The physical consequence follows immediately under the one-bit horizon area calibration $\lambda_{\mathrm{rec}}^2 = 4\ell_{\mathrm{P}}^2 \ln 2$ ($\ell_{\mathrm{P}}^2 = \hbar G/c^3$): assigning $\ln 2$ nats per raw

Table 2 Exact verification of the universal 3/2 three-dimensional Voronoi Crofton factor across the simple cubic ($\mathbb{Z}^3$), face-centred cubic (D_3, spatial slice of D_4), and body-centred cubic (D_3^*, spatial slice of D_4^*) Voronoi tessellations (Theorem 7.2). The pointwise column reports the exact global directional range over $n \in S^2$: for FCC D_3, $\sqrt{3/2} \approx 1.225$ along $[1,1,1]$ (3/2 along $[1,0,0]$) and global maximum $\sqrt{5/2} \approx 1.581$ along $\langle 2,1,0\rangle$; for BCC D_3^*, $(2\sqrt{2}+3\sqrt{6})/8 \approx 1.272$ along $[1,1,0]$ and $\sqrt{30+6\sqrt{3}}/4 \approx 1.589$ along $(1+3\sqrt{3},1,1)$. Increasing lattice isotropy narrows the pointwise directional spread while leaving the global spherical Crofton factor strictly invariant.

3D Lattice (Voronoi cell)	Vol. V	Antipodal face pairs (a_k, h_k)	Pointwise	Global $\iint / A_H$
Simple Cubic $\mathbb{Z}^3$ (cube)	1	3 square pairs: $(1, \frac{1}{2})$	$[1, \sqrt{3}]$	3/2
FCC D_3 (rhombic dodec.)	2	6 rhombic pairs: $(\frac{\sqrt{2}}{2}, \frac{\sqrt{2}}{2})$	$[\sqrt{3/2}, \sqrt{5/2}]$	3/2
BCC D_3^* (trunc. octah.)	4	3 sq. $(\frac{1}{2}, 1)$ + 4 hex. $(\frac{3\sqrt{3}}{4}, \frac{\sqrt{3}}{2})$	[1.272, 1.589]	3/2

Voronoi face crossing the horizon without the directional projection factor yields

$$S_{\text{raw}} = (\ln 2)\,\frac{\frac{3}{2}A_H}{\lambda_{\text{rec}}^2} = \frac{3A_H}{8\ell_{\text{P}}^2} = \frac{3c^3 A_H}{8G\hbar} = 1.5\,S_{\text{BH}}, \tag{124}$$

an exact 50% overcount across *every* three-dimensional Voronoi tessellation. Passing from simple cubic $\mathbb{Z}^3$ to more isotropic cells such as FCC D_3 or BCC D_3^* shrinks the global pointwise directional spread ($[1, 1.732] \to [1.225, 1.581]$ and $[1.272, 1.589]$), yet cannot budge the integrated spherical factor 3/2. The directional Cauchy–Crofton projection factor 2/3 is therefore forced geometrically by three-dimensional pyramidal volume scaling, completely independently of lattice isotropy [75].

7.2 Exact $SU(2)$ Weyl closure integral and forced uniqueness of $\gamma_{\log} = 3/2$ for arbitrary finite spin ceilings

We now determine the logarithmic correction to black-hole entropy for a quantum horizon punctured by an arbitrary finite list $L = [N_1, \dots, N_m]$ of $m = |L|$ faces carrying $SU(2)$ representations of spin $j_i = N_i/2$ ($N_i \in \mathbb{N}_{\geq 1}$, each puncture carrying $N_i + 1$ magnetic substates). Let

$$\chi_N(\theta) := \sum_{k=0}^{N} \cos\big((N-2k)\theta\big), \qquad \chi_L(\theta) := \prod_{N \in L} \chi_N(\theta) \tag{125}$$

denote the $SU(2)$ character of a single spin-$N/2$ puncture and the product character of the shell L, and write $D(L) := \prod_{N\in L}(N+1)$ for the unconstrained Hilbert-space dimension. Physical horizon microstates are restricted to the $SU(2)$-invariant (closed) intertwiner subspace $\mathcal{H}_{\text{closed}}(L)$ annihilated by the total angular-momentum generators.

Theorem 7.3 (Operator-to-Weyl-integral bridge for arbitrary valence and mixed spins)**.** *For every finite list L of twice-spins $N \in \mathbb{N}$, the complex dimension of the $SU(2)$-closed subspace equals the exact weight difference and Weyl group integral*

$$\dim_{\mathbb{C}} \mathcal{H}_{\text{closed}}(L) = w_0(L) - w_2(L) = \frac{1}{\pi}\int_{-\pi}^{\pi} \sin^2\theta\,\chi_L(\theta)\,d\theta, \tag{126}$$

where $w_q(L)$ counts basis states of total $2J_z$-weight q. Moreover, $\dim_{\mathbb{C}} \mathcal{H}_{\text{closed}}(L)$ is strictly invariant under arbitrary permutations of L, obeys the exact Clebsch–Gordan fusion and triangle selection rules, vanishes identically whenever $\sum_{N\in L} N$ is odd, and evaluates explicitly on mixed-spin intertwiner nodes to

$$[1,1,2] \mapsto 1 \text{ (Pauli vector)}, \quad [1,1,2,2] \mapsto 2, \quad [2,2,2,2] \mapsto 3, \quad [1,2,2] \mapsto 0, \quad [1,2,3] \mapsto 1. \tag{127}$$

The key analytic ingredient that unlocks arbitrary finite twice-spin ceilings $N_{\max} \geq 1$—without restricting to spin-1/2 or spin-1—is a pair of elementary Gaussian character envelopes whose upper decay rate is strictly independent of the spin N.

Lemma 7.4 (Spin-independent Gaussian upper and small-angle lower character bounds)**.** *For every integer $N \geq 1$:*

$$|\chi_N(\theta)| \leq (N+1)\, e^{-\theta^2/\pi^2} \qquad (\forall\, |\theta| \leq \pi/2), \tag{128}$$

$$\chi_N(\theta) \geq (N+1)\, e^{-N^2\theta^2} \qquad (\forall\, \theta \text{ with } N^2\theta^2 \leq 1). \tag{129}$$

Integrating Eq. (128) and Eq. (129) against the Haar measure factor $\sin^2\theta \sim \theta^2$ in Eq. (126) yields sharp two-sided counting bounds, an explicit two-sided entropy-area window, and forced uniqueness of the logarithmic coefficient $\gamma_{\log} = 3/2$.

Theorem 7.5 (Arbitrary-spin entropy-area window and forced uniqueness $\gamma_{\log} = 3/2$)**.** *Let L be a list of $m = |L| \geq 1$ punctures with $N \geq 1$ for all $N \in L$, and set $D(L) := \prod_{N\in L}(N+1)$.*

1. Unconditional upper bound (no spin cap, arbitrary parity):

$$\dim_{\mathbb{C}} \mathcal{H}_{\text{closed}}(L) \leq \frac{100\, D(L)}{m\sqrt{m}}. \tag{130}$$

2. Admissible lower bound for any twice-spin ceiling $N_{\max} \geq 1$: *Call L $N_{\max}$-admissible if $1 \leq N \leq N_{\max}$ for all $N \in L$, $\sum_{N\in L} N$ is even, and $m \geq 6{,}000\, N_{\max}^6$. For every $N_{\max}$-admissible shell L,*

$$\frac{D(L)}{32\, N_{\max}^3\, m\sqrt{m}} \leq \dim_{\mathbb{C}} \mathcal{H}_{\text{closed}}(L). \tag{131}$$

   In the specialized mixed spin-1/2 and spin-1 regime of $2n_{1/2}$ spin-1/2 and n_1 spin-1 punctures with $n_{1/2} + n_1 \geq 12$, $D = 4^{n_{1/2}} 3^{n_1}$, and $s := n_{1/2}/4 + n_1/3$, the tighter exact bracket $\frac{D}{240\, s\sqrt{s}} \leq \dim_{\mathbb{C}} \mathcal{H}_{\text{closed}} \leq \frac{D}{4\, s\sqrt{s}}$ holds, giving $S = \frac{A}{4\ell_{\mathrm{P}}^2} - \frac{3}{2}\ln\frac{A}{\ell_{\mathrm{P}}^2} + c$ with $\frac{3}{2}\ln 12 - \ln 240 \leq c \leq \frac{3}{2}\ln 23 - \ln 4$ (in particular $-2 \leq c \leq 4$), witnessed explicitly at $(n_{1/2} = 6, n_1 = 6, \ell_{\mathrm{P}} = 1)$.

3. Two-sided entropy-area window (*Working Input* area footprint): *Under the per-face area footprint $a_N := 4\ln(N+1)\,\ell_{\mathrm{P}}^2$ so that $A(L) := \sum_{N\in L} a_N$ satisfies $\frac{A(L)}{4\ell_{\mathrm{P}}^2} = \ln D(L)$, the Boltzmann entropy $S(L) := \ln \dim_{\mathbb{C}} \mathcal{H}_{\text{closed}}(L)$ of every $N_{\max}$-admissible shell obeys*

$$\begin{aligned} -(3\ln N_{\max} + \ln 32) + \frac{3}{2}\ln(4\ln 2) &\leq S(L) - \left(\frac{A(L)}{4\ell_{\mathrm{P}}^2} - \frac{3}{2}\ln\frac{A(L)}{\ell_{\mathrm{P}}^2}\right) \\ &\leq \ln 100 + \frac{3}{2}\ln\big(4\ln(N_{\max}+1)\big), \end{aligned} \tag{132}$$

   which lies strictly inside $\big[-3\ln N_{\max} - 2,\ 5 + \frac{3}{2}\ln(4\ln(N_{\max}+1))\big]$.

4. Forced uniqueness of $\gamma_{\log} = 3/2$: *For any fixed finite twice-spin ceiling $N_{\max} \geq 1$, if there exists a constant $C \geq 0$ such that*

$$\left| S(L) - \left(\frac{A(L)}{4\ell_{\mathrm{P}}^2} - \gamma_{\log}\ln\frac{A(L)}{\ell_{\mathrm{P}}^2}\right)\right| \leq C \tag{133}$$

   holds uniformly over all $N_{\max}$-admissible shells L, then necessarily $\gamma_{\log} = \frac{3}{2}$.

The theorem is accompanied by zero-hypothesis concrete witnesses at $N_{\max} = 4$ (spin 2, $m = 24{,}576{,}000$, $\ell_{\mathrm{P}} = 1$) and across arbitrary permutations of mixed spin sets $\{1/2, 1, 3/2, 2\}$. Physically, the factor $m^{-3/2}$—and hence the universal logarithmic slope $\gamma_{\log} = 3/2$—stems directly from the three-dimensional $SU(2)$ gauge-closure saddle: the Weyl Haar measure supplies $\sin^2\theta \sim \theta^2$ near $\theta = 0$ (and $\theta = \pi$ for even $\sum N$), while the product of m characters has Gaussian width $\Delta\theta \sim m^{-1/2}$, producing $\int \theta^2 e^{-cm\theta^2}\, d\theta \propto m^{-3/2}$.

This result clarifies an important comparison across the quantum-gravity literature. Unconstrained puncture counting produces no logarithmic suppression ($\gamma_{\log} = 0$). In loop quantum gravity, Meissner[77] obtains $\gamma_{\log} = 1/2$ by imposing the single $U(1)$ projection constraint ($\sum_i m_i = 0$, contributing

one factor $m^{-1/2}$), whereas imposing full $SU(2)$ gauge closure enforces all three angular-momentum constraints ($m^{-3/2} \implies \gamma_{\log} = 3/2$), matching Kaul and Majumdar[76], Ghosh and Mitra[78], and Engle, Noui, and Perez[79] and generalizing them to arbitrary finite spin ceilings $N_{\max} \geq 1$ with explicit non-asymptotic bounds. By contrast, Sen's one-loop Euclidean path-integral calculation[80] yields a logarithmic coefficient sensitive to the spectrum of massless bulk matter fields. Two honest scope boundaries apply to Theorem 7.5: the per-face area footprint $a_N = 4\ln(N+1)\,\ell_{\mathrm{P}}^2$ is adopted as a working normalization (*Working Input*)—distinct from loop quantum gravity's linear-in-j area spectrum $8\pi\gamma_{\mathrm{BI}}\ell_{\mathrm{P}}^2\sqrt{j(j+1)}$—and the exact $O(1)$ additive constant limit inside Eq. (132) is not determined.

7.3 Deterministic exterior-only Hayden–Preskill decoding and one-step Uhlmann recovery isometry

Finally, we turn from horizon state counting to post-Page-time information recovery in the finite-dimensional Hayden–Preskill mirror protocol[81;82]. Let Alice's thrown-in message register M ($\dim M = d_M$) be maximally entangled with a reference register N ($\dim N = d_M$), and let the old black hole B ($\dim B = d_B$) be maximally entangled with Bob's early Hawking radiation B' ($\dim B' = d_B$). A unitary scrambler $U : M \otimes B \to K \otimes T$ maps the combined black hole onto a retained interior K ($\dim K = d_K$) and newly emitted late radiation T ($\dim T = d_T$), obeying the exact unitary dimension identity

$$d_M\, d_B = d_K\, d_T. \tag{134}$$

Let $|\Psi_{NKTB'}\rangle$ denote the resulting pure state on $(N \otimes K) \otimes (T \otimes B')$, with bipartition amplitude matrix $\Psi : \mathcal{H}_T \otimes \mathcal{H}_{B'} \to \mathcal{H}_N \otimes \mathcal{H}_K$ so that the reduced interior-reference density matrix is $\rho_{NK} = \Psi\Psi^\dagger$. Measure the decoupling of Alice's reference N from the retained interior K by the decoupling defect

$$\Delta_{\mathrm{dec}} := \rho_{NK} - \rho_N \otimes \rho_K, \qquad \eta := d_M d_K \operatorname{Tr}\big(\Delta_{\mathrm{dec}}^2\big) = \frac{1}{F_{\mathrm{YK}}} - 1 \geq 0, \tag{135}$$

where F_{YK} is the probabilistic Yoshida–Kitaev post-selected decoding fidelity[83;84].

In the Yoshida–Kitaev decoding circuit, Bob holds strictly the exterior registers T and B', prepares an auxiliary maximally entangled pair $M'N'$ of dimension d_M (so that $d_{M'}d_{B'} = d_M d_B = d_K d_T$ by Eq. (134)), and applies the conjugate scrambler $U^* : M' \otimes B' \to K' \otimes T'$. This yields the exterior Grover workspace $\mathcal{H}_{\mathrm{Bob}} = T \otimes (K' \otimes T') \otimes N'$, leaving the interior-reference factor $N \otimes K$ untouched. Post-selection onto the maximally entangled state of TT' succeeds only with probability $P_{\mathrm{YK}} = (1+\eta)/d_M^2 = O(d_M^{-2})$. Adjoining a single exterior ancilla qubit ($\mathbb{C}^2$) to $\mathcal{H}_{\mathrm{Bob}}$ and executing Grover amplitude amplification strictly on $\mathcal{H}_{\mathrm{Bob}} \otimes \mathbb{C}^2$ eliminates post-selection completely.

Theorem 7.6 (Deterministic exterior-only Yoshida–Kitaev Grover decoding)**.** *Adjoin one ancilla qubit to Bob's exterior workspace $\mathcal{H}_{\mathrm{Bob}} = T \otimes (K' \otimes T') \otimes N'$. Both Grover reflections R_{mark} and R_{prep} act strictly as $I_{NK} \otimes O_{\mathrm{Bob}}$, commuting identically with every operator on $N \otimes K$, and the resulting Grover iterate G_A is unitary.*

1. Exact single-round qubit recovery ($d_M = 2$): *For a single-qubit message ($d_M = 2$, rotation angle $\alpha = \pi/6$) and exact decoupling ($\Delta_{\mathrm{dec}} = 0$), a single Grover round achieves unit-probability exact recovery with zero post-selection.*
2. Exact tuned-ancilla recovery for any $m \geq d_M$: *Tuning the ancilla preparation angle via $\sin\beta = d_M \sin\big(\frac{\pi}{2(2m+1)}\big)$, whenever $\Delta_{\mathrm{dec}} = 0$ the m-round unitary G_A^m maps the initial state identically onto the target recovered Bell state with probability* 1.
3. Unconditional deterministic fidelity bound: *For* every *scrambling unitary U on $M \otimes B \to K \otimes T$ and every integer $m \geq d_M$, the deterministic exterior-only recovery fidelity obeys*

$$F_{\mathrm{det}} \geq 1 - \frac{8}{\sqrt{3}}\frac{m}{d_M}\sqrt{\eta} \qquad \xrightarrow{m=d_M} \qquad F_{\mathrm{det}} \geq 1 - \frac{8}{\sqrt{3}}\sqrt{\eta}. \tag{136}$$

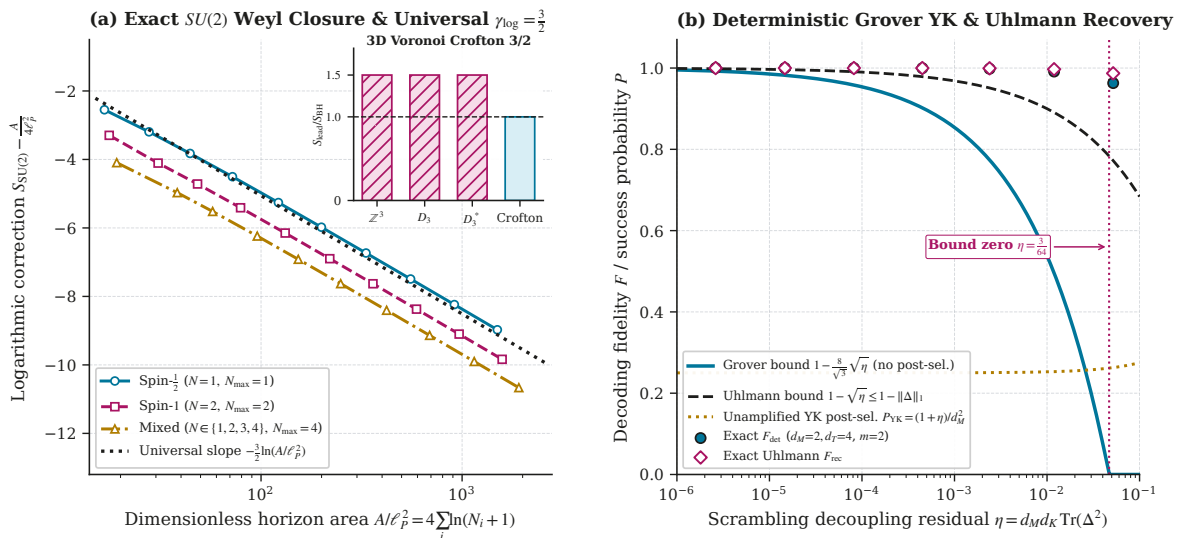

Fig. 6 Quantum horizon entropy scaling and deterministic post-Page decoding. (a) Exact $SU(2)$ Weyl closure logarithmic corrections $S_{SU(2)} - A/(4\ell_{\mathrm{P}}^2)$ versus dimensionless area $A/\ell_{\mathrm{P}}^2 = 4\sum_i \ln(N_i+1)$ for pure spin-1/2 ($N=1$), pure spin-1 ($N=2$), and mixed shells ($N \in \{1,2,3,4\}$), locking onto the universal slope $-\frac{3}{2}\ln(A/\ell_{\mathrm{P}}^2)$ (Theorems 7.3 and 7.5); inset shows the universal 3/2 raw Voronoi overcount across $\mathbb{Z}^3$, D_3, and D_3^* (Theorem 7.2). (b) Deterministic exterior-only Hayden–Preskill decoding fidelity versus scrambling decoupling residual $\eta = d_M d_K \,\mathrm{Tr}(\Delta_{\mathrm{dec}}^2)$, comparing the zero-post-selection Yoshida–Kitaev Grover bound $1 - \frac{8}{\sqrt{3}}\sqrt{\eta}$ (Theorem 7.6, crossing zero at the vertical dotted line $\eta = 3/64$), the one-step Uhlmann Stinespring recovery bound $1 - \|\Delta_{\mathrm{dec}}\|_1 \geq 1 - \sqrt{\eta}$ (Theorem 7.7), exact finite-dimensional realizations ($d_M = 2, d_T = 4, m = 2$), and the unamplified post-selected success probability $P_{\mathrm{YK}} = (1+\eta)/d_M^2$.

4. Exact unitary 2-design guarantee: *In every exact unitary 2-design on $K \otimes T$—which exists whenever $d_K d_T = p^n$ is a prime power—there exists a scrambling unitary U achieving*

$$F_{\mathrm{det}} \geq 1 - \frac{8}{\sqrt{3}}\frac{d_M}{d_T}. \tag{137}$$

The Grover decoder achieves deterministic recovery using explicit unitary reflections (assuming Bob can apply U^* on his exterior registers), at the cost of the $8/\sqrt{3}$ prefactor and $O(d_M)$ rounds. If instead we seek the sharpest information-theoretic recovery guarantee in a single exterior operation, Uhlmann's theorem[85] yields an explicit Stinespring isometry directly from the spectral decomposition of $\rho_{NK} = \Psi\Psi^\dagger$.

Theorem 7.7 (Explicit one-step Stinespring/Uhlmann recovery isometry and trace-norm bound)**.** *For every scrambling unitary U obeying Eq. (134), let $\Psi : \mathcal{H}_T \otimes \mathcal{H}_{B'} \to \mathcal{H}_N \otimes \mathcal{H}_K$ be the bipartition amplitude matrix ($\rho_{NK} = \Psi\Psi^\dagger$), let $(\rho_{NK}^+)^{1/2}$ denote the positive square root of the Moore–Penrose pseudoinverse of ρ_{NK} acting on $\mathrm{supp}(\rho_{NK})$, set $C := \left(\Psi^\dagger(\rho_{NK}^+)^{1/2}\right)^\top$, and let E satisfy $E^\dagger E = I - C^\dagger C$. Then the explicit exterior-only block operator $V = \binom{C}{E} : T \otimes B' \to (N' \otimes K') \oplus (T \otimes B')$ is an exact isometry ($V^\dagger V = I$) obeying*

$$1 - \|\Delta_{\mathrm{dec}}\|_1 \;\leq\; F_{\mathrm{Uhlmann}} = \frac{\left(\mathrm{Tr}\sqrt{\rho_{NK}}\right)^2}{d_M d_K} \;\leq\; P_{\mathrm{pair}\,NN'} \;\leq\; 1, \tag{138}$$

where $P_{\mathrm{pair}\,NN'}$ is the fidelity of the recovered Bell pair across NN', and $F_{\mathrm{Uhlmann}} = 1$ whenever $\Delta_{\mathrm{dec}} = 0$ (witnessed explicitly at $d_M = d_B = 2$ with $F_{\mathrm{Uhlmann}} = 1$). Moreover, in every exact unitary 2-design on $K \otimes T$ (and in particular whenever $d_K d_T = p^n$ is a prime power), there exists a scrambling unitary U achieving

$$F_{\mathrm{Uhlmann}} \geq 1 - \frac{d_M}{d_T}. \tag{139}$$

Figure 6 displays both the arbitrary-spin logarithmic entropy window and the deterministic exterior decoding bounds. The scope boundaries of Theorems 7.6 and 7.7 are sharp: (i) the Grover protocol

assumes Bob has oracle access to U^* on his exterior registers and $m = d_M$ is not claimed minimal; (ii) the Uhlmann isometry V is constructed spectrally in the eigenbasis of ρ_{NK} without formalizing gate-level circuit complexity or Petz-map optimality; (iii) the unitary 2-design results Eq. (137) and Eq. (139) are existential over the design; and (iv) both theorems operate strictly in finite-dimensional Hilbert spaces—dynamical curved-spacetime Hawking evaporation and self-consistent gravitational back-reaction remain open (Section 8.3).

8 Observational consequences, scope accounting, and open frontier

The theorems and obstructions established across this paper separate what classical general relativity, effective capacity-limited collapse, and discrete horizon microstructure strictly enforce from what remains phenomenologically assumed. Bringing the organizing structure, falsifiable consequences, and open technical problems together clarifies what the proved results establish and where the frontier begins.

8.1 Organizing role of the reciprocal cost and local D_4^* horizon stationarity

It is essential to distinguish two logical layers in this manuscript. On the one hand, the nonlinear black-hole, ADM, BMS_4, three-dimensional Voronoi Crofton, $SU(2)$-intertwiner, and finite-dimensional Hayden–Preskill theorems of Sections 3, 4 and 7 are self-contained theorems of differential geometry, representation theory, and quantum information that hold independently of any phenomenological collapse ansatz. On the other hand, across the strong-field models of Sections 4 to 6 and the discrete D_4^* action of Section 2.2, the canonical reciprocal cost $J(x) = \frac{1}{2}(x + x^{-1}) - 1$ and its compact phase branch $J_{\mathrm{phase}}(\theta) = 1 - \cos\theta$[4–6] serve as a single organizing parameterization linking four strong-field regimes to our linearized D_4^* graviton analysis[1]:

1. *Schwarzschild throat geometry (Section 4):* On the time-symmetric isotropic Schwarzschild slice, the sphere area $A(r) = 16\pi M^2\big(1 + \frac{1}{2}J(2r/M)\big)^2$ expresses both the unique minimal surface ($r = M/2$, saturating the Riemannian Penrose inequality[36–38]) and the exact inversion isometry $r \mapsto M^2/(4r)$ directly through $J(x) \geq 0$ and $J(x) = J(1/x)$.
2. *Effective capacity-ceiling collapse (Section 5):* Pricing the collapse rate variable through J_{phase} introduces the ceiling $\rho_c = 3/(8\pi G\ell^2)$ and the exact reciprocal-cost density law Eq. (9), matching the effective polymerized collapse dynamics of Refs.[65;67–69]. This yields uniform curvature caps in homogeneous bounces ($K_{\mathrm{int}} \leq 27/\ell^4$, $K_{\mathrm{ext}} \leq 360/\ell^4$) and sub-critical LTB profiles ($|\eta_{\mathrm{sh}}| < 1$), while cleanly isolating post-turn shell-crossing divergence at $\eta_{\mathrm{sh}} = 5/4$ (**Obstruction I**[49]).
3. *Rotating regular core parameterization (Section 6):* The Gürses–Gürsey capacity mass profile obeys the matching reciprocal-cost gradient Eq. (10), replacing Kerr's $48M_g^2/r^6$ equatorial divergence with the globally bounded core $|K_{\mathrm{GG}}| \leq 896/\ell^4$ (Theorems 6.6 and 6.7) while openly exposing the 0 vs. $24/\ell^4$ directional discontinuity at the ring.
4. *Local 104-hinge D_4^* stationarity across Kerr horizons (Sections 2.2 and 3):* By Eq. (12), the fine-lattice first variation of $\mathcal{C}_{104}(g, n)$ is unconditionally equivalent to the weak vacuum Einstein equation on C^6 periodic nondegenerate metrics in both signatures. Embedding any regular point of ingoing rotating Kerr spacetime ($r > 0$, $0 < \theta < \pi$)—including points directly on r_+, r_-, and the extremal horizon $\Delta = 0$—into a periodic local patch proves exact local first-variation stationarity across the horizon without asymptotic-boundary extrapolation.

8.2 Concrete observational and falsifiable consequences

Four quantitative predictions and exclusions follow directly from the proved theorems:

1. *Exclusion of naive regular-core bounce echoes returning to Exterior I for supercritical mergers.* Every stellar-mass and supermassive astrophysical black hole satisfies the supercritical horizon condition $27(GM)^2 > 64\ell^2$ by more than 70 orders of magnitude when $\ell \sim \ell_{\mathrm{P}}$. By **Obstruction II** (Section 5.3), the advanced time $V(\tau)$ of the matched ingoing bounce chart diverges as $\tau \to \tau_-^-$, and no causal trajectory of the re-expanding stellar surface can pass from Exterior I through the bounce back to Exterior I; post-bounce expansion enters a second asymptotic exterior described

by the outgoing chart (matching the global causal structure of quantum Oppenheimer–Snyder bounce models[68;69;71]). Consequently, regular-black-hole bounce models cannot produce classical post-merger gravitational-wave echoes[60–62] returning to the original exterior observer through the matched bounce spacetime. Any confirmed observational detection of late-time echoes from a macroscopic merger would either signal a horizonless ultracompact object ($M < M_{\rm crit}$ or $a > M_g$) or require non-classical exterior tunneling dynamics[63;64] outside classical causal propagation.

2. $O(\ell^2 r^{-6})$ *suppression of exterior Kerr deviations.* On the rotating capacity core (Theorem 6.6), the Ricci scalar and curvature eigenvalues decay as $|R| \le 72 M_g^2 \ell^2/r^6$ and $|\lambda_i| \le 36 M_g^2 \ell^2/r^6$, while the mass function departs from constant Kerr mass M_g by $-2M_g^2\ell^2/r^3$. At photon-sphere, shadow, and ISCO radii ($r \sim M_g$), fractional deviations from exact vacuum Kerr scale as $(\ell/M_g)^2$. For Planck-scale $\ell \sim \ell_{\rm P}$, $(\ell/M_g)^2 \lesssim 10^{-76}$ for stellar-mass mergers and $\lesssim 10^{-96}$ for M87* and Sgr A*, placing the rotating capacity core in full agreement with current Event Horizon Telescope shadow measurements and LIGO/Virgo/KAGRA ringdown observations. Conversely, any confirmed $O(1)$ macroscopic departure from Kerr shadow contours or quasinormal ringdown frequencies at astrophysical masses would immediately falsify a Planck-scale capacity core.
3. *Pure-vacuum Christodoulou memory and* BMS_4 *soft-graviton Ward benchmark.* Our explicit C^2 pure-vacuum radiative burst provides an analytic, zero-matter benchmark for nonlinear gravitational-wave memory[41] with exact Bondi mass loss $\Delta M_{\rm Bondi} = -\frac{429}{350G}$, equatorial permanent strain offset $\Delta C_+(\pi/2) = -\frac{429}{350}$, and nonzero quadrupole soft charge $Q_{\rm soft}[3\cos^2\theta - 1] = -\frac{429(3\pi-8)}{700G} < 0$. Paired with the exact massive-scattering bridge $\Delta C_{+,\times} = -4G\omega \cdot$ Weinberg soft factor[42;43] and the circular-binary axial angular-momentum flux $\frac{8}{5}\omega Q^2/G$[44], these closed-form identities supply exact calibration benchmarks for memory searches in next-generation interferometers (LISA, Einstein Telescope, Cosmic Explorer).
4. *Universal* $\gamma_{\log} = 3/2$ *logarithmic black-hole entropy signature.* Under the working per-face area footprint $a_N = 4\ln(N+1)\,\ell_{\rm P}^2$, Theorem 7.5 forces the logarithmic correction $-\frac{3}{2}\ln(A/\ell_{\rm P}^2)$ across every finite $SU(2)$ twice-spin ceiling $N_{\max} \ge 1$. This cleanly separates unconstrained puncture counting ($\gamma_{\log} = 0$) and $U(1)$-projected loop quantum gravity counting ($\gamma_{\log} = 1/2$[77]) from full $SU(2)$ gauge-closed microstates ($\gamma_{\log} = 3/2$, matching and generalizing Refs.[76;78;79]), as well as from bulk matter-dependent one-loop Euclidean shifts[80].

8.3 Concrete priorities along the open frontier

Each of the five open problems delineated in Section 1.3 points to a concrete next derivation rather than a vague ambition:

- *Beyond dust and symmetry:* Extending the two-sided LTB threshold ($|\eta_{\rm sh}| < 1$ vs. $\eta_{\rm sh} = 5/4$) to collapse with nonzero pressure, angular momentum, and no spatial symmetry, and comparing shell-crossing formation against polymerized shock-wave collapse models[68;70].
- *Inner Cauchy-horizon dynamics and* $r < 0$ *geometry:* Testing whether dynamical perturbations of supercritical capacity cores trigger exponential Poisson–Israel mass inflation at r_-[30;56;58] or ergoregion/quasinormal instabilities in rotating cores[59], alongside smooth $r < 0$ continuation and general rotating timelike geodesics.
- *Bulk-to-boundary* BMS_4 *bridge:* Deriving the Bondi mass-aspect and angular-momentum-aspect flux laws directly from four-dimensional asymptotically flat Einstein evolution in Bondi–Sachs coordinates, and extending the classical massive-body Ward identity to null radiation ($\sigma = 0$) and quantum S-matrix amplitudes.
- *Interacting continuum quantum measure and dynamical evaporation:* Constructing a diffeomorphism-gauge-fixed continuum path-integral measure from the D_4^* action Eq. (11) (handling lightlike second variations and discrete spin-2 gauge fixing[1;3]), deriving the per-face area footprint a_N and exact $O(1)$ entropy constant from first principles, and upgrading the finite-dimensional Grover and Uhlmann decoders (Theorems 7.6 and 7.7) to curved-spacetime Hawking evaporation with self-consistent metric back-reaction.

Acknowledgements

The author thanks E. Allahyarov, M. Simons, and M.Lj. Zlatanović for technical discussions on D_4^* lattice gravity, reciprocal-cost foundations, and formal verification design, and gratefully acknowledges the Recognition Physics Institute for computational support.

Data availability

All mathematical theorems, explicit analytic witnesses, counterexamples, and curvature bounds reported in this manuscript are contained in the article and its accompanying machine-verified Lean 4 formalization and symbolic–numerical cross-check scripts; no external experimental datasets were generated or analyzed.

Code availability

A frozen verification archive containing the standalone manuscript source, the complete theorem-to-module index for the clean-room-audited Lean 4 formalization baseline (1,012 modules indexed in Section A), the independent 30-check Python symbolic–numerical verification suite (`verify_sota_paper.py`) with its recorded pass log, and the vector figure-generation pipeline (`generate_figures.py`) is permanently archived on Zenodo under DOI 10.5281/zenodo.24509808.

Competing interests

The author declares no competing financial or non-financial interests.

Use of AI tools

Large language model assistants were used to aid Lean 4 proof engineering, independent Python symbolic–numerical verification scripts, and manuscript drafting. Every mathematical theorem, identity, witness, and obstruction reported in this paper was independently machine-checked by the Lean 4 kernel strictly on standard mathematical axioms with zero unproven gaps, and all physical interpretations, scope boundaries, and final text were reviewed and verified by the author.

Appendix A Formal verification ledger

Every theorem, explicit analytic witness, counterexample, and obstruction in Sections 2–7 has been machine-verified in Lean 4 against a clean-room-audited baseline of 1,012 modules (711 strong-field, collapse, geodesic, and quantum-horizon modules together with 301 foundational lattice and closure modules), with zero unproven obligations (`0 sorry`, `0 admit`, `0 native_decide`) and resting strictly on standard mathematical foundations (`propext`, `Classical.choice`, `Quot.sound`).

Table A1 maps each major result block of the manuscript to its audited status, controlling Lean 4 module(s), and exact scope boundary. Status tags distinguish unconditional mathematical theorems (*Proved*), theorems resting on an explicitly identified structural ansatz (*Proved (Working Input)*), theorems taking named asymptotic flux laws as explicit hypotheses (*Proved (Conditional)*), and proved negative refutations or causal impossibilities (*Proved (Obstruction)*).

Table A1: Theorem-to-module formal verification ledger mapping every result and obstruction in Sections 2–7 to its audited status, controlling Lean 4 module(s), and exact scope boundary.

Section / Result Block	Audited Status	Controlling Lean 4 Module(s)	Explicit Scope Boundary
Sec. 2 / Sec. 8: Canonical reciprocal cost $J(x)$, 104-hinge D_4^* real-time first variation $\mathcal{C}_{104}$, and local Kerr stationarity across $r_\pm, \Delta = 0$	Proved	`W3B_RealTimeNullUnitarity`, `W4A_KerrFieldVacuum`, `W4A_KerrLocalFullCost`, `FableE8_JcostRateLaw`	C^6 periodic / local Kerr patch ($r > 0, 0 < \theta < \pi$); non-perturbative $a_{\text{lat}} \to 0$ continuum quantum measure and lightlike second-variation regularization remain open.

Continued on next page

Table A1 (continued)

Section / Result Block	Audited Status	Controlling Lean 4 Module(s)	Explicit Scope Boundary
Sec. 3: Maximally extended Kruskal–Szekeres Schwarzschild (C^2 Fréchet jets, all 16 vacuum Einstein eqs., PPN $\beta = \gamma = 1$, orbits)	Proved	`T2_KruskalSmoothJet VerificationR47`, `W4A_ SchwarzschildFieldCurvature`, `W4A_IsotropicPPN`, `W4A_ SchwarzschildOrbits`	Maximal smooth domain $X^2 - T^2 > -1$, $\sin\theta \neq 0$, $M > 0$; classical $r = 0$ excluded.
Sec. 3: Smooth ingoing Kerr across both horizons (16 vacuum eqs., Killing eq., Zeroth Law κ_H, ergosphere, Penrose, BPT light ring / ISCO, shadow, Komar $M, J_{\rm BH} = Ma$, Petrov Type D, $K = 48\,\mathrm{Re}(\Psi_2^2)$)	Proved	`T2_KerrFieldLevel VacuumEinsteinR56`, `T2_ KerrErgosphere SuperradianceAnd IrreducibleMassR59`, `T2_ KerrPhotonSphere AndISCOEquatorialR61`, `T2_ KerrZerothLaw SurfaceGravityAndBPTISCOR63`, `T2_KerrShadowAnd KerrNewmanThermoR65`, `W3Opus_ KerrISCOLightRingR11D`, `W3Opus_KerrPetrovTypeDR11A`, `W3Opus_ KerrKomarIntegralsR11B`, `W3Opus_KerrISCOKomarAnd PetrovTypeDR11`	Smooth on $\varrho^2 \neq 0, W \neq 0$; classical ring $\varrho^2 = 0$ excluded; ISCO stability uses effective-potential criterion $V'' < 0$, not nonlinear dynamical stability.
Sec. 3: Charged rotating Kerr–Newman across both horizons (16 Einstein–Maxwell, 4 Maxwell, 64 Bianchi, direct on-horizon $\kappa_\pm$, both Zeroth Laws κ_H, Φ_H, Smarr, First Law, Gauss Q, 256-comp. Riemann/Weyl, 8-index $K_{\rm KN}$, Petrov Type D & $\Psi_2 = 0$ locus)	Proved	`T2_KerrNewmanFieldLevel EinsteinMaxwellR66`, `T2_ KerrNewmanZerothLaw AndElectricPotentialR68`, `W3Opus_KerrNewman EinsteinMaxwellR12E`, `R12F`, `W3Opus_IngoingKerrNewman HorizonEinsteinMaxwell R13A–R13C`, `W3Opus_ KerrNewmanPetrovTypeD AndKretschmannR14A–R14D`, `R14`	Smooth on $\varrho^2 \neq 0, W \neq 0$ (zero $1/\Delta$ denominators); finite-r KN Komar integrals with EM volume term and Type O reconstruction at $r = Q^2/M, \chi = 0$ not formalized.
Sec. 3: Kerr–Newman Penrose extraction ($E \geq \Omega_H L + \Phi_H q$, $M_{\rm irr}$), charged-scalar superradiance ($\omega < m\Omega_H + q\Phi_H$), and 4D Kerr Teukolsky separation, static solutions & Frobenius exponents	Proved	`W3Opus_KerrNewmanPenrose ExtractionR16A`, `W3Opus_ KerrNewman SuperradianceFluxR16B`, `W3Opus_KerrTeukolsky SeparationR16C`	$s = 0$ Teukolsky derived from 4D $\Box_g$; $s \neq 0$ master PDE taken from Teukolsky (1973); asymptotic reflection matching and test-particle back-reaction open.
Sec. 4: 4D ADM $3+1$ LDU/det, unique $D = 3$ Yamabe $p = 4$, Lichnerowicz–York constraints, Brill–Lindquist, Bowen–York barriers & mass bracket, Schwarzschild J-cost throat, spherical & IMCF Penrose rigidity, 6 Bardeen invariants, bounce $f_{\rm NL}^{\rm loc} = \frac{5}{2}(1+w)$	Proved	`W3Neon_FourDimADMConstraints LichnerowiczPenroseR1`, `W3Neon_LichnerowiczBarriers HawkingMassBardeenR4`	Unconditional from Mathlib Fréchet calculus; general non-spherical IMCF existence open.
Sec. 4: 4D contracted Bianchi, symmetric-hyperbolic ADM constraint propagation, 7 inhomogeneous ADM evolution eqs., exact Kasner witness $p^* = (-\frac{1}{3}, \frac{2}{3}, \frac{2}{3})$, Bianchi-I holonomy shear cap	Proved (Working Input for holonomy cap)	`W3Neon_FourDimADMEvolution BianchiPropagationR3`	4D Bianchi, ADM evolution, and Kasner blow-up unconditional; Bianchi-I holonomy constraint $h_i = \sin(\ell H_i)/\ell$ explicitly tagged Working Input.
Sec. 4: Pure-vacuum Christodoulou memory ($\Delta M = -\frac{429}{350G}$), S^2 spin-2 E/B Hodge, Flanagan–Nichols local superrotation balance ($k_{\rm sr}$), BMS_4 supertranslation Ward identity & Weinberg leading soft-graviton pole	Proved (Conditional)	`W3Fable_ PureVacuumChristodoulou MemoryR2`, `W3Fable_ Spin2HodgeAnd SuperrotationBalanceR2`, `W3Fable_BMS4SoftGravitonWard AndMemoryR4`	Calculus and algebraic identities unconditional; `MassAspectLaw` and `AngMomAspectLawAt` are explicit named hypotheses; classical massive timelike bodies only (null $\sigma = 0$ and quantum S-matrix open).

Continued on next page

Table A1 (continued)

Section / Result Block	Audited Status	Controlling Lean 4 Module(s)	Explicit Scope Boundary
Sec. 5: Compact-phase cost rate law, homogeneous Oppenheimer–Snyder bounce ($K_{\text{int}} \le 27/\ell^4$, $K_{\text{ext}} \le 360/\ell^4$), critical mass $27G^2M^2 = 64\ell^2$, outgoing EF $9+9$ Israel–Darmois junction	Proved (Working Input)	`FableE8_JcostRateLaw`, `FableE8_BouncingStar`, `FableE8_DynamicalCollapse JcostBounce`, `FableE8_Junction`, `FableE8_OutgoingChart`, `FableE8_SingularityResolution Capstone`	Equations, curvature bounds, and $9+9$ matching unconditional for all $G, M, \ell, r_b > 0$; compact-phase rate pricing tagged Working Input.
Sec. 5 (Obstruction I): Two-sided inhomogeneous LTB dust collapse: uniform bound $K \le C_{\text{LTB}}(\lvert\eta_{\text{sh}}\rvert)/\ell^4$ for $\lvert\eta_{\text{sh}}\rvert < 1$ (witness $\eta_{\text{sh}} = \frac{1}{2}$) vs. post-turn shell-crossing blow-up at $\eta_{\text{sh}} = \frac{5}{4}$	Proved (Two-Sided / Obstruction)	`FableE8_LTBCurvature`, `FableE8_LTBShellCrossing`, `FableE8_LTBBounceKretschmann`, `FableE8_Wave2LTBCurvatureAnd GeodesicsCapstone`	Marginally bound C^3 spherically symmetric dust; blow-up occurs approaching post-turn shell crossing at $s = +\ell/3$ ($N \to 0^+, R' \to 0^+$); generic $3+1$ asymmetric collapse with pressure open.
Sec. 5.3 (Obstruction II): Supercritical two-exterior / no-exterior-echo horizon obstruction ($27G^2M^2 > 64\ell^2$, $V(\tau) \to +\infty$ as $\tau \to \tau_-$)	Proved (Obstruction)	`FableE8_NoExteriorReturn`, `FableE8_OutgoingChart`, `FableE8_Junction`	Rules out causal return of the bouncing stellar surface to Exterior I in the matched bounce geometry; horizonless objects or non-classical tunneling outside scope.
Sec. 6: Global causal completeness of bouncing dust interior & bouncing stellar surface across glued ingoing/outgoing charts (Theorems 6.1 and 6.2)	Proved	`FableE8_InteriorGeodesic Completeness`, `FableE8_ExteriorGeodesics`	Unconditional for all $G, M, \ell, r_b > 0$ (subcritical, critical, and supercritical) on $a(\tau) \ge a_{\min} > 0$ and along the glued surface trajectory ($R \ge R_{\min}, K \le 360/\ell^4$).
Sec. 6: Global proper-time completeness on static Hayward capacity core ($r(\tau) \ge r_0 e^{-\tau/\ell}$, $\lvert K\rvert \le 896/\ell^4$; Theorem 6.3)	Proved	`FableE8_HaywardRainGeodesics`	Unit-energy ($E = 1$) radial rain timelike geodesics on $r > 0$; higher-energy ($E > 1$) trajectories reaching $r = 0$ in finite proper time outside scope.
Sec. 6: Rotating Gürses–Gürsey capacity core (J-cost mass law, $\lvert K_{\text{GG}}\rvert \le 896/\ell^4$, equatorial $24/\ell^4$ vs. flat $r = 0$ disk, $O(\ell^2 r^{-6})$ decay, complete principal null rays vs. Kerr $48M_g^2/r^6$; Theorems 6.5 to 6.7)	Proved (Working Input)	`FableE8_RotatingKerrRing SingularityResolution`, `FableE8_CoreNullGeodesics`, `FableE8_RotatingKretschmann`	Chart $r \ge 0, \varrho^2 \ne 0$; choice of m_{cap} tagged Working Input; $r < 0$ continuation, general rotating timelike geodesics, and inner Cauchy-horizon mass-inflation stability open.
Sec. 7: Exact $SO(3)$ curved-horizon spherical integral & universal 3/2 3D Voronoi Crofton theorem across $\mathbb{Z}^3, D_3, D_3^*$ (Theorems 7.1 and 7.2)	Proved	`T2_Universal3DVoronoi CroftonAndKerrR51`, `T2_UniversalSO3Crofton IntegralR55`	Unconditional geometric integral theorem forcing the 2/3 directional Crofton projection independently of 3D Voronoi lattice isotropy.
Sec. 7: Exact $SU(2)$ Weyl closure integral, Gaussian character bounds, arbitrary-spin two-sided entropy-area window & forced uniqueness $\gamma_{\log} = 3/2$ (Theorems 7.3 to 7.5)	Proved (Working Input for footprint)	`W2Fable_WeylClosureIntegral MixedSpin`, `W2Fable_GeneralValenceAndMixed SpinHorizonR16`, `W2Fable_ArbitrarySpinLogAreaLawR19`	Operator bridge, counting bounds, and uniqueness $\gamma_{\log} = 3/2$ unconditional for all finite $N_{\max} \ge 1$; per-face area footprint $a_N = 4\ln(N+1)\,\ell_{\text{P}}^2$ tagged Working Input; exact $O(1)$ constant not determined.
Sec. 7: Deterministic exterior-only Yoshida–Kitaev Grover decoder ($F_{\text{det}} \ge 1 - \frac{8}{\sqrt{3}}\sqrt{\eta}$) & one-step Stinespring/Uhlmann recovery isometry ($F_{\text{Uhlmann}} \ge 1 - \lVert\Delta_{\text{dec}}\rVert_1, 1 - d_M/d_T$; Theorems 7.6 and 7.7)	Proved	`W2Fable_DeterministicYoshida KitaevGroverR15`, `W2Fable_UhlmannRecoveryTraceNormR17`	Finite-dimensional Hilbert-space matrix theorems ($d_M d_B = d_K d_T$); Grover assumes exterior U^* access; Uhlmann isometry uses Moore–Penrose pseudoinverse on $\text{supp}(\rho_{NK})$ (circuit complexity and Petz optimality not formalized); dynamical Hawking evaporation & back-reaction open.

References

[1] J. Washburn, E. Allahyarov, Birefringent gravitons in Lorentzian Regge calculus. Submitted to Eur. Phys. J. C (2026)

[2] J. Washburn, E. Allahyarov, Flat geometries select the Regge action in Lorentzian Regge calculus. Submitted to Eur. Phys. J. C (2026)

[3] J. Washburn, *Quantum Gravity on the Recognition Ledger: Exact Theorems, Proved Obstructions, and the Open Frontier*, Version 3.0 (23 November 2026), Recognition Physics Institute. https://recognitionphysics.org/papers/quantum-gravity-from-the-recognition-ledger/

[4] J. Washburn, M.Lj. Zlatanović, Uniqueness of the canonical reciprocal cost. Mathematics **14**, 935 (2026). https://doi.org/10.3390/math14060935

[5] J. Washburn, M.Lj. Zlatanović, E. Allahyarov, The d'Alembert inevitability theorem. Mathematics **14**, 1386 (2026). https://doi.org/10.3390/math14081386

[6] S. Pardo-Guerra, A. Thapa, M. Simons, J. Washburn, Coherent comparison as information cost: axiomatic foundations for discrete ledger dynamics. Foundations **6**, 17 (2026). https://doi.org/10.3390/foundations6020017

[7] M. Simons, E. Allahyarov, J. Washburn, A discrete informational framework for classical gravity: ledger foundations and galaxy rotation curve constraints. Entropy **28**(4), 477 (2026). https://doi.org/10.3390/e28040477

[8] T. Regge, General relativity without coordinates. Nuovo Cimento **19**, 558 (1961). https://doi.org/10.1007/BF02733251

[9] G. Bhanot, K. Bitar, U.M. Heller, H. Neuberger, φ^4 on F_4: analytical results. Nucl. Phys. B **343**, 467 (1990). https://doi.org/10.1016/0550-3213(90)90479-W

[10] R.M. Wald, *General Relativity* (University of Chicago Press, Chicago, 1984). https://doi.org/10.7208/chicago/9780226870373.001.0001

[11] R.P. Kerr, Gravitational field of a spinning mass as an example of algebraically special metrics. Phys. Rev. Lett. **11**, 237 (1963). https://doi.org/10.1103/PhysRevLett.11.237

[12] E.T. Newman, E. Couch, K. Chinnapared, A. Exton, A. Prakash, R. Torrence, Metric of a rotating, charged mass. J. Math. Phys. **6**, 918 (1965). https://doi.org/10.1063/1.1704351

[13] M.D. Kruskal, Maximal extension of Schwarzschild metric. Phys. Rev. **119**, 1743 (1960). https://doi.org/10.1103/PhysRev.119.1743

[14] G. Szekeres, On the singularities of a Riemannian manifold. Publ. Math. Debrecen **7**, 285 (1960); reprinted in Gen. Relativ. Gravit. **34**, 2001 (2002)

[15] R.H. Boyer, R.W. Lindquist, Maximal analytic extension of the Kerr metric. J. Math. Phys. **8**, 265 (1967). https://doi.org/10.1063/1.1705193

[16] R. Penrose, Gravitational collapse and space-time singularities. Phys. Rev. Lett. **14**, 57 (1965). https://doi.org/10.1103/PhysRevLett.14.57

[17] R. Penrose, Gravitational collapse: the role of general relativity. Riv. Nuovo Cimento **1**, 252 (1969); reprinted in Gen. Relativ. Gravit. **34**, 1141 (2002)

[18] S.W. Hawking, R. Penrose, The singularities of gravitational collapse and cosmology. Proc. R. Soc. Lond. A **314**, 529 (1970). https://doi.org/10.1098/rspa.1970.0021

[19] D. Christodoulou, R. Ruffini, Reversible transformations of a charged black hole. Phys. Rev. D **4**, 3552 (1971). https://doi.org/10.1103/PhysRevD.4.3552

[20] J.M. Bardeen, W.H. Press, S.A. Teukolsky, Rotating black holes: locally nonrotating frames, energy extraction, and scalar synchrotron radiation. Astrophys. J. **178**, 347 (1972). https://doi.org/10.1086/151796

[21] J.M. Bardeen, Timelike and null geodesics in the Kerr metric, in *Black Holes (Les Astres Occlus)*, ed. by C. DeWitt, B.S. DeWitt (Gordon and Breach, New York, 1973), pp. 215–239

[22] J.M. Bardeen, B. Carter, S.W. Hawking, The four laws of black hole mechanics. Commun. Math. Phys. **31**, 161 (1973). https://doi.org/10.1007/BF01645742

[23] S.A. Teukolsky, Perturbations of a rotating black hole. I. Fundamental equations for gravitational, electromagnetic, and neutrino-field perturbations. Astrophys. J. **185**, 635 (1973). https://doi.org/10.1086/152444

[24] W.H. Press, S.A. Teukolsky, Perturbations of a rotating black hole. II. Dynamical stability of the Kerr metric. Astrophys. J. **185**, 649 (1973). https://doi.org/10.1086/152445

[25] R. Brito, V. Cardoso, P. Pani, *Superradiance: Energy Extraction, Black-Hole Bombs and Implications for Astrophysics and Particle Physics*, Lecture Notes in Physics, vol. 906 (Springer, Cham, 2015). https://doi.org/10.1007/978-3-319-19000-6

[26] B. Carter, Global structure of the Kerr family of gravitational fields. Phys. Rev. **174**, 1559 (1968). https://doi.org/10.1103/PhysRev.174.1559

[27] E. Newman, R. Penrose, An approach to gravitational radiation by a method of spin coefficients. J. Math. Phys. **3**, 566 (1962). https://doi.org/10.1063/1.1724257

[28] A. Komar, Covariant conservation laws in general relativity. Phys. Rev. **113**, 934 (1959). https://doi.org/10.1103/PhysRev.113.934

[29] R.C. Henry, Kretschmann scalar for a Kerr–Newman black hole. Astrophys. J. **535**, 350 (2000). https://doi.org/10.1086/308819

[30] E. Poisson, W. Israel, Internal structure of black holes. Phys. Rev. D **41**, 1796 (1990). https://doi.org/10.1103/PhysRevD.41.1796

[31] R. Arnowitt, S. Deser, C.W. Misner, The dynamics of general relativity, in *Gravitation: An Introduction to Current Research*, ed. by L. Witten (Wiley, New York, 1962), pp. 227–265; reprinted in Gen. Relativ. Gravit. **40**, 1997 (2008). https://doi.org/10.1007/s10714-008-0661-1

[32] A. Lichnerowicz, L'intégration des équations de la gravitation relativiste et le problème des n corps. J. Math. Pures Appl. **23**, 37 (1944)

[33] J.W. York, Jr., Gravitational degrees of freedom and the initial-value problem. Phys. Rev. Lett. **26**, 1656 (1971). https://doi.org/10.1103/PhysRevLett.26.1656

[34] D.R. Brill, R.W. Lindquist, Interaction energy in geometrostatics. Phys. Rev. **131**, 471 (1963). https://doi.org/10.1103/PhysRev.131.471

[35] J.M. Bowen, J.W. York, Jr., Time-asymmetric initial data for black holes and black-hole collisions. Phys. Rev. D **21**, 2047 (1980). https://doi.org/10.1103/PhysRevD.21.2047

[36] R. Geroch, Energy extraction. Ann. N.Y. Acad. Sci. **224**, 108 (1973). https://doi.org/10.1111/j.1749-6632.1973.tb41445.x

[37] G. Huisken, T. Ilmanen, The inverse mean curvature flow and the Riemannian Penrose inequality. J. Differ. Geom. **59**, 353 (2001). https://doi.org/10.4310/jdg/1090349447

[38] H.L. Bray, Proof of the Riemannian Penrose inequality using the positive mass theorem. J. Differ. Geom. **59**, 177 (2001). https://doi.org/10.4310/jdg/1090349428

[39] H. Bondi, M.G.J. van der Burg, A.W.K. Metzner, Gravitational waves in general relativity VII. Waves from axi-symmetric isolated systems. Proc. R. Soc. Lond. A **269**, 21 (1962). https://doi.org/10.1098/rspa.1962.0161

[40] R.K. Sachs, Gravitational waves in general relativity VIII. Waves in asymptotically flat space-time. Proc. R. Soc. Lond. A **270**, 103 (1962). https://doi.org/10.1098/rspa.1962.0206

[41] D. Christodoulou, Nonlinear nature of gravitation and gravitational-wave experiments. Phys. Rev. Lett. **67**, 1486 (1991). https://doi.org/10.1103/PhysRevLett.67.1486

[42] S. Weinberg, Infrared photons and gravitons. Phys. Rev. **140**, B516 (1965). https://doi.org/10.1103/PhysRev.140.B516

[43] A. Strominger, On BMS invariance of gravitational scattering. J. High Energy Phys. **2014**(07), 152 (2014). https://doi.org/10.1007/JHEP07(2014)152

[44] É.É. Flanagan, D.A. Nichols, Conserved charges of the extended Bondi–Metzner–Sachs algebra. Phys. Rev. D **95**, 044002 (2017); Erratum: Phys. Rev. D **108**, 069902 (2023). https://doi.org/10.1103/PhysRevD.95.044002

[45] J.R. Oppenheimer, H. Snyder, On continued gravitational contraction. Phys. Rev. **56**, 455 (1939). https://doi.org/10.1103/PhysRev.56.455

[46] G. Lemaître, L'Univers en expansion. Ann. Soc. Sci. Bruxelles A **53**, 51 (1933); English translation: Gen. Relativ. Gravit. **29**, 641 (1997)

[47] R.C. Tolman, Effect of inhomogeneity on cosmological models. Proc. Natl. Acad. Sci. U.S.A. **20**, 169 (1934). https://doi.org/10.1073/pnas.20.3.169

[48] H. Bondi, Spherically symmetrical models in general relativity. Mon. Not. R. Astron. Soc. **107**, 410 (1947). https://doi.org/10.1093/mnras/107.5-6.410

[49] C. Hellaby, K. Lake, Shell crossings and the Tolman model. Astrophys. J. **290**, 381 (1985); Erratum: Astrophys. J. **300**, 461 (1986). https://doi.org/10.1086/162995

[50] W. Israel, Singular hypersurfaces and thin shells in general relativity. Nuovo Cimento B **44**, 1 (1966). https://doi.org/10.1007/BF02710419

[51] S.A. Hayward, Formation and evaporation of nonsingular black holes. Phys. Rev. Lett. **96**, 031103 (2006). https://doi.org/10.1103/PhysRevLett.96.031103

[52] J.M. Bardeen, Non-singular general-relativistic gravitational collapse, in *Proceedings of the International Conference GR5* (Tbilisi, 1968), p. 174

[53] M. Gürses, F. Gürsey, Lorentz covariant treatment of the Kerr–Schild geometry. J. Math. Phys. **16**, 2385 (1975). https://doi.org/10.1063/1.522480

[54] C. Bambi, L. Modesto, Rotating regular black holes. Phys. Lett. B **721**, 329 (2013). https://doi.org/10.1016/j.physletb.2013.03.025

[55] V.P. Frolov, Notes on nonsingular models of black holes. Phys. Rev. D **94**, 104056 (2016). https://doi.org/10.1103/PhysRevD.94.104056

[56] R. Carballo-Rubio, F. Di Filippo, S. Liberati, C. Pacilio, M. Visser, On the viability of regular black holes. J. High Energy Phys. **2018**(07), 023 (2018). https://doi.org/10.1007/JHEP07(2018)023

[57] R. Carballo-Rubio, F. Di Filippo, S. Liberati, M. Visser, Geodesically complete black holes. Phys. Rev. D **101**, 084047 (2020). https://doi.org/10.1103/PhysRevD.101.084047

[58] R. Carballo-Rubio, F. Di Filippo, S. Liberati, C. Pacilio, M. Visser, Regular black holes without mass inflation instability. J. High Energy Phys. **2022**(09), 118 (2022). https://doi.org/10.1007/JHEP09(2022)118

[59] E. Franzin, S. Liberati, J. Mazza, R. Dey, S. Chakraborty, Scalar perturbations around rotating regular black holes and wormholes: quasinormal modes, ergoregion instability, and superradiance. Phys. Rev. D **105**, 124051 (2022). https://doi.org/10.1103/PhysRevD.105.124051

[60] V. Cardoso, E. Franzin, P. Pani, Is the gravitational-wave ringdown a probe of the event horizon? Phys. Rev. Lett. **116**, 171101 (2016); Erratum: Phys. Rev. Lett. **117**, 089902 (2016). https://doi.org/10.1103/PhysRevLett.116.171101

[61] V. Cardoso, P. Pani, Testing the nature of dark compact objects: an overview. Living Rev. Relativ. **22**, 4 (2019). https://doi.org/10.1007/s41114-019-0020-4

[62] J. Abedi, H. Dykaar, N. Afshordi, Echoes from the abyss: tentative evidence for Planck-scale structure at black hole horizons. Phys. Rev. D **96**, 082004 (2017). https://doi.org/10.1103/PhysRevD.96.082004

[63] C. Rovelli, F. Vidotto, Planck stars. Int. J. Mod. Phys. D **23**, 1442026 (2014). https://doi.org/10.1142/S0218271814420267

[64] H.M. Haggard, C. Rovelli, Quantum-gravity effects outside the horizon spark black to white hole tunneling. Phys. Rev. D **92**, 104020 (2015). https://doi.org/10.1103/PhysRevD.92.104020

[65] A. Ashtekar, T. Pawlowski, P. Singh, Quantum nature of the big bang. Phys. Rev. Lett. **96**, 141301 (2006). https://doi.org/10.1103/PhysRevLett.96.141301

[66] J.G. Kelly, R. Santacruz, E. Wilson-Ewing, Effective loop quantum gravity framework for vacuum spherically symmetric spacetimes. Phys. Rev. D **102**, 106024 (2020). https://doi.org/10.1103/PhysRevD.102.106024

[67] J.G. Kelly, R. Santacruz, E. Wilson-Ewing, Black hole collapse and bounce in effective loop quantum gravity. Class. Quantum Gravity **38**, 04LT01 (2021). https://doi.org/10.1088/1361-6382/abd3e2

[68] V. Husain, J.G. Kelly, R. Santacruz, E. Wilson-Ewing, Quantum gravity of dust collapse: shock waves from black holes. Phys. Rev. Lett. **128**, 121301 (2022). https://doi.org/10.1103/PhysRevLett.128.121301

[69] J. Lewandowski, Y. Ma, J. Yang, C. Zhang, Quantum Oppenheimer–Snyder and Swiss cheese models. Phys. Rev. Lett. **130**, 101501 (2023). https://doi.org/10.1103/PhysRevLett.130.101501

[70] K. Giesel, M. Han, B.-F. Li, H. Liu, P. Singh, Spherical symmetric gravitational collapse of a dust cloud: polymerized dynamics in reduced phase space. Phys. Rev. D **107**, 044047 (2023). https://doi.org/10.1103/PhysRevD.107.044047

[71] M. Bobula, T. Pawłowski, Rainbow Oppenheimer–Snyder collapse and the entanglement entropy production. Phys. Rev. D **108**, 026016 (2023). https://doi.org/10.1103/PhysRevD.108.026016

[72] J.D. Bekenstein, Black holes and entropy. Phys. Rev. D **7**, 2333 (1973). https://doi.org/10.1103/PhysRevD.7.2333

[73] S.W. Hawking, Particle creation by black holes. Commun. Math. Phys. **43**, 199 (1975). https://doi.org/10.1007/BF02345020

[74] T. Jacobson, Thermodynamics of spacetime: the Einstein equation of state. Phys. Rev. Lett. **75**, 1260 (1995). https://doi.org/10.1103/PhysRevLett.75.1260

[75] L.A. Santaló, *Integral Geometry and Geometric Probability* (Addison-Wesley, Reading, 1976)

[76] R.K. Kaul, P. Majumdar, Logarithmic correction to the Bekenstein–Hawking entropy. Phys. Rev. Lett. **84**, 5255 (2000). https://doi.org/10.1103/PhysRevLett.84.5255

[77] K.A. Meissner, Black-hole entropy in loop quantum gravity. Class. Quantum Gravity **21**, 5245 (2004). https://doi.org/10.1088/0264-9381/21/22/015

[78] A. Ghosh, P. Mitra, An improved lower bound on black hole entropy in the quantum geometry approach. Phys. Lett. B **616**, 114 (2005). https://doi.org/10.1016/j.physletb.2005.05.003

[79] J. Engle, K. Noui, A. Perez, Black hole entropy and $SU(2)$ Chern–Simons theory. Phys. Rev. Lett. **105**, 031302 (2010). https://doi.org/10.1103/PhysRevLett.105.031302

[80] A. Sen, Logarithmic corrections to Schwarzschild and other non-extremal black hole entropy in different dimensions. J. High Energy Phys. **2013**(04), 156 (2013). https://doi.org/10.1007/JHEP04(2013)156

[81] D.N. Page, Information in black hole radiation. Phys. Rev. Lett. **71**, 3743 (1993). https://doi.org/10.1103/PhysRevLett.71.3743

[82] P. Hayden, J. Preskill, Black holes as mirrors: quantum information in random subsystems. J. High Energy Phys. **2007**(09), 120 (2007). https://doi.org/10.1088/1126-6708/2007/09/120

[83] B. Yoshida, A. Kitaev, Efficient decoding for the Hayden–Preskill protocol. arXiv:1710.03363 [hep-th] (2017). https://arxiv.org/abs/1710.03363

[84] B. Yoshida, N.Y. Yao, Disentangling scrambling and decoherence via quantum teleportation. Phys. Rev. X **9**, 011006 (2019). https://doi.org/10.1103/PhysRevX.9.011006

[85] A. Uhlmann, The "transition probability" in the state space of a $*$-algebra. Rep. Math. Phys. **9**, 273 (1976). https://doi.org/10.1016/0034-4877(76)90060-4